A THESIS

FOR THE DEGREE OF DOCTOR OF PHYLOSOPHY

Boundary Estimation in EIT using Expectation Maximization Algorithm

Anil Kumar Khambampati

Department of Electrical and Electronic Engineering

GRADUATE SCHOOL

JEJU NATIONAL UNIVERSITY

2010. 02

Boundary Estimation in EIT using Expectation Maximization Algorithm

Anil Kumar Khambampati

(Supervised by Professor Kyung Youn Kim)

A thesis submitted in partial fulfillment of the requirement for the degree of Doctor of Philosophy

2010. 02

The thesis has been examined and approved.

Thesis director, Min Jae Kang, Professor, Department of Electronic Engineering

Seok Jun Ko, Assistant Professor, Department of Electronic Engineering

Sin Kim, Professor, Department of Nuclear and Energy Engineering

Seoung Dal Jung, Professor, Department of Mathematics

Kyung Youn Kim, Professor, Department of Electronic Engineering

Date

Department of Electrical and Electronic Engineering
GRADUATE SCHOOL
JEJU NATIONAL UNIVERSITY
REPUBLIC OF KOREA

To

My Parents

Acknowledgements

The work with this dissertation has been extensive and trying, but in the first place exciting, instructive, and fun. This thesis is the result of four years of work whereby I have been accompanied and supported by many people. It is a pleasant aspect that I have now the opportunity to express my gratitude for all of them.

The first person I would like to thank is my supervisor Kyung Youn Kim. I have been with him since 2006 when I started my Ph.D. assignment. During these years I have known Prof. Kyung Youn Kim as a sympathetic and principle-centered person. His overly enthusiasm and integral view on research and his mission for providing only high quality work and not less, has made a deep impression on me. I owe him lot of gratitude for having me shown this way of research. He could not even realize how much I have learned from him. Besides of being an excellent supervisor, Prof Kim was as close as a relative and a good friend to me. I am really glad that I have come to get know Prof. Kyung Youn Kim in my life.

I would like to thank Professor Sin Kim for his guidance, stimulating suggestions and encouragement had helped me in all the time of research and writing of this dissertation. His deep physical insight and wide knowledge in the field of EIT was always of great assistance. I would also like to thank the other members of my Ph.D. committee who monitored my work and took effort in reading and providing me with valuable comments on earlier versions of this thesis: Prof. Min Jae Kang, Prof. Seok Jun Ko, and Prof. Seoung Dal Jung. I thank you all.

Also, I wish to offer my humble gratitude to professors of my department, Prof. Yang Hoi Doh, Prof. Kyung Sik Kim, Prof. Kwang Man Lee, and Prof. Sung Taek Ko for their inspiring and encouraging way to guide me to a deeper understanding of knowledge, and their invaluable comments during the course work.

I am fortunate enough to have chance to work with many people directly or indirectly. Dr. Umer Zeeshan Ijaz has helped me initially when I joined the lab. He has been a real mentor and provided motivation to achieve something big in life. Dr. Bong Seok Kim has been so kind and helped me when ever I faced some difficulty in the work. I always remember Mr. Ahmar Rashid for the long discussions we had in the lab about life and work. He always motivated me to work and I never

felt alone or stressed with work. Even though I spent only few months with Liu Dong, he has been very helpful and assisted me in arranging the thesis. In acquiring the knowledge about the experimental studies, Jeong Seong Lee helped me study and perform the experiments. The experiments performed in this thesis are performed with his help. Rong Li, Murtuza, Minseok, Boan Lee have been good friends and even though I did not have chance to work with them directly, they provided good support and were helpful in assisting me in numerous ways.

Staying away from home is always challenging and tough. However, I am glad to have friends in Jeju who always made be believe they are there when it matters and has been part of my happiness and hard ships. Vijay Ramu, Anji Reddy, Abhijit saha, Shrikant, Gunasekaran, Sueng Hyun Oh, Mahanama, Chamilani, Mahinda, Jin Long, Dr Ganesh, Dr. hari, Dr. Rajneesh, Mr. Syed Shanu, Purushottaman, Nandeesh, Umasuthan, Ganesh Thangaraj and Nauman. I thank them all for giving me so many memories to cherish during my stay in Jeju. I also thank all the members of JISO who has been very cooperative and supportive.

I am also grateful for the department of Electronic Engineering at Jeju University for providing me an excellent work environment during my study and I also thank Mi Na Hyun, Suk-In Kang for their cheerful assistance in the office work.

Many thanks to institute for information technology advancement (IITA) funded by Korean government for supporting me during my stay in Korea. Also, Graduate school of Jeju University has been grateful to wave the tuition fee for my doctoral studies. I thank Brain Korea 21 which provided the funds for presenting the research work held in Korea and abroad.

Finally, I will never find words enough to express the gratitude that I owe to my parents and family members. Their tender love and affection has always been the cementing force for building the blocks of my academic career. The all round support rendered by them provided the much needed stimulant to sail through the phases of stress and strain.

I would like to thank all those whom I have not mentioned above but helped me in numerous ways to my success.

Abbreviations and notations

BEM	Boundary element method
CEM	Complete electrode model
EIT	Electrical impedance tomography
EM	Expectation maximization
EKF	Extended Kalman filter
EKS	Extended Kalman smoother
FEM	Finite element method
GRV	Gaussian random variable
IMM	Interactive multiple model
LKF	Linearized Kalman filter
ML	Maximum likelihood
MNN	Multi-layered Neural network
OT	Optical tomography
PDE	Partial differential equation
RMSE	Root mean square error
STD	Standard deviation
UT	Unscented transform
UKF	Unscented Kalman filter

I	Identity matrix
T	Transpose of a matrix
i, j	indices
Ω	Object to be imaged
$\partial\Omega$	Boundary of the object
J	Current density, Jacobian
J^o	Ohmic current
J^s	Current source
ε	Permittivity
μ	Permeability
e_l	lth electrode
σ	Conductivity
L	Number of electrodes, Likelihood estimate
L_R	Regularization matrix
U_l , V_l	Voltage on lth electrode
I_l	Current applied to the lth electrode
υ	Outward unit normal
u, $u(x)$	Potential distribution inside an object
z_l	Contact impedance of lth electrode
α_i , β_i	Parameters used in FEM formulation

$u^h(x,y)$	Finite element approximation of potential distribution
U^h	Finite element approximation of boundary voltages
$\hat{\mathbf{U}}$	Voltages from the measurement electrodes
M	Measurement matrix
$\bar{M}$	Extended measurement matrix
$\bar{N}$	Extended mapping matrix
ϕ_i	Two-dimensional first-order basis function
$\lvert e_j \rvert$	Area of the electrode j
N	Number of nodes in the finite element mesh
ρ_n	Resistivity of nth element
A	Magnetic vector potential, Stiffness matrix,
B	Magnetic induction, Component of stiffness matrix
C	Component of stiffness matrix
D	Electric displacement, Component of stiffness matrix
$\bar{R}$	Pseudo resistance matrix
x	State vector
$\bar{n}$	Dimension of state vector
$\bar{m}$	Dimension of observation vector
k	Discrete time step
F_k	State transition model
H_k	Observation model
w_k	Process noise
v_k	Measurement noise
Q_k	Process noise covariance
R_k	Measurement noise covariance
z_k	Measurements
$x_{k\|k-1}$	Priori state estimate
$x_{k\|k}$	Posteriori state estimate
$e_{k\|k-1}$	Priori state estimate error
$e_{k\|k}$	Posteriori estimate error
E	Expectation, electric field
H	Magnetic field
K_k	Kalman gain
P_k	Error covariance
P	Number of current patterns, probability
y_k	Pseudo measurement
θ	Model parameters
μ	Mean of the initial state
Π	Covariance of initial state
x_0	Initial state
$\log L$	Log-likelihood function
n	Number of observations recorded in EM implementation

$x_{k\|n}$, $\gamma_{k\|n}$	Smoothed state estimate
$P_{k\|n}$	Smoothed covariance estimate
$P_{k,k-1\|n}$	Smoothed cross covariance estimate
G	Smoother gain
P	Number of phase boundaries in flow field
χ_k	Characteristic function of the sub region A_k
A_k	Disjoint region
$C_k(s)$	Closed boundary
Ω_m	Mesh elements which cross the boundary
N_θ	Number of basis functions
γ_k^α	Fourier coefficients representing closed boundary
γ_k	State vector for closed boundary
Γ	Coefficient vector representing closed boundary coefficients
θ_n	Periodic and smooth basis function
$U_k(d_k), U_k(\gamma_k)$	Forward solver using FEM
d_λ	Front points to be estimated
Λ	Total number of front points to be estimated
A, B, C	Parameters used in EM algorithm
RMSE_γ	Root mean square error for estimated Fourier coefficients
S_k	Distinct regions in open boundary
R	Radius of pipe
σ_e	Area weighted conductivity
RMSE_d	Root mean square error for estimated front points
RMSE_U	Root mean square error for computed voltages

Contents

List of Figures

List of Tables

요약

이상(two-phase) 유동의 시각화는 유동 파라미터의 특징에 관한 이해를 제공해 주므로, 유동 과정(flow process)을 모니터링 하는데 도움이 된다. 고시간(high temporal) 특성을 갖는 전기 임피던스 단층촬영법은 빠른 천이 과정을 모니터링 할 수 있다. 전기 임피던스 단층촬영법에서는, 프로세스 대상체의 경계면에 부착된 전극을 통해 전류 소스를 주입하고, 전극에 유기되는 전압을 측정한다. 이 전류-전압 관계를 기반으로 내부의 도전율 분포(conductivity distribution)가 복원된다. 이상 유동에서 도전율 분포는 미리 알 수가 있으므로, 이 사전 정보를 이용하여 이상 사이의 경계를 추정할 수가 있다. 상 경계(phase boundary)는 경계의 토폴로지에 따라 개경계(open boundary)와 폐경계(closed boundary) 형태로 분류될 수 있다. 폐경계 문제는 유동 과정에서 공동(void)들의 추정 문제를 수반한다. 전형적인 개경계 문제는 서로 혼합되지 않는 두 유체 사이의 표면 경계를 추정하는 것이다. 유동 과정에서 형성된 공동(void)들은 불안정하고 대상체 내부를 무작위로 움직이므로, 영역의 경계면을 추정하는데 있어서 동적 추정 알고리즘이 필요하다. 폐경계는 푸리에 급수를 이용하여 표현되는 반면에, 개경계는 이산 프런트 포인트(discrete front points)의 보간법으로 표현된다. 이상 사이의 경계는 시변(time variant)이고 유동 과정은 꽤 복잡하다. 빠른 경계 변화를 추적하기 위해서는 동적 추정 알고리즘이 필요하다.

동적 추정 문제에서, 역문제(inverse problem)는 상태 추정 문제로 취급되고 시변하는 경계 계수들은 추정할 상태 변수들이 된다. 확장 칼만 필터(EKF), unscented 칼만 필터(UKF) 등과 같은 칼만-형태의 추정기들을 적용함에 있어서, 전개(evolution)의 정확한 동역학과 초기 상태들과 프로세스의 잡음 공분산과 측정 모델 등이 미리 정의되어야만 한다. 실제로, 대상체의 전개에 관한 사전 정보가 알려져 있지 않다면 random-walk 모델이 종종 사용된다. 어떤 경우에 있어서는, 등속도와 등가속도와 같은

Kinematic 모델이 사용된다. 잡음 공분산의 값들은 경험상 설정되거나, 수동으로 조절되는데, 이는 파라미터 추정에 있어서 확장 칼만 필터(EKF)의 주요 단점이다. 실제 상황에서 전개의 동역학은 복잡하고 미리 경계의 전개를 모델링 하는 것은 어렵다. 또한, 프로세스 잡음은 표적의 동역학과 주변 환경에 좌우된다. 모델 파라미터들을 결정함에 있어서 불확실성이 존재하는 상황에서 칼만-형태의 필터들의 추정 성능은 영향을 받는다. 따라서 본 연구에서는, 폐경계와 개경계를 추정함에 있어서 모델의 불확실성을 줄이기 위해 역문제 알고리즘으로서 기대치-최대화(EM) 알고리즘을 적용한다. EM 은 경계 추정을 위해 칼만 스무더(smoother)를 사용한다. 모델 파라미터들(상태 전개 행렬, 잡음 공분산 행렬, 초기 상태)은 기대치 단계와 최대화 단계를 통해 추정된다. EM 을 사용하는 장점으로는, 우도함수(log-likelihood function)를 항상 증가시키려 하고 그렇게 함으로써 수렴을 보장해 준다. 본 연구에서는, 경계 추정에 대해 다음의 두 가지 응용분야에 EM 을 적용하였다. 하나(폐경계)는 유동 과정에서 공동(void)들의 추정 문제를 수반하는 반면에, 다른 하나(개경계)는 서로 혼합되지 않는 두 유체 사이의 움직이는 표면 경계를 추정하는 것이다. 위 두 응용에 대해 수치적 연구와 실험적 연구가 수행되었고, 추정 성능은 EKF 와 비교하였다. 전형적인 EKF 와 비교해서, EM 이 경계(위치, 모양, 크기)에서의 동적 변화에 대해 더 나은 추정성능을 보여 주고 있다.

동적 변화에 대해 더 나은 추정성능을 보여 주고 있다.

1. Introduction

1.1 Electrical impedance tomography

Tomography is defined as the technology to view the cross sectional image of the domain. Through the tomogram the inner details of the domain can be investigated. There are several tomography techniques developed based on application of different energy source and applied in different applications. Electrical impedance tomography (EIT) is one such imaging technology which involves use of electrical quantities as energy source. In EIT, electrical current or voltage is passed across the electrodes placed around the object to be imaged and the resulting excitations caused due to the presence of the medium inside the domain are measured on the surface of the electrode. Based on the current-voltage relationship, internal distribution inside the object is reconstructed. Schematic diagram which explains the principle of EIT is shown in figure 1.1. EIT comes under soft field imaging techniques as the electrical quantities are dispersed inside the object and are effected by the inside objects. Thus EIT has lower spatial resolution. The main advantage with EIT technology is that it is very cheap, portable and safe. Apart from that, EIT has high-speed data acquisition system thus has high temporal characteristics.

EIT has been applied to numerous fields in medicine, industry and geophysical applications. Medical applications using EIT include detection and classification of tumors from breast tissue (Muller *et al*. 1999, Osterman *et al*. 2000), studying gastric function (Smallwood *et al*. 1994, Dijkstra *et al*. 1993, Brown *et al*. 1985, Smallwood *et al*. 1992), pulmonary ventilation, perfusion, and hyperthermia (Cheney *et al*. 1999, Leathard *et al*. 1994, Newell *et al*. 1996). EIT has been applied to clinical applications such as lung imaging (Brown 2001, Mueller *et al*. 2001), head imaging (Holder 1992) and breast imaging (Cherepenin *et al*. 2001, Cherepenin *et al*. 2002, Kerner *et al*. 2002(a), Kerner *et al*. 2002(b), Osterman *et al*. 2000). In industry, EIT has been used to monitor flow processes, mixing in pipes, multiphase flows and non destructive testing (Dickin and Wang 1996, Pinheiro *et al*. 1997, Mann *et al*. 1997,

Jones *et al*. 1993, Friedman and Vogelius 1989). In regard of the application of EIT to geophysics, resistivity imaging is widely used in exploring mineral resources, ground water, detection of faults, fractures, contaminant plumes, waste dumps, geological mapping, geotechnical and environmental applications (Maillol *et al*. 1999; Barker *et al*. 1998; Daily *et al*. 1992; Spies *et al*. 1995; Hou *et al*. 2008; Daily *et al*. 1998; Reynolds *et al*. 1996; Casas *et al*. 2008; Meads *et al*. 2003).

The physical relationship between the injected currents and the measured boundary voltages is governed by a partial differential equations derived from Maxwell equations. There are many physical models that can be considered. Continum, average-gap, shunt and complete electrode model (CEM) are the most popular. CEM takes care of the discreteness, shunting, contact impedance between the electrode and the outer boundary of the object. The performance of CEM is better as compared to others as it is close to the real situation. Image reconstruction with EIT is computed using forward and inverse problem. In forward problem, given the conductivity distribution inside the domain and the injected currents we calculate the boundary voltages on the electrode surface. In inverse problem, with the measured voltage and current data, the internal conductivity distribution is estimated. Analytical solution of Laplace equation is only possible for simple regular geometries. Analytical solution for a homogeneous cube based on the average-gap electrode model was derived in (Choi *et al*. 2004). In Kim *et al*. (2007a), analytical model with complete electrode model was presented. For complex geometry, it is difficult to obtain analytical solution therefore numerical methods are used instead. Numerical method which has been widely studied for the EIT problem is the finite-element method (FEM) (Jain *et al*. 1997, Polydorides and Lionheart 2002). Another numerical method which has been used for solving Laplace equation in the interior of the volume with appropriate boundary conditions is the boundary element method (BEM) (also known as the boundary integral method) (Cartwright *et al*. 2001). Inverse problem in EIT is to estimate the internal conductivity distribution based on measured voltages on the surface of the object. Inverse problem in EIT is highly nonlinear and ill-posed. Ill-posedness is because voltage has a weak relation with respect to conductivity distribution i.e. small change in voltage measurements result in large change in conductivity distribution. Regularization methods which consider

the prior information of initial conductivity distribution inside and the knowledge of the measurement noise covariance are helpful in mitigating the effect of ill-posedness. Spatial resolution in EIT is not good due to ill-posedness. However, EIT has high temporal resolution so it has better performance for fast transient processes.

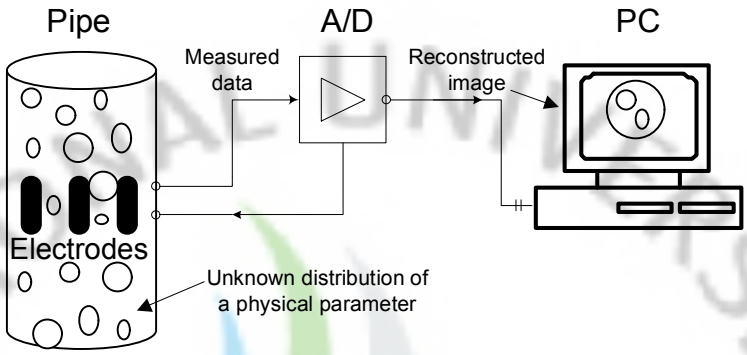

Figure 1.1. Schematic diagram which explains the principle of EIT.

Image reconstruction in EIT is classified as static and dynamic imaging. In static imaging, the properties inside the object or domain remain constant within the time to obtain the complete set of independent measurements. In dynamic imaging, the properties of the medium inside the domain changes before acquiring complete set of measurements. If the properties of the medium are changing rapidly then the conventional methods of static imaging do not give desirable results. In these dynamic approaches, the temporal resolution can be improved by a factor of p (p is the number of current patterns in a conventional frame). Analysis of current patterns to find the optimal current patterns is necessary in case of dynamic scenarios. Optimal current patterns can be determined by evaluating the norm and power distinguishabilities (Isaacson 1986, Gisser *et al.* 1988, Newell *et al.* 1988). State-space model is used to represent the dynamic problems and the problem is treated as state estimation problem and the time varying state is estimated using a suitable reconstruction method. Kalman type filters are the most popular algorithms used in tracking the dynamic changes.

1.2 Phase boundary estimation

In industrial applications we often come across flows in pipelines involving mixture of fluids. In mechanical systems such as condensers, evaporators and combustion systems we come across liquid-gas or liquid-vapor mixtures (Holand and Bragg 1995, Perry *et al.* 1997). Few applications involve transportation of slurry composed of solid particles in a liquid from one place to other. Liquid-liquid mixtures are seen in emulsions as well as a combination of two immiscible liquids. It is of interest to determine the phase boundaries in the flow process. Phase distribution of the flow field helps us to know about the hydrodynamics and heat transfer between the fluids. Void fraction which is one of the key flow parameters can be determined by estimating the phase boundaries. Visualization of these flow processes and phase boundaries without disturbing the flow field is necessary to determine flow parameters which can be used in monitoring and designing the mechanical systems.

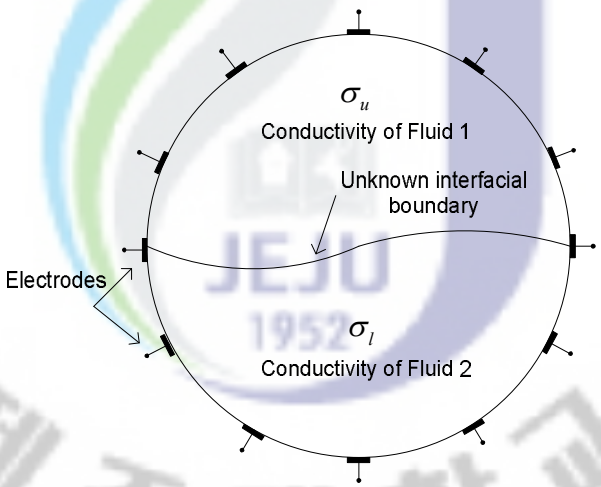

Figure 1.2. Estimation of unknown boundary surface in flow field using EIT.

There are several tomography techniques applied to visualize two-phase flows with noninvasive and nonintrusive characteristics. For example, gamma densitometry (Shollenberger *et al.* 1997), ultrasonic imaging (Xu *et al.* 1997) and nuclear magnetic resonance imaging (Gladden and Alexander, 1996) are used to visualize the flow processes. The techniques such as gamma densitometry are hazardous to health and also expensive. Ultrasound imaging involves usage of transducers as energy source

which are expensive and the data acquisition rate is not so fast. Changes in flow field are relatively fast and therefore we need a technique which is relatively cheap, portable and has a high data acquisition rate. Electrical impedance tomography can be a promising method to measure the phase boundary due to its non-intrusive characteristics and high temporal resolution. The data acquisition is very fast in electrical impedance tomography therefore it can be used for fast transient processes like two-phase flows. Electrodes are attached around the pipe in the region of interest and electrical currents are applied across the electrodes and the voltages are measured. With the voltage data the inner phase distribution can be reconstructed using inverse algorithm. In flow process such as two-phase flow, the knowledge of conductivities of the fluids can be known *a priori*. The prior information can be used in the inverse algorithm to estimate the boundary size, shape and location. The process of estimating the boundary rather than conductivities from the measured voltages is known as phase boundary estimation problem.

Phase boundary estimation can be classified into two types based on the topology of the boundary to be estimated. First is the closed boundary problem where the flow region is composed discrete region boundaries of different conductivities to that of background (figure 1.1). These problems are observed in two-phase flows in the condensers or heat exchangers when the pressure of the liquid becomes less than the vapor pressure resulting in voids or bubbles. The other is the open boundary problem where the flow region is separated into two regions separated by interfacial boundary (figure 1.2). Open boundary problems can be observed in case of flow of two immiscible liquids for example liquid hydrocarbons transported in pipelines over a long distance in petroleum industry. Crude oil transported in pipelines often contains free water and the interfacial boundary is useful to analyze the amount of the water present in the mixture (Fairuzov 2000).

1.3 Related work for boundary estimation in EIT

Various researchers have developed different methods to estimate the phase boundary using EIT. In context of closed boundary problem, Han *et al*. (1999) considered shape decomposition based on boundary element method where the

boundary of each target was represented in terms of Fourier series. Using the boundary data, Kolehmainen *et al*. (1999) recovered the region boundaries of piece-wise constants of an elliptic partial differential equation (PDE) for an application to optical tomography (OT) which is similar to EIT. Efficient method to estimate the Fourier coefficients was the main focus therefore there were many methods introduced in that perspective. Multi-layered neural network (MNN) was used to estimate the Fourier coefficients in Jeon *et al.*(2005) as it is conceptually simple, easier in implementation and the principal advantage is that it does not require computation of Jacobian matrix. Kim *et al*. (2007b) proposed the use of front points in polar coordinates to represent closed boundary because the higher modes of Fourier series are necessary to represent a complex shape and these higher modes are more sensitive to noise. Boundary detection could also be considered using the well-known level set methods. The level set method was first proposed by Osher *et al*. (1988) for tracing interfaces between different phases of fluid flows. Rondi *et al.* (2001) applied and analyzed phase-filled methods to the reconstruction of piecewise constant conductivities in EIT. Although, level set method was initially introduced for tracking propagating boundaries, they are generally used for tracking static interfaces for the reason that they are slow. Therefore, it is desirable to have a cost-effective inverse algorithm which not only tracks dynamic interfaces, but can also handle higher level of noise in the measurement and requires less measurement data. Therefore, the Kalman-type reconstruction algorithms serve this purpose as they are modeled on a Markov chain and traditionally built on linear operators perturbed by Gaussian noise. Since, image reconstruction in EIT is a nonlinear problem, therefore, the nonlinear version of Kalman-type filters should be considered. In that perspective, Kim *et al.* (2004) used interactive multiple model (IMM) to estimate the Fourier coefficients by considering multiple extended Kalman filter (EKF) each working on different measurement noise model. The problem with EKF is that it can only be used with Gaussian assumption. It is only accurate up to second order for Gaussian distribution. Also, the linearization in EKF is possible only if the Jacobian matrix exists. To overcome the difficulties with EKF, the unscented transform (UT) which was developed by Julier and Uhlmann (1997) and subsequently in Julier and Uhlmann (2004) as a method to propagate mean and covariance information through

a nonlinear transformation is used to estimate Fourier coefficients. It is more accurate, easier to implement, and uses the same order of calculations as EKF. Unscented Kalman filter (UKF) is applied in Ijaz *et al*. (2008) to estimate the Fourier series and it is shown that UKF has better performance than EKF.

In context of open boundary problems, Butler and Bonnecaze (2000), an open channel filled with conducting liquid was considered and electrodes are placed at the bottom of the channel and the EIT data is obtained through a array of the electrodes. The boundary was parameterized with Chebyshev polynomials, whose coefficients are the unknown to be estimated. In Tossavainen *et al.* (2004), pipe which is partially filled with water and has a void region of zero conductivity is considered and the boundary is parameterized using Bezier curve. The endpoints of the boundary are fixed in this case which is undesirable. An improved method for the free surface and admitttivity distribution was given in Tossavainen *et al.* (2006) where the boundary is restricted within the domain. Kim *et al*.(2007b) represented the interfacial boundary between immiscible liquids using front points and EKF is used to track the time varying interfacial boundary. EKF is suboptimal nonlinear filter and has linearization error also it needs the computation of Jacobian therefore UKF is introduced in Ijaz *et al.* 2008 to track front points and the performance is compared with EKF.

1.4 Expectation maximization algorithm

Dynamic phase boundary estimation is achieved by representing the problem as state estimation problem. The state space model consists of linear state equation which describes the evolution of state parameters with time. Measurement equation with EIT is represented as nonlinear. To solve the non-linear set of equations Kalman type filters such as EKF and UKF are generally applied (Bar-Shalom and Li 1993, Khambampati *et al*. 2009, Julier and Uhlmann 2004). In the implementation of Kalman type filters it is assumed that the knowledge of state transition matrix, initial states, process and measurement noise covariance matrices are predefined. In many situations, there can be uncertainty in the model parameters or difficult to obtain. In EIT we do not have any information regarding the evolution of the boundary

therefore random-walk model is adopted. Kinematic models (Bar-Shalom and Li 1993, Li 1997) can be used if we assume the boundary is moving with constant velocity or acceleration. In a real time situation this is not the case, as the motion of boundary is complicated and it is difficult to model as a prior form. Also the values for noise matrices, process noise depends on the motion of boundary and the environment surrounding. The performance of EKF largely depends on the values of the model parameters. These model parameters can be estimated using three methods. One method is using classical method where we treat the model parameters also as state parameters and are augmented with the state vector and estimated. The other method involves using multiple models like IMM (Mazor *et al*. 1996, Li and Zhang 1996). The third method is to use join estimation method. Expected Maximization algorithm belongs to third category. EM algorithm is a kind of maximum likelihood estimator which estimates the state variables and model parameters by minimizing the likelihood function. It is formulated such that it always increases the log-likelihood therefore the convergence is guaranteed (Wu *et al*. 1981). EM contains two steps, E and M step. Using the two steps iteratively the model parameters are estimated. EM algorithm is applied in many applications areas ranging from medicine (Jiang 1994), signal processing (Shepp and Yardi 1982), statistics (Little and Rubin 1983), pattern recognition (Byrne 1992), time-delay estimation (Antoniadis and Hero 1994) to name a few.

1.5 Aims and contents of the thesis

The purpose of this thesis is to develop novel dynamic reconstruction technique for estimating phase boundary using EIT. The boundary estimation is done for two cases, closed boundary and open boundary. Closed boundary involves estimation of voids in the flow process. Open boundary is to estimate the interfacial boundary between the two immiscible fluids. The Expectation maximization algorithm is used as an inverse algorithm to reduce model uncertainties in estimating the closed and open boundaries. All the examples considered in this thesis are using two-dimensional (2D) and the three-dimension (3D) extension of these problems is pretty straight forward.

EM algorithm is formulated for boundary estimation using EIT. The model parameters are estimated using E and M steps. The advantage of the EM algorithm is that it always tries to increase the likelihood function thereby guaranteeing the convergence. The two steps are iterated until the convergence of the model parameters is attained. The proposed algorithm is tested with numerical and experiment data.

This thesis contains five chapters. Chapter 1 gives a brief introduction about EIT, its applications and methodology. It also presents the idea of boundary estimation using the prior information of phase distribution and its classification and applications where it can be used. The related work done with regard to closed and open boundary is presented and an overview of the thesis is given.

Chapter 2 deals with the mathematical models used in solving EIT problem. Complete electrode model which is used as the physical model in the thesis is explained. Finite element formulation based on CEM is explained briefly. Various data collection methods used in EIT is discussed and Jacobian is formulated for change in conductivity with voltage. The forward solution and Jacobian are necessary in the implementation of inverse algorithm.

In chapter 3, the dynamic image reconstruction methods are studied. State estimation formulation is presented. Methods to solve the state estimation problem using Kalman-type filters are discussed. Linearized Kalman filter (LKF) and Extended Kalman filter (EKF) are derived in the view of solving the inverse problem using EIT. Smoothening of the estimates considering the future measurements gives a better estimation performance. In Kalman smoothers, fixed interval Kalman filter (RTS smoother) is derived which is used in the EM algorithm for calculating the expectation of hidden variables. Maximum likelihood estimation (ML) which involves the estimation of model parameters is explained. The EM algorithm, which is the main focus of this thesis, is derived based on Kalman smoother.

Chapter 4 and 5 present the core part of the thesis. Two applications are described, one for closed boundary and the other for open boundary. Chapter 4 deals with the estimation of voids in flow process which is an application to closed boundary problem. Representation of smooth closed boundary using Fourier series is presented. State-estimation model and Jacobian are devised to solve the inverse

problem. EM is formulated for closed boundary estimation using EIT. The performance of the EM is tested using numerical and experimental studies and the performance is compared against the EKF. The results are then analyzed and discussed.

Chapter 5 is about estimation of interfacial boundary between two immiscible liquids. Boundary representation of open boundary using front points is described. The Jacobian has been formulated for the front point implementation. EM algorithm for front point estimation is discussed and it is tested with numerical and experimental data. Finally, reconstructed results with EM are compared against EKF.

Finally, in chapter 6 the conclusions of the thesis is given and future work is envisaged.

2. Forward problem

EIT reconstruction problem can be summarized into two steps, forward problem and inverse problem. In forward problem, the voltages are computed inside the domain Ω and on the electrode surface $\partial\Omega$ with the given current injection and known conductivity distribution. In inverse problem, using a set of voltage measurements and the currents the internal properties are reconstructed. To derive the forward problem in EIT we should first construct a physical model (mathematical model) to describe the problem. The equations which relate the currents, voltage measurements and conductivity distribution have to be modeled. The physical model for EIT can be derived through Maxwell equations of electromagnetism (Nunez 1981, Isaacson and Cheney 1990, Malmivuo and Plonsey 1995, Doerstling 1995). The governing equation which describes the potential distribution of the domain and the boundary conditions necessary to solve the governing equation are discussed. Among all the physical models, CEM is considered to be efficient and accurate compared to other models (Cheng *et al.* 1989, Sommersalo *et al.* 1992). In this study in solving the boundary estimation problem we use the CEM as a physical model. In this chapter various physical models used in the EIT are described. The forward problem for CEM is formulated using finite element method (FEM). Various data collection methods are discussed and Jacobian is derived.

2.1 Background

The electromagnetic field in the domain $\Omega \in \Re^2$ can be described using the Maxwell's equation (Somersalo *et al.* 1992, Ola *et al.* 1993)

$$\nabla \times E = -\frac{\partial B}{\partial t} \tag{2.1}$$

$$\nabla \times H = J + \frac{\partial D}{\partial t}, \tag{2.2}$$

such that E is the electric field, H magnetic field, D electric displacement, B magnetic induction, and J current density.

Assuming that the domain Ω consists of linear and isotropic medium, following holds true

$$D = \varepsilon E \tag{2.3}$$
$$B = \mu H \tag{2.4}$$
$$J = \sigma E, \tag{2.5}$$

where ε is permittivity, μ permeability, and σ conductivity of the medium. Assuming that the injected currents are time harmonic with frequency ω, we get

$$E = \tilde{E}e^{i\omega t} \tag{2.6}$$
$$B = \tilde{B}e^{i\omega t}. \tag{2.7}$$

Solving equations (2.1) and (2.2) using equations (2.3) to (2.7), we get

$$\nabla \times E = -\frac{\partial B}{\partial t} = -\frac{\partial(\tilde{B}e^{i\omega t})}{\partial t}$$
$$= -iw\tilde{B}e^{i\omega t} - \frac{e^{i\omega t}\partial(\tilde{B})}{\partial t} = -i\omega\mu H - \frac{e^{i\omega t}\partial(\tilde{B})}{\partial t}$$
$$\nabla \times H = J + \frac{\partial D}{\partial t} = J + \frac{\partial(\varepsilon E)}{\partial t} = J + \frac{\varepsilon\partial(\tilde{E}e^{i\omega t})}{\partial t}$$
$$= J + i\omega\varepsilon\tilde{E}e^{i\omega t} + \frac{\varepsilon e^{i\omega t}\partial(\tilde{E})}{\partial t} = J + i\omega\varepsilon E + \frac{\varepsilon e^{i\omega t}\partial(\tilde{E})}{\partial t}.$$

The current density J can be separated into two components ohmic current ($J^0 = \sigma E$) and current source (J^s). Putting the value of J and canceling out the oscillatory exponential terms, we get the following simplified Maxwell equations (Somersalo *et al*. 1992, Ola *et al*. 1993, Doerstling 1995)

$$\nabla \times E = -i\omega\mu H \tag{2.8}$$
$$\nabla \times H = (\sigma + i\omega\varepsilon)E + J^s. \tag{2.9}$$

Now the electric field, E, can be derived as

$$E = -\nabla u - \frac{\partial A}{\partial t}, \tag{2.10}$$

where u is electric potential and A magnetic vector potential.

In EIT, we assume static conditions, which mean that the effect of magnetic induction which produces an induced electric field is neglected. The second assumption we make is that the capacitive effects $i\omega\varepsilon E$ in (2.9) can be neglected (Barber and Brown 1984, Baker 1989). Using these assumptions, the above equations can be simplified as

$$E = -\nabla u \tag{2.11}$$

$$\nabla \times H = \sigma E + J^s. \tag{2.12}$$

Taking the divergence on both sides of (2.12), putting the value of (2.11) into (2.12), and also because $J^s = 0$ in the given frequency range in EIT, we get

$$\nabla \cdot (\nabla \sigma u) = 0, \tag{2.13}$$

where $u = u(x,y)$, for $x,y \in \Omega$. The equation (2.13) serves as the governing equation for EIT. Now we need to have a set of boundary conditions to solve this equation. A number of different boundary conditions, usually referred to as physical models in EIT, are presented the next subsection.

2.2 Physical models in EIT

2.2.1 Continuum model

This is the most basic physical model. It assumes the entire surface is a conductor with no specific electrodes attached to the surface, with j as a continuous source current

$$j(\xi) = C\cos(k\xi), \tag{2.14}$$

where C is a constant. There is, however, up to a 25% (resistivity) estimation error using this model due to the fact that the effect of electrodes is not considered here (Cheng *et al*. 1989, Sommersalo *et al*. 1992).

2.2.2 Gap model

In this model, it is assumed that the current density is constant over electrodes while it is assumed to be zero between the electrodes

$$j = \begin{cases} \dfrac{I_l}{|e_l|} & x \in e_l, \ \ l = 1, 2, ...L \\ 0 & x \in \partial\Omega \setminus \bigcup_{l=1}^{L} e_l, \end{cases} \tag{2.15}$$

where $|e_l|$ is the area of the *l*th electrode, I_l is the current applied to the *l*th electrode e_l, and L is the number of electrodes.

2.2.3 Average-gap model

The average-gap model is based upon the same boundary conditions as the gap model. The main difference between the two models is that the gap model considers the voltage values measured at the centre of each electrode whereas the average-gap model considers the average value of potential at each electrode. Since both the gap and average-gap models ignore the shunting effect as well as the contact impedance of the electrodes, they still overestimate the resistivity distribution inside the body (Somersalo *et al*. 1992).

2.2.4 Shunt model

As the name implies, this model takes into account the shunting effect of the electrode. This means that the potential on the electrode is assumed to be constant. The boundary condition, in this case, will be as follows

$$\int_{e_l} \sigma \frac{\partial u}{\partial \upsilon} dS = I_l \,,\ (x,y) \in e_l \,,\ l = 1,2,\cdots,L, \tag{2.16}$$

where the shunting effect is compensated by introducing the following condition

$$u = U_l \,,\ (x,y) \in e_l \,,\ l = 1,2,\cdots,L, \tag{2.17}$$

where U_l is the measured voltage on the lth electrode. Also, υ in (2.16) is the outward normal unit vector on the surface $\partial\Omega$. Since the contact impedances are still ignored in this model, it underestimates the resistivity distribution.

2.2.5 Complete electrode model (CEM)

The complete electrode model (CEM) considers both the shunting effect as well as the contact impedance between the electrodes and the surface of the body. This model consists of the following boundary conditions

$$\int_{e_l} \sigma \frac{\partial u}{\partial \upsilon} dS = I_l \,,\ (x,y) \in e_l \,,\ l = 1,2,\cdots,L \tag{2.18}$$

$$\sigma \frac{\partial u}{\partial \upsilon} = 0 \,,\ (x,y) \in \partial\Omega \setminus \bigcup_{l=1}^{L} e_l . \tag{2.19}$$

The total current applied through electrodes attached on the boundary of the object is given by (2.18) and (2.19) is the insulated condition where there is no current applied other than at the electrode surface.

Apart from (2.18) and (2.19) we have additional condition which considers the contact impedance between the electrode and electrolyte inside the domain

$$u + z_l \sigma \frac{\partial u}{\partial \upsilon} = U_l \,,\ (x,y) \in e_l \,,\ \ l = 1,2,\cdots,L, \tag{2.20}$$

where z_l is the effective contact impedance. The CEM (2.18-2.20) has better approximation of the boundary voltages when compared to average-gap model or

shunt model. Also, to ensure the existence and uniqueness of the solution, we impose the following conditions (Somersalo *et al*. 1992)

$$\sum_{l=1}^{L} I_l = 0 \quad \text{and} \quad \sum_{l=1}^{L} U_l = 0 . \tag{2.21}$$

2.3 Finite element method formulation of EIT

In the FEM implementation of above problem, the object Ω is discretized into small triangular elements. We assume that the resistivity is uniform within each element. If N is the number of nodes in the finite element mesh, the potential distribution u within the object is approximated as

$$u \approx u^h (x, y) = \sum_{i=1}^{N} \alpha_i \varphi_i (x, y), \tag{2.22}$$

and the potential on the electrodes is represented as

$$U^h = \sum_{j=1}^{L-1} \beta_j \mathbf{n}_j , \tag{2.23}$$

where

ϕ_i = two-dimensional first-order basis function,
$\mathbf{n}_1 = (1, -1, 0, \cdots, 0)^{\mathrm{T}}$ and
$\mathbf{n}_2 = (1, 0, -1, 0, \cdots, 0)^{\mathrm{T}} \in \Re^L$

are the bases for the measurements. α_i and β_i are the coefficients to be determined. The finite element formulation gives the following system of linear equations

$$\mathbf{Ab} = \tilde{\mathbf{I}}, \tag{2.24}$$

where

$$\mathbf{A} = \begin{pmatrix} \mathbf{B} & \mathbf{C} \\ \mathbf{C}^T & \mathbf{D} \end{pmatrix}, \qquad \mathbf{b} = \begin{pmatrix} \boldsymbol{\alpha} \\ \boldsymbol{\beta} \end{pmatrix} \quad \text{and} \quad \tilde{\mathbf{I}} = \begin{pmatrix} \mathbf{0} \\ \boldsymbol{\zeta} \end{pmatrix} \tag{2.25}$$

$$\boldsymbol{\alpha} = (\alpha_1, \alpha_2, \cdots, \alpha_N)^{\mathrm{T}} \in \Re^N,$$
$$\boldsymbol{\beta} = (\beta_1, \beta_2, \cdots, \beta_{L-1})^{\mathrm{T}} \in \Re^{L-1},$$
$$\mathbf{0} \in \Re^N, \text{ and}$$
$$\boldsymbol{\zeta} = (I_1 - I_2, I_1 - I_3, \cdots, I_1 - I_L)^{\mathrm{T}} \in \Re^{L-1}.$$

and the stiffness matrix $\mathbf{A}$ is of the form

$$\mathbf{B}(i,j) = \int_\Omega \sigma \nabla \varphi_i \cdot \nabla \varphi_j d\Omega + \sum_{\ell=1}^{L} \frac{1}{z_\ell} \int_{e_l} \varphi_i \varphi_j dS, \quad i,j = 1,2,\cdots,N \tag{2.26}$$

$$\mathbf{C}(i,j) = -\frac{1}{z_1} \int_{e_1} \varphi_i dS + \frac{1}{z_{j+1}} \int_{e_{j+1}} \varphi_i dS, \quad i = 1,2,\cdots,N, \quad j = 1,2,\cdots,L-1 \tag{2.27}$$

$$\mathbf{D}(i,j) = \begin{cases} \dfrac{|e_1|}{z_1} & i \neq j \\ \dfrac{|e_1|}{z_1} + \dfrac{|e_{j+1}|}{z_{j+1}} & i = j \end{cases}, \quad i,j = 1,2,\cdots,L-1, \tag{2.28}$$

where $|e_j|$ is the area of the electrode j.

In some cases, the voltages are measured only at some selected electrodes, not every electrode. Also, the selected electrodes may be different at each current pattern. The measured voltages at the measurement electrodes $\hat{\mathbf{U}}$ can be obtained as

$$\hat{\mathbf{U}} = \mathbf{M}^{\mathrm{T}} \mathbf{U}^h = \mathbf{M}^{\mathrm{T}} \mathbf{N} \boldsymbol{\beta} \in \Re^{E \times P}, \tag{2.29}$$

where, E is the number of the measurement electrodes, P is the number of current patterns and $\mathbf{M} \in \Re^{L \times E}$ is the measurement matrix. Furthermore, $\mathbf{U}^h$ can be extracted directly from $\mathbf{b}$ by introducing the extended mapping matrix $\tilde{\mathbf{N}}$

$$\tilde{\mathbf{N}} = (\mathbf{0}, \mathbf{N}) \in \Re^{L \times (N+L-1)} \text{ and } \mathbf{U}^h = \tilde{\mathbf{N}} \mathbf{b}, \tag{2.30}$$

where $\mathbf{0} \in \Re^{L \times N}$. Therefore, we have

$$\hat{\mathbf{U}} = \mathbf{M}^{\mathrm{T}}\mathbf{U}^{h} = \mathbf{M}^{\mathrm{T}}\tilde{\mathbf{N}}\mathbf{b} = \tilde{\mathbf{M}}\mathbf{b}, \tag{2.31}$$

where the extended measurement matrix is defined as

$$\tilde{\mathbf{M}} = \mathbf{M}^{\mathrm{T}}\tilde{\mathbf{N}} \in \Re^{E\times(N+L-1)}. \tag{2.32}$$

2.4 Current injection methods

To estimate the conductivity distribution inside the domain, the currents are applied through the electrodes and the voltages are measured. Current injection mechanism can affect the performance as the sensitivity is different for each case. Various methods have been proposed for the current injection (Webster *et al*. 1990, Isaacson 1986, Cheney and Isaacson 1992, Cheng *et al*. 1988) and also the methods to obtain the optimal current patterns (Paulson *et al*. 1992). The most common current injection protocols used in EIT are the adjacent method, the opposite method, the cross method and the trigonometric method.

In static EIT, all the independent current patterns are injected to reconstruct a single frame of image and the number of independent current patterns is determined by the current pattern and the number of electrodes. However, when the conductivity distribution inside the body changes rapidly we use the so-called *dynamic imaging techniques.* Recalling that in the dynamic EIT only one current injection is allowed for each image reconstruction, each current pattern comprising a current injection protocol can be an independent current pattern. For example, in the trigonometric pattern, each mode of cosine and sine pattern can be an independent pattern. Hence, variety of current patterns is possible in the dynamic EIT. The minimum number of current patterns required to get an optimal solution in a dynamic scenario can be achieved by the analysis of different current patterns. Isaacson (1986) investigated the optimal current pattern in a two-dimensional cylindrical object with concentric inhomogeneity and showed that the trigonometric pattern is optimal to distinguish a central concentric inhomogeneity inside an otherwise homogeneous circular conductor when the L_2 norm of the current is kept constant. However, if the total

injected current is kept constant, Köksal and Eyüboğlu (1995) found that the opposite method gives the best distinguishability. Kim *et al*. (2005) reported a qualitative comparison of the reconstructed dynamic images obtained with various current patterns. The comparison shows that the trigonometric and the opposite methods generate the best reconstructed images.

Gisser *et al.* (1988) compared the distinguishabilities by using adjacent, opposite and performed a distinguishability analysis by injecting trigonometric (cosine), opposite and adjacent current patterns into a circular phantom with no circular inhomogeneity inside, and demonstrated that cosine pattern with the maximum magnitude which is equal to the magnitude of either adjacent or the opposite current pattern is the optimal current pattern. Similarly, Newell *et al.* (1988) showed that cosine current patterns perform better than the opposite and adjacent current patterns to distinguish the smaller inhomogeneities. In general, if the sum of the amplitude of the injected currents is constant, opposite current pattern is optimal current patterns Vauhkonen (1997, 1998) developed many dynamic estimation techniques by considering the inverse problem to be a nonlinear state estimation problem and estimating the time-varying state using the linearized Kalman filter (LKF).

As for the trigonometric pattern, only the first modes are considered because the higher modes tend to deteriorate the reconstruction performance (Kim *et al*. 2005). To explain the current pattern used in this work it would be helpful to illustrate the configuration of the electrodes attached on a circular object (see figure 2.1). With a 16-electrode system, the injected current of the *l*th electrode, I_l, for the cosine and the sine patterns are defined as

$$I_l = \begin{cases} I_0 \cos(2\pi l / 16) \\ I_0 \sin(2\pi l / 16) \end{cases} \quad l = 1, 2, \cdots, 16. \tag{2.33}$$

While injecting the designed currents, the induced voltages at the electrodes, V_l , are measured.

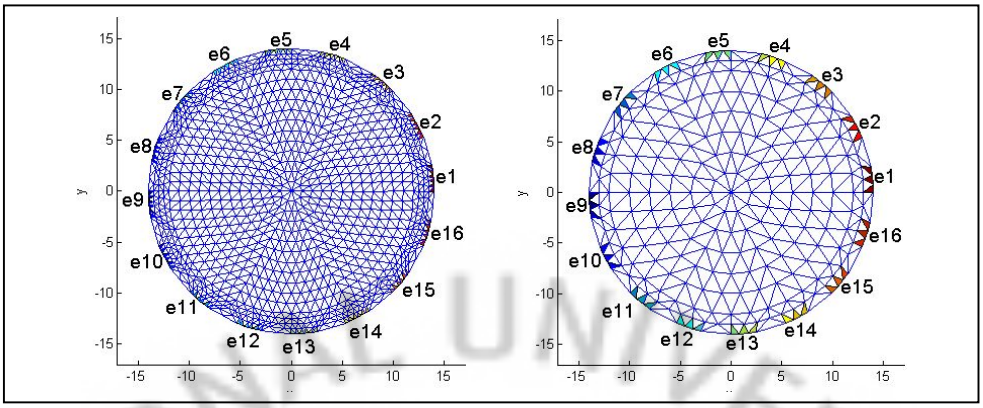

Figure 2.1. Electrode configurations and mesh structure.

In the opposite pattern, a pair of electrodes is selected to inject the predetermined current and to discharge the same amount of current while other electrodes are remained insulated. The basic mode chooses an electrode pair (e_1, e_9) and the current pattern will be ($I_1 = I_0$, $I_9 = -I_0$). It should be noted that the boundary voltages are measured only at the insulated electrodes.

2.5 Jacobian

The rate of change of potential with respect to the conductivity is popularly known as Jacobian and the resulting matrix is defined as the Jacobian matrix. Jacobian determines how sensitive the measurements are with respect to change of the resistivity inside the domain (Yorkey and Webster 1987).

If the measurement matrix $\mathbf{M} \in \Re^{L \times E}$ is used the voltages on the electrodes can be given by (2.32). The Jacobian can be written as

$$J = \frac{d\hat{\mathbf{U}}}{d\rho_n} = \frac{d(\tilde{\mathbf{M}}\mathbf{b})}{d\rho_n} = \tilde{\mathbf{M}} \frac{dA^{-1}}{d\rho_n} \tilde{\mathrm{I}}, \tag{2.34}$$

where n is the column of Jacobian matrix.

If the pseudo-resistance matrix is defined as

$$\tilde{\mathbf{R}} = \mathbf{A}^{-1}\tilde{\mathbf{M}}^{\mathrm{T}} \in \Re^{(N+L-1)\times E} \quad \text{or} \quad \mathbf{A}\tilde{\mathbf{R}} = \tilde{\mathbf{M}}^{\mathrm{T}}. \tag{2.35}$$

The pseudo-resistance matrix can be easily obtained by the solution of the system equation as given below

$$\mathbf{A}\begin{pmatrix}\tilde{\mathbf{R}} & \mathbf{b}\end{pmatrix} = \begin{pmatrix}\tilde{\mathbf{M}}^{\mathrm{T}} & \tilde{\mathbf{I}}\end{pmatrix}. \tag{2.36}$$

Using (2.32) and (2.25) the above equation can be written as

$$\mathbf{A}\begin{pmatrix}\tilde{\mathbf{R}}_1 & \boldsymbol{\alpha} \\ \tilde{\mathbf{R}}_2 & \boldsymbol{\beta}\end{pmatrix} = \begin{pmatrix}\mathbf{0} & \mathbf{0} \\ \mathbf{N}^{\mathrm{T}}\mathbf{M} & \mathbf{N}^{\mathrm{T}}\hat{\mathbf{I}}\end{pmatrix}, \tag{2.37}$$

where

$$\tilde{\mathbf{R}}_1 = \tilde{\mathbf{R}}(1:N,:) \in \Re^{N\times E} \text{ and } \tilde{\mathbf{R}}_2 = \tilde{\mathbf{R}}(N+1:N+L-1,:) \in \Re^{(L-1)\times E}. \tag{2.38}$$

The Jacobian $\partial\hat{\mathbf{U}} / \partial\rho_n$ will be

$$\frac{\partial\hat{\mathbf{U}}}{\partial\rho_n} = \tilde{\mathbf{M}}\mathbf{A}^{-1}\frac{\partial\mathbf{A}}{\partial\rho_n}\mathbf{A}^{-1}\tilde{\mathbf{I}} = \tilde{\mathbf{R}}^{\mathrm{T}}\frac{\partial\mathbf{A}}{\partial\rho_n}\mathbf{b}, \tag{2.39}$$

$(A^{-1})^{\mathrm{T}} = A^{-1}$, this is due to the symmetry of the stiffness matrix $\mathbf{A}$. In $\mathbf{A}$, the matrix $\mathbf{B}$ is the only term dependent on ρ_n and the Jacobian will be

$$\frac{\partial\hat{\mathbf{U}}}{\partial\rho_n} = -\begin{pmatrix}\tilde{\mathbf{R}}_1 \\ \tilde{\mathbf{R}}_2\end{pmatrix}^{\mathrm{T}}\begin{pmatrix}\frac{\partial\mathbf{B}}{\partial\rho_n} & \mathbf{0} \\ \mathbf{0} & \mathbf{0}\end{pmatrix}\begin{pmatrix}\boldsymbol{\alpha} \\ \boldsymbol{\beta}\end{pmatrix} = -\begin{pmatrix}\tilde{\mathbf{R}}_1^{\mathrm{T}} & \tilde{\mathbf{R}}_2^{\mathrm{T}}\end{pmatrix}\begin{pmatrix}\frac{\partial\mathbf{B}}{\partial\rho_n}\boldsymbol{\alpha} \\ \mathbf{0}\end{pmatrix} = -\tilde{\mathbf{R}}_1^{\mathrm{T}}\frac{\partial\mathbf{B}}{\partial\rho_n}\boldsymbol{\alpha}, \tag{2.40}$$

in which the term $\dfrac{\partial\mathbf{B}}{\partial\rho_n}$ can be calculated as

$$\frac{\partial \mathbf{B}(i.j)}{\partial \rho_n} = -\frac{1}{\rho_n^2}\int_{\square_n} \nabla\varphi_i \cdot \nabla\varphi_j . \quad i,j = 1,2,\cdots,N. \tag{2.41}$$

Here, φ_i , φ_j are basis functions and $\square_n$ is the element with which the derivative is computed.

3. Dynamic state estimation

In the inverse problem, the conductivity distribution is estimated based on the injected currents and the measured voltages. Reconstruction algorithms for EIT are generally classified into static and dynamic algorithms. The static algorithms are usually employed for visualization of time-invariant internal conductivity distribution. Those cases which involve fast changes, dynamic algorithms are used (Kim *et al.* 2001, Kim *et al.* 2007a). In the dynamic estimation, the underlying inverse problem is treated as a state estimation problem (Kim *et al*. 2001) which consists of a state equation that models the temporal evolution of the state, and an observation equation that gives the relationship between the state and the boundary voltages. In this chapter, the nonlinear system of equations is solved using the state-space model. For solving the nonlinear system of equations, LKF and EKF are derived to estimate the state variable. These Kalman filters assume predefined model parameters which are difficult to predict in most of the cases. Expectation maximization algorithm (EM) is introduced which reduces the uncertainty in the system by estimating the model parameters. EM algorithm is formulated using the extended Kalman smoother (EKS) approach (Dempster *et al*. 1977, Shaumway and Stoffer 1982, Gaharamani and Beal 1999, Sam and Ghahramani 2001). E step is obtained using EKS (RTS) approach and M step is done by differentiating the log-likelihood function.

3.1 Linearized Kalman filter

We consider the estimation of the state $x \in \Re^n$ of a discrete-time controlled process that is governed by the linear stochastic difference equation

$$x_k = F_{k-1} x_{k-1} + w_{k-1} \tag{3.1}$$

with a measurement $z \in \Re^{\bar{m}}$ that is

$$z_k = H_k x_k + v_k, \tag{3.2}$$

where $F_k \in \Re^{\bar{n}\times\bar{n}}$ is the state transition model and $H_k \in \Re^{\bar{m}\times\bar{n}}$ is the observation model. The random variables $w_k \in \Re^{\bar{n}}$ and $v_k \in \Re^{\bar{m}}$ denote the process and the measurement noise, respectively. They are assumed to be white noises and independent of each other with normal probability distributions

$$p(w_k) \sim N(0, Q_k) \tag{3.3}$$

$$p(v_k) \sim N(0, R_k), \tag{3.4}$$

where $Q_k \in \Re^{\bar{n}\times\bar{n}}$ and $R_k \in \Re^{\bar{m}\times\bar{m}}$ are the process and the measurement noise covariance, respectively.

Our goal is to set a recursive procedure to estimate x_k with the previous states $x_1, \cdots, x_k$ and the measurements $z_1, \cdots, z_k$. Let us define $x_{k|k-1} \in \Re^{\bar{n}}$ to be *a priori* state estimate at step k given knowledge of the process up to step $k-1$, and $x_{k|k} \in \Re^{\bar{n}}$ to be *a posteriori* state estimate at step k given measurement z_k. Then, *a priori* and *a posteriori* estimate errors can be defined as

$$e_{k|k-1} = x_k - x_{k|k-1} \tag{3.5}$$

$$e_{k|k} = x_k - x_{k|k}, \tag{3.6}$$

respectively.

The *a priori* state estimate will be

$$x_{k|k-1} = E[x_k \mid Z_{k-1}] = E[F_{k-1}x_{k-1} + w_k \mid Z_{k-1}] = F_{k-1}x_{k-1|k-1}, \tag{3.7}$$

where

$$Z_k = (z_1, \cdots, z_k)^{\mathrm{T}} \tag{3.8}$$

because of (3.3) and the definition of the *a posteriori* state estimate. The *a posteriori* state estimate is set to be a linear combination of the *a priori* state estimate $x_{k|k-1}$ and a weighted difference between an actual measurement z_k and a measurement prediction $H_k x_{k|k-1}$

$$x_{k|k} = x_{k|k-1} + K_k(z_k - H_k x_{k|k-1}), \tag{3.9}$$

where $K_k \in \Re^{\bar{n}\times\bar{m}}$ is the gain or blending factor. The Kalman filter can be determined by minimizing the *a posteriori* error covariance $P_{k|k}$

$$P_{k|k} = E[e_{k|k}e_{k|k}^{\mathrm{T}} \mid Z_k] = (I - K_k H_k)P_{k|k-1}(I - K_k H_k)^{\mathrm{T}} + K_k R_k K_k^{\mathrm{T}} \tag{3.10}$$

and

$$K_k = P_{k|k-1}H_k^{\mathrm{T}}\left(H_k P_{k|k-1}H_k^{\mathrm{T}} + R_k\right)^{-1}, \tag{3.11}$$

where the *a priori* error covariance $P_{k|k-1}$ is defined as

$$P_{k|k-1} = E[e_{k|k-1}e_{k|k-1}^{\mathrm{T}} \mid Z_{k-1}]. \tag{3.12}$$

In this,

$$\begin{aligned} e_{k|k} &= x_k - x_{k|k} = x_k - x_{k|k-1} - K_k(z_k - H_k x_{k|k-1}) \\ &= e_{k|k-1} - K_k(H_k x_k + v_k - H_k x_{k|k-1}) \\ &= (I - K_k H_k)e_{k|k-1} - K_k v_k \end{aligned}$$

$$\frac{\partial P_{k|k}}{\partial K_k} = \frac{\partial}{\partial K_k}E[e_{k|k}e_{k|k}^{\mathrm{T}} \mid Z_k] = -2(I - K_k H_k)P_{k|k-1}H_k^{\mathrm{T}} + 2K_k R_k = 0,$$

$$K_k(H_k P_{k|k-1}H_k^{\mathrm{T}} + R_k)\varepsilon_k = P_{k|k-1}H_k^{\mathrm{T}}.$$

If the observation model becomes more credible $R_k \to 0$, the gain weights the residual more heavily

$$\lim_{R_k \to 0} K_k = H_k^{-1}. \tag{3.13}$$

On the other hand, as the a priori state estimate becomes more credible $P_{k|k-1} \to 0$, the gain weights the residual less heavily

$$\lim_{C_{k|k-1} \to 0} K_k = 0. \tag{3.14}$$

The a priori error covariance $P_{k|k-1}$ and the *a posteriori* error covariance $P_{k|k}$ can be obtained as

$$P_{k|k-1} = F_{k-1} P_{k-1|k-1} F_{k-1}^{\mathrm{T}} + Q_{k-1}, \tag{3.15}$$

$$P_{k|k} = (I - K_k H_k) P_{k|k-1}. \tag{3.16}$$

In this

$$\begin{aligned} P_{k|k-1} &= E[e_{k|k-1} e_{k|k-1}^{\mathrm{T}} \mid Z_{k-1}] \\ &= E\left[\left(F_{k-1} e_{k-1|k-1} + w_{k-1} \right) \left(F_{k-1} e_{k-1|k-1} + w_{k-1} \right)^{\mathrm{T}} \mid Z_{k-1} \right] \\ &= F_{k-1} P_{k-1|k-1} F_{k-1}^{\mathrm{T}} + Q_{k-1}, \end{aligned}$$

$$\begin{aligned} P_{k|k} &= E\left[e_{k|k} e_{k|k}^{\mathrm{T}} \mid Z_k \right] = (I - K_k H_k) P_{k|k-1} (I - K_k H_k)^{\mathrm{T}} + K_k R_k K_k^{\mathrm{T}} \\ &= (I - K_k H_k) P_{k|k-1} - (I - K_k H_k) P_{k|k-1} H_k^{\mathrm{T}} K_k^{\mathrm{T}} + K_k R_k K_k^{\mathrm{T}} \\ &= (I - K_k H_k) P_{k|k-1} - \left[P_{k|k-1} H_k^{\mathrm{T}} - K_k H_k P_{k|k-1} H_k^{\mathrm{T}} - K_k R_k \right] K_k^{\mathrm{T}} \\ &= (I - K_k H_k) P_{k|k-1} - \left[P_{k|k-1} H_k^{\mathrm{T}} - K_k \left(H_k P_{k|k-1} H_k^{\mathrm{T}} + R_k \right) \right] K_k^{\mathrm{T}} \\ &= (I - K_k H_k) P_{k|k-1}. \end{aligned}$$

Finally, we have a full set of recursive equations to estimate the state variable as following

Time Update Equations

$$x_{k|k-1} = F_{k-1} x_{k-1|k-1} \tag{3.17}$$

$$P_{k|k-1} = F_{k-1} P_{k-1|k-1} F_{k-1}^{\mathrm{T}} + Q_{k-1}. \tag{3.18}$$

Measurement Update Equations

$$K_k = P_{k|k-1} H_k^{\mathrm{T}} \left(H_k P_{k|k-1} H_k^{\mathrm{T}} + R_k \right)^{-1} \tag{3.19}$$

$$x_{k|k} = x_{k|k-1} + K_k (z_k - H_k x_{k|k-1}) \tag{3.20}$$

$$P_{k|k} = \left(I - K_k H_k \right) P_{k|k-1}. \tag{3.21}$$

3.2 Extended Kalman filter

Let us consider a case where the process model and the observation model are nonlinear.

$$x_k = f\left(x_{k-1}, w_{k-1} \right) \tag{3.22}$$

$$z_k = h\left(x_k, v_k \right). \tag{3.23}$$

The *a priori* state estimate at step k given knowledge of the process up to step $k-1$, $x_{k|k-1} \in \Re^{\bar{n}}$, and the measurement estimate at step k, $z_{k|k-1} \in \Re^{\bar{m}}$, will be

$$x_{k|k-1} = f\left(x_{k-1|k-1}, 0 \right) \tag{3.24}$$

$$z_{k|k-1} = h\left(x_{k|k-1}, 0 \right). \tag{3.25}$$

Now, we linearize the process model about *a posteriori* state estimate at step $k-1$, $x_{k|k-1} \in \Re^{\bar{n}}$, and the observation model about a priori state estimate at step k, $x_{k|k-1}$.

$$x_k \approx f\left(x_{k-1|k-1},0\right)+\frac{\partial f}{\partial x}\left(x_{k-1|k-1},0\right)\left(x_{k-1}-x_{k-1|k-1}\right)+\frac{\partial f}{\partial w}\left(x_{k-1|k-1},0\right)w_{k-1}$$
$$=f\left(x_{k-1|k-1},0\right)+F_{k-1}\left(x_{k-1}-x_{k-1|k-1}\right)+W_{k-1}w_{k-1}, \tag{3.26}$$

$$z_k \approx h\left(x_{k|k-1},0\right)+\frac{\partial h}{\partial x}\left(x_{k|k-1},0\right)\left(x_k-x_{k-1|k-1}\right)+\frac{\partial h}{\partial v}\left(x_{k|k-1},0\right)v_k$$
$$=h\left(x_{k|k-1},0\right)+H_k\left(x_k-x_{k|k-1}\right)+V_k v_k. \tag{3.27}$$

A pseudo measurement is introduced

$$y_k \equiv z_k - h(x_{k|k-1},0)+H_k x_{k|k-1}=H_k x_k+V_k v_k. \tag{3.28}$$

The Jacobians will be defined as

$$F_k=\frac{\partial f}{\partial x}\left(x_{k|k},0\right), \qquad W_k=\frac{\partial f}{\partial w}\left(x_{k|k},0\right), \tag{3.29}$$

$$H_k=\frac{\partial h}{\partial x}\left(x_{k|k-1},0\right), \qquad V_k=\frac{\partial h}{\partial v}\left(x_{k|k-1},0\right). \tag{3.30}$$

Our system to be estimated become

$$x_k=x_{k|k-1}+F_{k-1}\left(x_{k-1}-x_{k-1|k-1}\right)+W_{k-1}w_{k-1},$$
$$y_k=H_k x_k+V_k v_k.$$

The a priori state estimate and measurement estimate become

$$x_{k|k-1}=f\left(x_{k-1|k-1},0\right),$$
$$y_{k|k-1}=H_k x_{k|k-1}. \tag{3.31}$$

The predicted error is obtained as

$$e_{k|k-1}=x_k-x_{k|k-1}=F_{k-1}\left(x_k-x_{k|k-1}\right)+W_{k-1}w_{k-1}$$
$$=F_{k-1}e_{k-1|k-1}+W_{k-1}w_{k-1},$$

and the predicted error covariance will be

$$P_{k|k-1} = \mathrm{cov}(e_{k|k-1}) = F_{k-1} P_{k-1|k-1} F_{k-1}^{\mathrm{T}} + W_{k-1} Q_{k-1} W_{k-1}^{\mathrm{T}}. \tag{3.32}$$

The pseudo measurement error is

$$\begin{aligned} \varepsilon_k &= y_k - y_{k|k-1} = H_k \left(x_k - x_{k|k-1} \right) + V_k v_k \\ &= H_k e_{k|k-1} + V_k v_k . \end{aligned} \tag{3.33}$$

and its variation is

$$S_k = \mathrm{cov}(\varepsilon_k) = H_k P_{k|k-1} H_k^{\mathrm{T}} + V_k R_k V_k^{\mathrm{T}}. \tag{3.34}$$

The updated state is assumed to be

$$x_{k|k} = x_{k|k-1} + K_k \varepsilon_k . \tag{3.35}$$

The updated error is

$$\begin{aligned} e_{k|k} &= x_k - x_{k|k} = e_{k|k-1} - K_k \varepsilon_k = e_{k|k-1} - K_k \varepsilon_k \left(H_k e_{k|k-1} + V_k v_k \right) \\ &= \left(I - K_k H_k \right) e_{k|k-1} - K_k V_k v_k , \end{aligned} \tag{3.36}$$

and the updated error covariance will be

$$P_{k|k} = \mathrm{cov}(e_{k|k}) = \left(I - K_k H_k \right) P_{k-1|k-1} \left(I - K_k H_k \right)^{\mathrm{T}} + K_k V_k R_k V_k^{\mathrm{T}} K_k^{\mathrm{T}}. \tag{3.37}$$

Now, the nonlinear model is written in a linearized form as (3.26) and (3.28). Comparing the linear model (3.1) and (3.2) with the above linearized model (3.26) and (3.28) and their error covariance, finally, we have a full set of recursive

equations to estimate the state variable when the process and observation models are nonlinear as following

Time Update Equations

$$x_{k|k-1} = f\left(x_{k-1|k-1}, 0\right),$$

$$P_{k|k-1} = F_{k-1} P_{k-1|k-1} F_{k-1}^{\mathrm{T}} + W_{k-1} Q_{k-1} W_{k-1}^{\mathrm{T}}.$$

Measurement Update Equations

$$K_k = P_{k|k-1} H_k^{\mathrm{T}} \left(H_k P_{k|k-1} H_k^{\mathrm{T}} + R_k\right)^{-1},$$

$$x_{k|k} = x_{k|k-1} + K_k (z_k - H_k x_{k|k-1}),$$

$$P_{k|k} = \left(I - K_k H_k\right) P_{k|k-1}.$$

3.3 Expectation maximization algorithm

Since the EKF is a sub optimal estimator based on linearisation of a nonlinear mapping, x_k is only an approximation to the expected value and P_k is an approximation to the covariance matrix. The EKF algorithm for state estimation suffers from serious shortcomings, namely choosing the initial states and covariance. It is necessary to estimate the system parameters in an effective way. Maximum likelihood techniques involving the use of scoring or Newton Raphson techniques are generally used to estimate the system parameters (Gupta and Mehra 1974). They involve differentiating the log-likelihood function obtained from non-linear equations to estimate the parameters. Feasibility of these methods applied to several cases has been shown in (Ledolter 1979, Goodrich and Caines 1979).

The likelihood methods explained above have some limitations which can be circumvented using EM algorithm (Dempster 1977). Firstly the correction steps involve large calculation of inverse of the second order partials and this is complicated if more number of parameters are involved. Furthermore, Newton methods may not necessarily increase the likelihood function sometimes it reduces

due to large number of steps. On the other hand, EM steps always increase the likelihood function and one is guaranteed convergence to a stationary point for an exponential family (Wu *et al*. 1981). One may find a local or global maximum there or one may be indefinitely along a ridge (Boyles 1980) depending on the shape of the likelihood function. EM algorithm is relatively simple in implementation unlike the Newton methods which involve the calculation of second order partials for maximizing log-likelihood function. EM does not consider the evaluation of second order partials therefore it is not available for estimating standard error. Another disadvantage in EM is that it has slow convergence in later stages of iterations therefore can switch to some other algorithm at this stage.

Using the Markovian property embedded in the evolved model, the likelihood of the complete data can be represented as below

$$\begin{aligned} L &= p(x,z\,|\,\theta) \\ &= p(x_0\,|\,\theta)\prod_{s=1}^{k} p(x_s\,|\,x_{s-1},\theta)\prod_{s=1}^{k} p(z_s\,|\,x_s,\theta), \end{aligned} \tag{3.38}$$

where $\theta=[\mu,\Pi,F,Q,R]$ denotes the unknown system parameters, μ and Π are the mean and covariance of the initial states x_0, F_k is the state evolution matrix, Q and R are the covariance of process and measurement noise, respectively.
The log-likelihood of the complete data is given by

$$\begin{aligned} \log L = &-\sum_{2}^{n}[\frac{1}{2}\{z_k - h(x_k)\}^{\mathrm{T}} R^{-1}\{z_k - h(x_k)\}] \\ &-\sum_{2}^{n}[\frac{1}{2}\{x_k - F_k x_{k-1}\}^{\mathrm{T}} Q^{-1}\{x_k - F_k x_{k-1}\}] \\ &-\frac{1}{2}\{x_1-\mu\}^{\mathrm{T}}\Pi^{-1}\{x_1-\mu\} - \frac{n(m+q)}{2}\log(2\pi) \\ &-\frac{n}{2}\log|R| - \frac{n-1}{2}\log|Q| - \frac{1}{2}\log|\Pi|, \end{aligned} \tag{3.39}$$

where log-likelihood function ($\log L$) is to be maximized with respect to the system parameters $\theta=[\mu,\Pi,F,Q,R]$. In the above notation the log-likelihood function depends on the unobserved data x_k, therefore in implementation of EM we consider

the expectation of the log-likelihood function based on the observations y_k $(k=1,2,\cdots,n)$

3.4 EM algorithm principle and implementation

The EM algorithm is a widely applicable iterative algorithm. It consists of two major steps; expectation step and maximization step. The expectation is with respect to the unknown hidden variables using the current estimate of the parameters and conditioned upon the observations. The maximization step provides a new estimate of the parameters. These two steps are iterated until convergence.

For the implementation of EM Algorithm we need to calculate the expectation of the log-likelihood equation (3.39) and then differentiate it with respect to the parameters so as to maximize it.

$$\begin{aligned} E(\log L \mid z_k) = &-\sum_{2}^{n}[\frac{1}{2}E[\{z_k - h(x_k)\}^{\mathrm{T}} R^{-1}\{z_k - h(x_k)\}]] \\ &-\sum_{2}^{n}[\frac{1}{2}E[\{x_k - F_k x_{k-1}\}^{\mathrm{T}} Q^{-1}\{x_k - F_k x_{k-1}\}]] \\ &-\frac{1}{2}E[\{x_1 - \mu\}^{\mathrm{T}} \Pi^{-1}\{x_1 - \mu\}] - \frac{n(m+q)}{2}\ln(2\pi) \\ &-\frac{n}{2}\ln(R) - \frac{n-1}{2}\ln(Q) - \frac{1}{2}\ln(\Pi). \end{aligned} \tag{3.40}$$

In order to calculate the expectations in (3.40), it is convenient to define conditional mean and covariance

$$x_{k|n} = E(x_k \mid z_1, ..., z_n) \tag{3.41}$$

$$P_{k|n} = \mathrm{COV}(x_k \mid z_1, ..., z_n) \tag{3.42}$$

$$P_{k,k-1|n} = \mathrm{COV}(x_k, x_{k-1} \mid z_1, ..., z_n). \tag{3.43}$$

Here, $x_{k|k}$ is the usual Kalman estimator whereas $x_{k|n}$ is the minimum square error smoothed estimator of x_k based on complete observed data i.e. $(k=1,2,\cdots,n)$. These expected values of states and covariance can be obtained using extended Kalman smoother

$$
\begin{aligned}
E(\log L \mid z_1,..,z_n) = &-\frac{1}{2}\log|\Pi| - \frac{1}{2}tr\{\Pi^{-1}(P_{0|n} + (x_{0|n} + \mu)(x_{0|n} + \mu)^{\mathrm{T}})\} \\
&-\frac{n}{2}\log|Q| - \frac{1}{2}tr\{C - BF^{\mathrm{T}} - FB^{\mathrm{T}} + FAF^{\mathrm{T}})\} \\
&-\frac{n}{2}\log|R| \\
&-\frac{1}{2}tr\left\{R^{-1}\sum_{k=1}^{n}[(z_n - h_k(x_k))(z_n - h_k(x_k))^{\mathrm{T}} + J_k P_{k|n} J_k^{\mathrm{T}}]\right\},
\end{aligned}
\tag{3.44}
$$

where

$$A = \sum_{k=1}^{n}(P_{k-1|n} + x_{k-1|n}x_{k-1|n}^{\mathrm{T}}) \tag{3.45}$$

$$B = \sum_{k=1}^{n}\left(P_{k,k-1|n} + x_{k|n}x_{k-1|n}^{\mathrm{T}}\right) \tag{3.46}$$

$$C = \sum_{k=1}^{n}\left(P_{k|n} + x_{k|n}x_{k|n}^{\mathrm{T}}\right). \tag{3.47}$$

Maximizing the last two lines of log-likelihood function (3.44) we obtain the values for system parameters which increase the log-likelihood function

$$F(r+1) = BA^{-1} \tag{3.48}$$

$$Q(r+1) = \frac{1}{n-1}(C - BA^{-1}B^{\mathrm{T}}) \tag{3.49}$$

$$R(r+1) = \frac{1}{n}\sum_{k=1}^{n}J_k^{\mathrm{T}}p_{k|n}J_k + \{(z_k - J_k x_{k|n})(z_k - J_k x_{k|n})^{\mathrm{T}}\} \tag{3.50}$$

$$\mu(r+1) = x_{1|n} \tag{3.51}$$

$$\Pi(r+1) = p_{1|n}. \tag{3.52}$$

In some cases we may want to add constraints to the elements in state transition matrix F such that $FM = G$ then (3.48) and (3.49) are modified as

$$F_c(r+1) = F - (FM - G)(M^{\mathrm{T}}A^{-1}M)^{-1}M^{\mathrm{T}}A^{-1} \tag{3.53}$$

$$Q_c(r+1) = Q + (FM - G)(M^{\mathrm{T}}A^{-1}M)^{-1}(FM - G)^{\mathrm{T}}. \tag{3.54}$$

The value of log-likelihood function can be evaluated at each step using the formula given below (Gupta and Mehra 1974)

$$\log L = -\frac{1}{2}\sum_{k=1}^{n}\log\left|J_k P_{k|k-1} J_k^{\mathrm{T}} + R_k\right| \\ = \frac{1}{2}\sum_{k=1}^{n}(z_k - h_k(x_{k|k-1})^{\mathrm{T}}(J_k P_{k|k-1} J_k^{\mathrm{T}} + R_k)(z_k - h_k(x_{k|k-1}). \tag{3.55}$$

The EM algorithm always increases the log-likelihood function in each step and this is used as convergence criteria when the value of log-likelihood function decreases then iterations are terminated.

3.5 Extended Kalman smoother

In EKF, it proceeds only forward in time to estimate the parameters. By incorporating the future measurements we can have improved estimates of the previous time steps. This is known as smoothing operation. The smoothing is done by using fixed point or fixed lag or fixed interval. Here we use fixed interval extended Kalman filter which entails forward and backward computations to estimate at each time step.

Step 1) Predicted (a priori) state

$$x_{k|k-1} = F_{k-1} x_{k-1|k-1}. \tag{3.56}$$

Step 2) Predicted (a priori) error covariance

$$P_{k|k-1} = \mathrm{cov}(e_{k|k-1}) = F_{k-1} P_{k-1|k-1} F_{k-1}^{\mathrm{T}} + Q_{k-1}. \tag{3.57}$$

Step 3) Predicted measurement error

$$\varepsilon_k = \tilde{z}_k - \tilde{z}_{k|k-1} = \tilde{z}_k - H_k x_{k|k-1}. \tag{3.58}$$

Step 4) Predicted measurement error covariance

$$S_k = \mathrm{cov}(\varepsilon_k) = H_k P_{k|k-1} H_k^{\mathrm{T}} + R_k. \tag{3.59}$$

Step 5) Kalman gain

$$K_k = P_{k|k-1} H_k^{\mathrm{T}} S_k^{-1}. \tag{3.60}$$

Step 6) Updated (a posteriori) state

$$x_{k|k} = x_{k|k-1} + K_k \varepsilon_k = x_{k|k-1} + K_k (\tilde{z}_k - H_k x_{k|k-1}). \tag{3.61}$$

Step 7) Updated (*a posteriori*) error covariance

$$P_{k|k} = (I - K_k H_k) P_{k|k-1}. \tag{3.62}$$

Step 8) Initialize Rauch-Tung-Stribel smoother

$$\begin{aligned} x_{n|n} &= x_n \\ P_{n|n} &= P_n. \end{aligned} \tag{3.63}$$

Step 9) Smoother gain

$$G_{k-1} = P_{k-1|k-1} F_k^{\mathrm{T}} (P_{k|k-1})^{-1}. \tag{3.64}$$

Step 10) Smoothed estimate

$$x_{k-1|n} = x_{k-1|k-1} + G_{k-1}(x_{k|n} - F_k x_{k-1|k-1}). \tag{3.65}$$

Step 11) Smoothed covariance update

$$P_{k-1|n} = P_{k-1|k-1} + G_{k-1}(P_{k|n} - P_{k|k-1}) G_{k-1}^{\mathrm{T}}. \tag{3.66}$$

Step 12) Compute smoothed cross-covariance

$$P_{k-1,k-2|n} = P_{k-1|k-1} G_{k-2}^{\mathrm{T}} + G_{k-1}(P_{k,k-1|n} - F_k P_{k-1|k-1}) G_{k-2}^{\mathrm{T}}. \tag{3.67}$$

In conventional maximum likelihood estimation procedure, the log-likelihood condition (3.39) is used along with nonlinear methods to solve for system parameters. These methods are difficult to implement and need to compute the inverse matrix of second order partial equations. Also, these methods do not increase the log-likelihood function value. However, through EM using (3.48), (3.49) and (3.50), the system parameters are estimated. These are simple to implement as they are just multivariate regression calculations. The better estimation performance of EM is achieved at the expense of additional computational effort needed to calculate the smoothed estimators $x_{k|n}$, $P_{k|n}$, $P_{k,k-1|n}$ needed to compute system parameters (3.42-3.44). For this one requires to apply backward recursions where as conventional methods needs forward computations to compute (3.39). In the conventional methods for solving maximum likelihood function, it requires a set of derivates for $x_{k|k-1}$, $P_{k|k-1}$ to solve for system parameters which also takes comparable amount of computation.

4. Estimation of region boundaries in flow field using expectation maximization algorithm

In many industrial processes such as heat exchangers and combustion systems, liquid-gas or liquid vapour phases are formed under normal or accidental conditions (Holand and Bragg 1995, Fairuzov 2000). Location of these region boundaries in the flow field is important for the safety operation of the mechanical systems. In this regard, there have been numerous methods proposed for the visualization of two-phase flows (Gladden and Alexander 1996, Xu *et al.* 1997, Shollenberger *et al.* 1997). Some of these methods such as gamma densitometry are expensive, hazardous and have side effects. A few other methods are intrusive and disturb the flow field. Finally, some techniques have large data acquisition time making it difficult to visualize two-phase flows. Electrical impedance tomography (EIT) is a non-intrusive method and has high temporal resolution characteristics thus making it a potential method for visualization of two-phase flows. Image reconstruction in EIT comprises of forward and inverse problem. In forward problem, a set of electrical currents are injected through the electrodes attached around the boundary of the object to be imaged and the excited voltages are measured on the electrodes. In inverse problem based on the current-voltage relationship, the internal conductivity distribution is reconstructed. The main disadvantage in EIT is its low spatial resolution because like many inverse problems, reconstruction using EIT is highly non-linear and ill-posed. To mitigate the ill-posedness, regularization methods are often employed (Lionheart 2004). If the process vessel contains some region boundaries (voids) enclosed by background and the knowledge of the conductivity distribution of the background and that of the voids are known *a priori*, then the unknown parameters will be the location and size of the boundaries. If the problem is to estimate the boundary of the void rather than the conductivity distribution then it is defined as phase boundary estimation problem. These boundary estimation problems can be classified as open and closed boundary problems according to the topology of the boundary to be estimated. The boundary is termed as closed boundary if the anomalies are enclosed by the background substance (Han and Prosperetti 1999). In case of the open

boundary problem, the domain is divided into disjoint zones separated by an interfacial open boundary (Butler and Bonnecaze 2000, Kim *et al.* 2007b). The methods used to describe the open boundary problems are not applicable to closed boundary problems. The work concerned here is about estimation of the region boundaries, which is a closed boundary problem.

Several methods have been proposed in literature to represent the closed boundary. Han and Prosperetti (1999) assumed the boundary to be smooth and described the boundary using Fourier series. Shape decomposition method based on boundary element method was used to solve the boundary problem. Kolehmainen *et al.* (1999) developed a method to recover the piece wise coefficients of an elliptic PDE for an application of optical tomography which is similar in principal with that of EIT. Using EIT, numerous methods have been proposed to recover the Fourier coefficients that represent the boundary. Static methods like Newton methods and neural networks were employed for boundary estimation (Jeon *et al.* 2005, Kim *et al.* 2006). These static methods offer slow convergence and therefore are not fast enough to track the transient changes of the object. In such situations, dynamic algorithms such as EKF and UKF filter give a better performance (Kim *et al.* 2007b, Ijaz *et al.* 2007).

The EKF is the most popular algorithm used to track the fast transient changes of the object. EKF uses a state-space model which consists of process and observation models to estimate the state parameters. The process model describes the dynamic behavior of the object while the observation model establishes the relationship between the measurements and the state vector. Statistical properties are used in the implementation of process and observation model. The process model is used to predict the motion of the object and the predicted values are corrected using the available measurements. Using this predictor-corrector mechanism, it approximates an optimal estimate due to linearization of the process and observation models. For the application of EKF, the exact dynamics of the evolution, initial states of the noise covariance of process and measurement models have to be predefined. In practice, we do not have any prior information about the evolution of the motion parameters, therefore, random-walk model is employed. In some cases, interactive multiple models such as constant velocity and constant acceleration are used (Bar

and Shalom and Li 1993). In real situations, the dynamics of the evolution are complex and it is difficult to represent the model parameters in a prior form. The values of noise covariance are set through experience or manually tuned which is a major drawback of EKF for parameter estimation. The determination of dynamic evolution matrix, noise covariance matrices and initial estimates are accomplished using expectation maximization algorithm. The EM algorithm is a method of finding a mode of the proposed likelihood function through the expectation and maximization. The most remarkable aspect of EM algorithm is that it ensures the increase in log likelihood function. A method of EM for learning a linear dynamic system has been studied in Grahahmani and Hinton (1996). Extension to the system of linear dynamics and nonlinear measurement are given in Grahahmani and Beal (1999). EM algorithm has been applied in field of medical and economics to estimate the hidden states using the missing data.

This study involves estimation of voids in the flow process using EIT as an application of process tomography to visualize two-phase flows. The smooth closed boundary is represented using truncated Fourier series and the Fourier coefficients are estimated using expectation maximization algorithm. The proposed model assumes that state transition obeys Gaussian distribution and the Markovian chain theory. The state transition matrix, initial states, process and measurement noise covariance matrices is estimated using EM algorithm and then the estimated system parameters are applied to EKF to estimate the unknown region boundaries. Numerical and experimental studies have been carried out to evaluate the performance of the proposed method. The results show that EM has better estimation performance of the void boundary (location, shape and size) as compared to conventional EKF.

4.1 Boundary representation

In this section, the shape parameterization and the recovery of smooth region boundaries are presented. Since the conductivities of the background and that of object are known *a priori,* the coefficients that represent the boundary are estimated

instead. The forward solver is then modified accordingly as a set of coefficients representing the boundary shape.

Let us assume that the problem domain $\Omega \in \Re^2$ is divided into $P+1$ disjoint regions A_k as shown in figure 4.1

$$\Omega = \bigcup_{k=0}^{P} A_k . \tag{4.13}$$

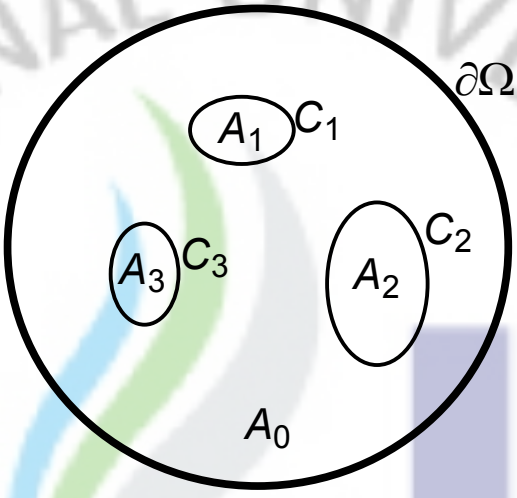

Figure 4.1. Region boundaries enclosed by background.

Let A_0 be the background region whose outer boundary is $\partial\Omega$ whereas the region $A_k \ \left(k = 1, \cdots, P\right)$ is bounded by smooth boundary $C_k \in \Omega (k = 1, \cdots, P)$ Let $\chi_k(r)$ be the characteristic function of sub region A_k, the conductivity in the region is a known constant and can be expressed as

$$\sigma = \sum_{k=0}^{P} \sigma_k \chi_k (r). \tag{4.14}$$

By substituting (4.14) into (4.10), we obtain

$$\mathbf{B}(i, j) = \sum_{k=0}^{P} \int_{\mathrm{supp}(\varphi_i \varphi_j) \cap A_k} \sigma_k \nabla \varphi_i \nabla \varphi_j dr + \sum_{l=1}^{L} \frac{1}{z_l} \int_{e_l} \varphi_i \varphi_j dS, \tag{4.15}$$

where supp($\varphi_i\varphi_j$) is a part of domain Ω where both the basis functions φ_i and φ_j is non-zero. The implementation of the integrals of the form (4.15) has been described previously in (Kolehmainen *et al.* 1999, Tossavainen *et al.* 2006). As a first step, mesh elements Ω_m are classified into sets of elements inside the region $A_k\,(k=0,1)$ for two-phase flow and a set of elements intercepted by the boundary C_k. For the elements that lie in the region A_k, they are assigned their corresponding conductivity values σ_k. However, for the elements that lie on the boundary C_k, the area weighted conductivity values are assigned as in Kolehmainen *et al.* (1999)

$$\sigma_e = \frac{\sigma_l S_l + \sigma_r S_r}{S_e (= S_l + S_r)}, \tag{4.16}$$

where S_l and S_r denotes the area of lower and upper regions of the splitted element, respectively. If phase boundaries of the objects C_k are sufficiently smooth, they can be approximated as a linear combination of known functions

$$C_k(s) = \begin{pmatrix} x_k(s) \\ y_k(s) \end{pmatrix} = \sum_{\omega=1}^{N_\theta} \begin{pmatrix} \gamma_\omega^{x_l} \theta_\omega^x(s) \\ \gamma_\omega^{y_l} \theta_\omega^y(s) \end{pmatrix}, \tag{4.17}$$

where $\theta_\omega^x(s)$ and $\theta_\omega^y(s)$ are periodic differentiable basis functions and N_θ is the number of basis functions. In this paper, we express the phase boundaries as Fourier series in two-dimensional coordinates with respect to parameter s, that is, we use the basis functions of the form

$$\theta_1^\alpha(s) = 1 \tag{4.18}$$

$$\theta_\omega^\alpha(s) = \sin(2\pi \frac{\omega}{2} s), \;\; \omega = 2,4,6.....N_\theta - 1 \tag{4.19}$$

$$\theta_\omega^\alpha(s) = \cos(2\pi \frac{(\omega-1)}{2} s), \;\; \omega = 1,3,5.....N_\theta, \tag{4.20}$$

where $s \in [0,1]$ and α denotes either x or y. Let Γ be the coefficient vector which represents the boundary, that is,

$$\Gamma = (\gamma_1^{x_1}, ..., \gamma_{N_\theta}^{x_1}, \gamma_1^{y_1}, ..., \gamma_{N_\theta}^{y_1}, ..., ..., \gamma_1^{x_s}, ..., \gamma_{N_\theta}^{x_s}, \gamma_1^{y_s}, ..., \gamma_{N_\theta}^{y_s})^{\mathrm{T}}, \tag{4.21}$$

where $\Gamma \in \Re^{2\bar{P}N_\theta}$. Now our goal is to estimate the coefficient vector with the information of injected currents and measured boundary voltages using an efficient inverse algorithm.

4.2 Inverse problem: Estimation of Fourier coefficients

4.2.1 State estimation approach

In this section, we present the state estimation formulation for boundary estimation using EIT. The voids formed inside the process vessel are not stable and they change position and shape during the time of data acquisition. If the target changes so fast that its characteristics changes significantly with in one single image frame then the conventional static imaging techniques will not give desirable results. In order to enhance the temporal resolution in EIT, dynamic image reconstruction algorithms are required. The unknown Fourier coefficients that represent the boundary of the void are regarded as state variables and the inverse problem is treated as a state estimation problem. Assuming that the evolution of the state variables $\gamma \in \Re^{\bar{n}}$ is smooth, the dynamic equation is modeled by a stochastic linear differential equation

$$\gamma_k = F_k \gamma_{k-1} + w_k, \tag{4.22}$$

where F_k is the state transition matrix, w_k is the process noise vector, $\bar{n}$ is the dimension of state vector $\left(\bar{n} = 2\bar{P}N_\theta\right)$, and the index k represents the discrete time step. EIT measurements are described by the nonlinear equation

$$V_k = U_k(\gamma_k) + v_k, \tag{4.23}$$

where V_k is the vector of voltages measured at time step k, v_k is the measurement noise vector and $U_k(\gamma_k)$ is the forward solution computed using FEM. Both the

process and observation noise, w_k and v_k, are assumed to be mutually independent and zero-mean normally distributed random variables with known covariance matrix,

$$w_k \sim N(0, Q) \tag{4.24}$$
$$v_k \sim N(0, R). \tag{4.25}$$

The equations (4.22) and (4.23) constitute the state-space representation of the boundary estimation problem. In solving the state estimation procedure, the conditional expectations have to be determined. The conditional estimates $\gamma_{k|k}$ are determined using recursive Kalman filter if the state and measurement equations are linear. In case of non-linear system of equations, suboptimal estimates can be obtained by applying the linear approximations of the state and/or observation equations. The method which has been formulated based on such an approach is known as extended Kalman filter (EKF) (Kim *et al.* 2008, Ijaz *et al.* 2008). State estimation using EKF assumes the prior knowledge of the model parameters (F, Q, R, γ_0, P_0). Evolution of the state is often very complicated in the case of two-phase flows. Moreover, the process noise is heavily dependant on the environment surrounding the object, therefore, it is difficult to have prior information of actual dynamics of the model parameters. The estimation performance of EKF is affected by the choice of these model parameters. The EM algorithm can be used to effectively estimate these model parameters and the estimated parameters are then used in EKF for state estimation. First, we introduce maximum likelihood function before deriving the EM algorithm for boundary estimation.

4.2.2 Maximum likelihood function

We assume that the initial conditions, evolution of the states and the likelihood of the measurement data can be represented by Gaussian distribution. The conditional probabilities for the state and the measurements can be written as follows

$$p(\gamma_0 \mid \theta) = (2\pi)^{-\bar{n}/2} (\Pi)^{-1/2} \exp[-\{(\gamma_0 - \mu)^{\mathrm{T}} \Pi^{-1} (\gamma_0 - \mu)\} / 2] \tag{4.26}$$
$$p(\gamma_k \mid \gamma_{k-1}, \theta) = (2\pi)^{-\bar{n}/2} (Q)^{-1/2} \exp[-\{(\gamma_k - F_k \gamma_{k-1})^{\mathrm{T}} Q^{-1} (\gamma_k - F_k \gamma_{k-1})\} / 2] \tag{4.27}$$

$$p(V_k \mid \gamma_k, \theta) = (2\pi)^{-m/2} (R)^{-1/2} \exp[-\{(V_k - U_k(\gamma_k))^{\mathrm{T}} R^{-1} (V_k - U_k(\gamma_k))\}/2], \tag{4.28}$$

where $\theta = [\mu, \Pi, F_k, Q, R]$ denotes the unknown system parameters, μ and Π are the mean and covariance of the initial states γ_0, F_k is the state evolution matrix, Q and R are the covariance of process and measurement noise, respectively. The likelihood of the complete data using the Markovian property embedded in state equations is given by

$$\begin{aligned} L &= p(\gamma_k, V_k \mid \theta) \\ &= p(\gamma_0 \mid \theta) \prod_{k=1}^{n} p(\gamma_k \mid \gamma_{k-1}, \theta) \prod_{k=1}^{n} p(V_k \mid \gamma_k, \theta). \end{aligned} \tag{4.29}$$

The log-likelihood of the complete data is given by

$$\begin{aligned} \log L = \text{constant} &- \frac{1}{2}\log|\Pi| - \frac{1}{2}\{\gamma_0 - \mu\}^{\mathrm{T}} \Pi^{-1} \{\gamma_0 - \mu\} \\ &- \frac{n}{2}\log|R| - \sum_{k=1}^{n} [\frac{1}{2}\{V_k - U_k(\gamma_k)\}^{\mathrm{T}} R^{-1} \{V_k - U_k(x_k)\}] \\ &- \frac{n}{2}\log|Q| - \sum_{k=1}^{n} [\frac{1}{2}\{\gamma_k - F_k\gamma_{k-1}\}^{\mathrm{T}} Q^{-1} \{\gamma_k - F_k\gamma_{k-1}\}], \end{aligned} \tag{4.30}$$

where log-likelihood function log L is to be maximized with respect to the system parameters $\theta = [\mu, \Pi, F, Q, R]$.

4.2.3 EM algorithm for boundary estimation

The EM algorithm is an iterative method for finding a mode of the likelihood function. The EM algorithm consists of two major steps; expectation step and maximization step. The expectation is with respect to the unknown variables using underlying variables using the current estimate of the parameters and conditioned upon the measurements. The maximization step provides a new estimate of the parameters. These two steps are iterated until convergence. The EM algorithm presented here is based on Shumway and Stoffer 1982 where the measurement matrix U is considered to be known.

For the implementation of EM Algorithm we need to calculate the expectation of the log-likelihood (4.30) and then differentiate it with respect to the parameters so as to

maximize it. The log-likelihood function (4.30) depends on the unobserved data γ_k, therefore in the implementation of EM we consider the expectation of the log-likelihood function based on the observations $V_k \quad (k=1,2,3\cdots,n)$

$$\begin{aligned} E(\log L \mid V_{k=1,2,\ldots,n}) = &-\sum_{k=1}^{n}[\frac{1}{2}E[\{V_k - U_k(\gamma_k)\}^{\mathrm{T}} R^{-1}\{V_k - U_k(\gamma_k)\}]] \\ &-\sum_{k=1}^{n}[\frac{1}{2}E[\{\gamma_k - F_k\gamma_{k-1}\}^{\mathrm{T}} Q^{-1}\{\gamma_k - F_k\gamma_{k-1}\}]] \\ &-\frac{1}{2}E[\{\gamma_1 - \mu\}^{\mathrm{T}} \Pi^{-1}\{\gamma_1 - \mu\}] - \frac{n(m+q)}{2}\ln(2\pi) \\ &-\frac{n}{2}\ln(R) - \frac{n-1}{2}\ln(Q) - \frac{1}{2}\ln(\Pi). \end{aligned} \tag{4.31}$$

To evaluate the conditional expectations in (4.31) we define the conditional mean and covariance

$$\gamma_{k|n} = E(\gamma_k \mid V_1,\ldots\ldots,V_n) \tag{4.32}$$

$$P_{k|n} = \mathrm{COV}(\gamma_k \mid V_1,\ldots\ldots,V_n) \tag{4.33}$$

$$P_{k,k-1|n} = \mathrm{COV}(\gamma_k,\gamma_{k-1} \mid V_1,\ldots\ldots,V_n). \tag{4.34}$$

Here, $\gamma_{k|n}$ is the smoothed estimate of γ_k based on all the available measured data i.e. $(k=1,2,3\cdots,n)$. Similarly, $P_{k|n}$, $P_{k,k-1|n}$ are the covariance and cross covariance smooth estimates, respectively. These smooth estimates for mean and covariance are obtained using extended Kalman smoother which is explained in subsequent subsection. Using the conditional expectations of mean and covariance, the expectation of log-likelihood function is written as below

$$\begin{aligned} E(\log L \mid V_{k=1,\ldots,n}) = &-\frac{1}{2}\log|\Pi| - \frac{1}{2}tr\{\Pi^{-1}(P_{0|n} + (\gamma_{0|n} + \mu)(\gamma_{0|n} + \mu)^{\mathrm{T}})\} \\ &-\frac{n}{2}\log|Q| - \frac{1}{2}tr\{\square - \square F^{\mathrm{T}} - F\square^{\mathrm{T}} + F\square F^{\mathrm{T}})\} \\ &-\frac{n}{2}\log|R| \\ &-\frac{1}{2}tr\left\{R^{-1}\sum_{k=1}^{n}[(V_n - U_k(\gamma_k))(V_n - U_k(\gamma_k))^{\mathrm{T}} + J_k P_{k|n} J_k^{\mathrm{T}}]\right\}, \end{aligned} \tag{4.35}$$

where

$$A = \sum_{k=1}^{n} (P_{k-1|n} + \gamma_{k-1|n}\gamma_{k-1|n}^{T}) \tag{4.36}$$

$$B = \sum_{k=1}^{n} \left(P_{k,k-1|n} + \gamma_{k|n}\gamma_{k-1|n}^{T} \right) \tag{4.37}$$

$$C = \sum_{k=1}^{n} \left(P_{k|n} + \gamma_{k|n}\gamma_{k|n}^{T} \right). \tag{4.38}$$

Maximizing the log-likelihood function (4.31) we obtain the values for system parameters which increase the log-likelihood function

$$F(r+1) = BA^{-1} \tag{4.39}$$

$$Q(r+1) = \frac{1}{n}(C - BA^{-1}B^{T}) \tag{4.40}$$

$$R(r+1) = \frac{1}{n}\sum_{k=1}^{n} J_k^{T} p_{k|n} J_k + \{(V_k - J_k\gamma_{k|n})(V_k - J_k\gamma_{k|n})^{T}\} \tag{4.41}$$

$$\mu(r+1) = \gamma_{1|n} \tag{4.42}$$

$$\prod(r+1) = p_{1|n}. \tag{4.43}$$

The detailed description about the computation of derivatives of log-likelihood function for the evaluation of system parameters can be found in Shaumway and Stoffer 1982, Ghaharamani and Hinton 1999.

4.2.4 Extended Kalman smoother

EKF is an iteration algorithm which only proceeds in forward-step in time to estimate the state parameters. By incorporating the future measurements we can have improved estimates of the previous time steps. This is known as smoothing operation. The smoothing is done by using fixed point or fixed lag or fixed interval. Here, we use fixed interval extended Kalman filter which entails forward and backward computations to estimate at each time step (Gelb 1981).

Rauch-Tung-Stribel smoother

Step 1) Predicted (*a priori*) state

$$\gamma_{k|k-1} = F_{k-1}\gamma_{k-1|k-1}. \tag{4.44}$$

Step 2) Predicted (*a priori*) error covariance

$$P_{k|k-1} = \mathrm{cov}(e_{k|k-1}) = F_{k-1} P_{k-1|k-1} F_{k-1}^{\mathrm{T}} + Q_{k-1}. \tag{4.45}$$

Step 3) Predicted measurement error

$$\varepsilon_k = V_k - V_{k|k-1} = V_k - H_k \gamma_{k|k-1}. \tag{4.46}$$

Step 4) Predicted measurement error covariance

$$S_k = \mathrm{cov}(\varepsilon_k) = H_k P_{k|k-1} H_k^{\mathrm{T}} + R_k. \tag{4.47}$$

Step 5) Kalman gain

$$K_k = P_{k|k-1} H_k^{\mathrm{T}} S_k^{-1}. \tag{4.48}$$

Step 6) Updated (a posteriori) state

$$\gamma_{k|k} = \gamma_{k|k-1} + K_k \varepsilon_k = \gamma_{k|k-1} + K_k (V_k - H_k \gamma_{k|k-1}). \tag{4.49}$$

Step 7) Updated (a posteriori) error covariance

$$P_{k|k} = (I - K_k H_k) P_{k|k-1}. \tag{4.50}$$

Step 8) Initialize RTS smoother

$$\gamma_{n|n} = \gamma_n, P_{n|n} = P_n. \tag{4.51}$$

Step 9) Smoother gain

$$G_{k-1} = P_{k-1|k-1} F_k^{\mathrm{T}} (P_{k|k-1})^{-1}. \tag{4.52}$$

Step 11) Smoothed estimate

$$\gamma_{k-1|n} = \gamma_{k-1|k-1} + G_{k-1} (\gamma_{k|n} - F_k \gamma_{k-1|k-1}). \tag{4.53}$$

Step 12) Compute smoothed covariance update

$$P_{k-1|n} = P_{k-1|k-1} + G_{k-1}(P_{k|n} - P_{k|k-1})G_{k-1}^{\mathrm{T}}. \tag{4.54}$$

Step 13) Compute smoothed cross-covariance

$$P_{k-1,k-2|n} = P_{k-1|k-1}G_{k-2}^{\mathrm{T}} + G_{k-1}(P_{k,k-1|n} - F_k P_{k-1|k-1})G_{k-2}^{\mathrm{T}} \tag{4.55}$$

4.2.5 Jacobian for closed boundary

In General, EIT has a nonlinear relationship between boundary voltages and conductivity hence measurement equation has to be linearized. The rate of change of potential with respect to the conductivity is popularly known as Jacobian and the matrix thus obtained is called the Jacobian matrix. Jacobian determines how sensitive the measurements are with respect to change of the conductivity inside the domain. However, for the case of boundary estimation the conductivity is replaced by the shape parameters which represent the boundary. The relative change of the measured voltage at the *l*th measurement electrode at the p th current pattern ($\hat{U}_l^p$) with respect to the change of the n th coefficient of the k th boundary ($\gamma_n^{\alpha_k}, \alpha = x, y$), that is

$$J = \frac{\partial \hat{U}_l^p}{\partial \gamma_n^{\alpha_k}}. \tag{4.56}$$

Using the FEM formulation for CEM (2.24~2.32), the expression for Jacobian for boundary coefficients can be written as follows

$$\frac{\partial \hat{\mathbf{U}}}{\partial \gamma_n^{\alpha_k}} = \tilde{\mathbf{M}}\mathbf{A}^{-1}\frac{\partial \mathbf{A}}{\partial \gamma_n^{\alpha_k}}\mathbf{A}^{-1}\tilde{\mathbf{I}} = \tilde{\mathbf{R}}^{\mathrm{T}}\frac{\partial \mathbf{A}}{\partial \gamma_n^{\alpha_k}}\mathbf{b}, \tag{4.57}$$

$(A^{-1})^{\mathrm{T}} = A^{-1}$, this is due to the symmetry of the stiffness matrix $\mathbf{A}$. In $\mathbf{A}$, the matrix $\mathbf{B}$ is the only term dependent on $\gamma_n^{\alpha_k}$ and the Jacobian will be

$$\frac{\partial \hat{\mathbf{U}}}{\partial \gamma_n^{\alpha_k}} = -\begin{pmatrix} \tilde{\mathbf{R}}_1 \\ \tilde{\mathbf{R}}_2 \end{pmatrix}^{\mathrm{T}} \begin{pmatrix} \frac{\partial \mathbf{B}}{\partial \gamma_n^{\alpha_k}} & \mathbf{0} \\ \mathbf{0} & \mathbf{0} \end{pmatrix} \begin{pmatrix} \boldsymbol{\alpha} \\ \boldsymbol{\beta} \end{pmatrix} = -\begin{pmatrix} \tilde{\mathbf{R}}_1^{\mathrm{T}} & \tilde{\mathbf{R}}_2^{\mathrm{T}} \end{pmatrix} \begin{pmatrix} \frac{\partial \mathbf{B}}{\partial \gamma_n^{\alpha_k}} \boldsymbol{\alpha} \\ \mathbf{0} \end{pmatrix} = -\tilde{\mathbf{R}}_1^{\mathrm{T}} \frac{\partial \mathbf{B}}{\partial \gamma_n^{\alpha_k}} \boldsymbol{\alpha}. \quad (4.58)$$

The evaluation of the term $\frac{\partial \mathbf{B}}{\partial \gamma_n^{\alpha_k}}$ can be found in (Tossavainen *et al.* 2007).

4. 3 Results

In this section we present the results for phase boundary estimation using expectation maximization algorithm. The method is tested with numerical and experiment data and the performance is compared with EKF. As a performance criterion, root mean square error (RMSE) of the estimated Fourier coefficients is computed. RMSE for boundary coefficients γ, RMSE_γ, is defined as

$$\mathrm{RMSE}_\gamma = \frac{\left\| \gamma_{\mathrm{estimated}} - \gamma_{\mathrm{true}} \right\|}{\left\| \gamma_{\mathrm{true}} \right\|}. \quad (4.55)$$

4.3.1 Results using simulated data

In this section, the estimation of voids using numerical simulations is presented. The geometry of the phantom is the same which is used in laboratory experiments. The characteristics of the flow inside the phantom are chosen such that the contrast of the conductivities is high between the background fluid and the void present. In this respect, the background conductivity is set to 0.0033 S/cm and the conductivity of the void is set as 0.1×10^{-10} S/cm. The contact impedance between the electrode and the medium is taken as 0.005 $\Omega\mathrm{cm}^2$. To describe a single elliptic boundary, six Fourier coefficients are required and three Fourier coefficients for circular boundary. If same discretization model is adopted in both forward and inverse computations it is termed as inverse crime. In order to avoid such a situation, two different finite element meshes are used for forward and inverse problem. A fine mesh with 2409 nodes and 4560 triangular elements is used in forward solver to generate the boundary voltage data. Inverse solver uses coarse mesh with 2121 nodes and 3984 triangular elements to

estimate the boundary coefficients that describe the target boundary. The voids formed in the flow process are not stable and they change their position and shape with respect to time. Three dynamic scenarios are considered in this respect for the evolution of the void. To generate the true data in all the three cases, first-order kinematic model is used to evolve the motion of the void. In inverse computation, it is assumed that we do not have the prior knowledge of the evolution, therefore, random-walk model is used. To simulate with that of actual conditions, random noise of zero-mean Gaussian noise having *STD* 2% of the value of the corresponding computed voltage is added to the computed voltage.

In case 1, (the moving case), the void changes its position as shown in figure 4.2(a). Initially, the void is positioned at (2, 1) in Cartesian system and it moves with each current pattern while the size and shape of void remain constant during its motion. As an initial guess for the boundary, we choose a circular shaped void with radius 1 cm at center (figure 4.2(b)). The reconstructed phase boundary for case 1 without noise is shown in figure 4.3. In figure 4.3, it can be noticed that EM has better estimation of the phase boundary as compared to EKF. Better initial guess and model parameters estimated by EM result in better estimation of the boundary. The transition period is less as compared to EKF. The void location estimation for case 1 without noise is shown in figure 4.4. EM has better estimation of x and y position of the void. Similarly, the size of the estimated void when there is no noise is shown in figure 4.5. Size and shape are estimated better by EM when compared to EKF. RMSE for boundary coefficients is computed and is shown in figure 4.6. It can be seen that EM has lower RMSE values as compared to EKF in all the iterations. Figures (4.7~4.10) show the reconstructed results with noise for case 1. The reconstructed phase boundaries are shown in Figure 4.7. Void location and size estimation is shown in figure 4.8 and 4.9. RMSE for boundary coefficients is shown in figure 4.10. From figures (4.7~4.10), it can be noticed EM has better estimation performance of phase boundaries, void location and size. The initial parameters used in the numerical simulation for case 1 are shown in Table 4.1.

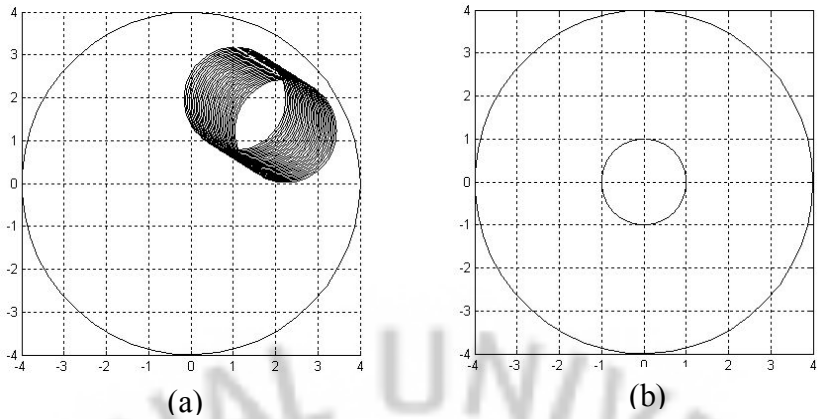

Figure 4.2. Numerical results for case 1 (moving scenario) (a) generated scenario (b) initial guess.

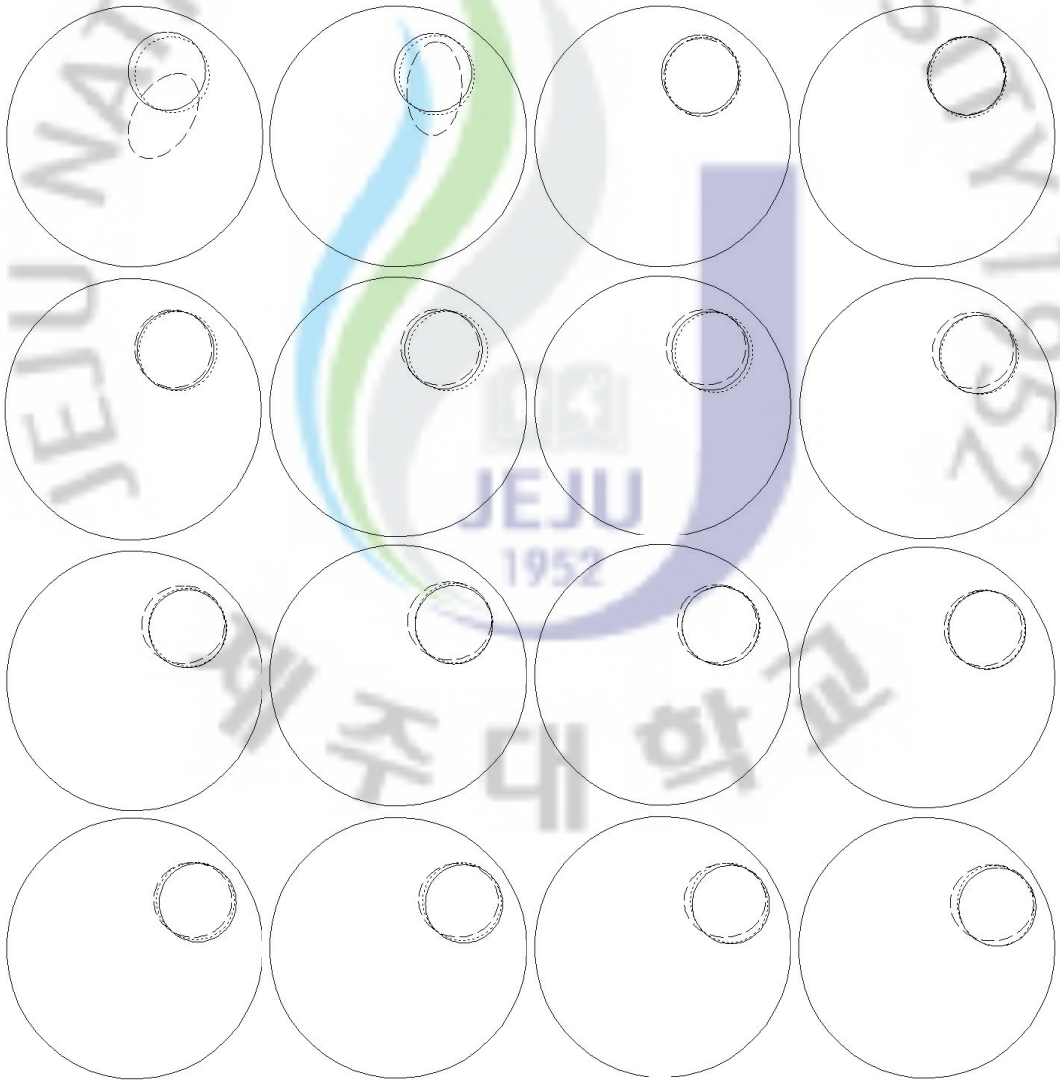

Figure 4.3. Reconstructed phase boundary estimation for case 1 without noise. Alternate images have been displayed. Solid line represents the true boundary, dotted line is with EM algorithm and dashed line is using EKF.

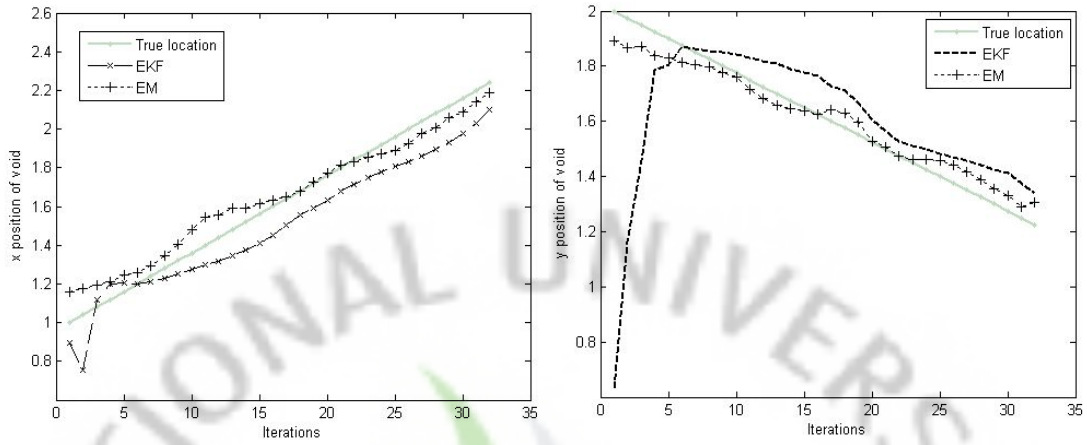

Figure 4.4. Estimation of boundary location for case 1 without noise (a) x position (b) y position.

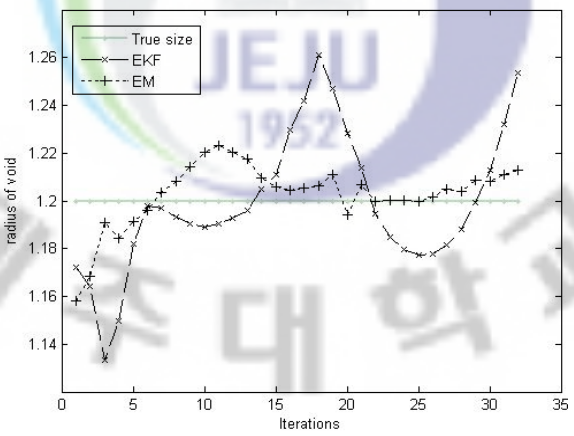

Figure 4.5. Void size estimation for case 1 without noise.

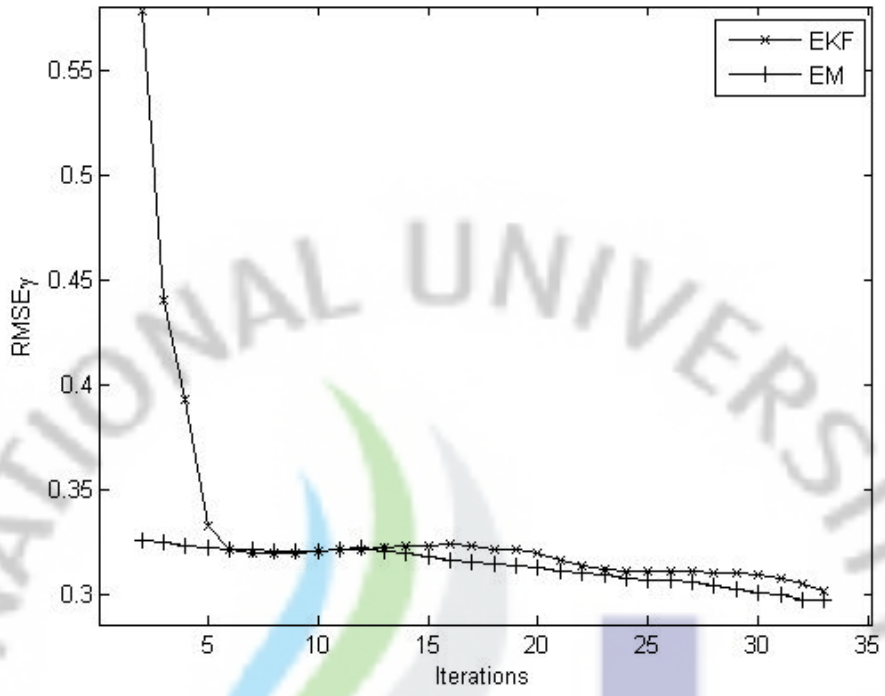

Figure 4.6. RMSE of estimated Fourier coefficients for case 1 without noise.

Table 4.1. Initial settings of model parameters used in EM and EKF for case 1.

Parameters	Noise	
	0 %	2 % white Gaussian Noise
F	$I_M \in \Re^{M\times M}$	$I_M \in \Re^{M\times M}$
Q	$0.01I_M$	$0.05I_M$
R	$500I_L$	$1000I_L$
$C_{0\|0}$	I_M	I_M

Figure 4.7. Reconstructed phase boundary estimation for case 1 with 2% noise. Alternate images have been displayed. Solid line represents the true boundary, dotted line is with EM algorithm and dashed line is using EKF.

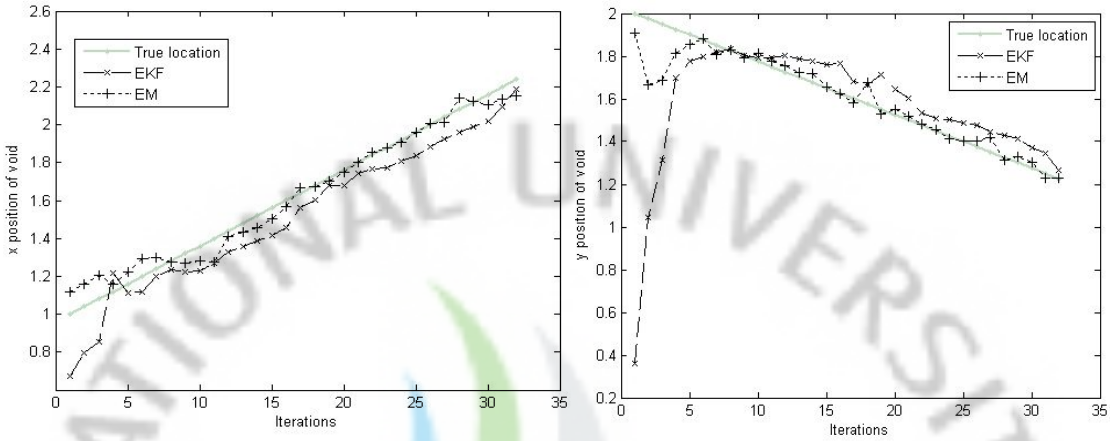

Figure 4.8. Estimation of boundary location for case 1 with 2% noise (a) x position (b) y position.

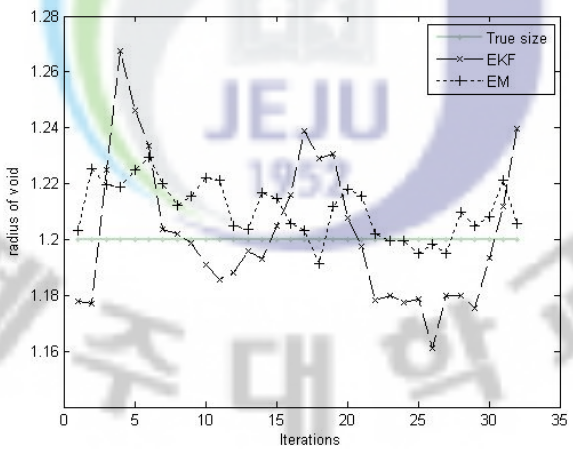

Figure 4.9. Void size estimation for case 1 with 2% noise.

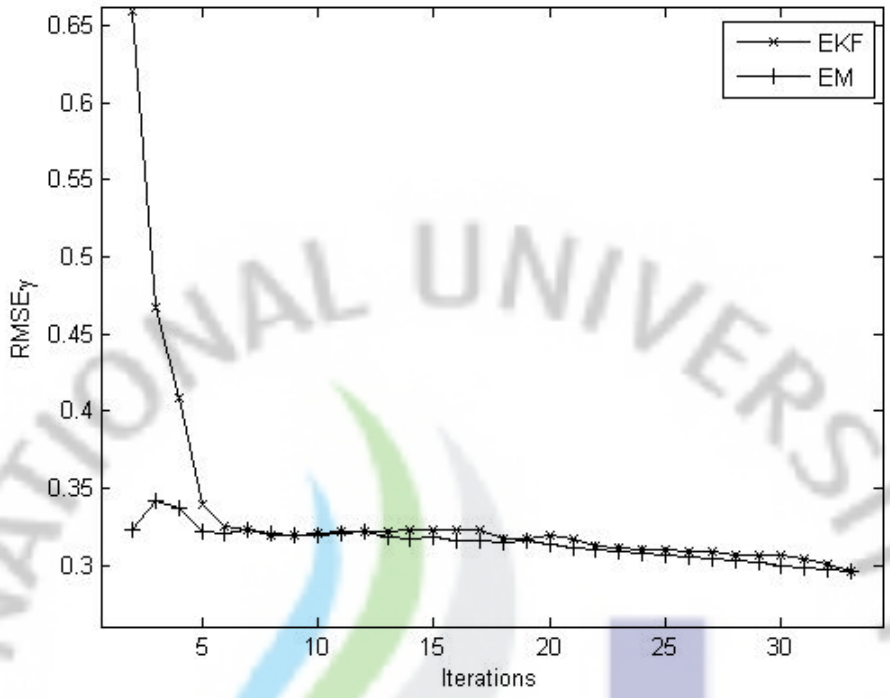

Figure 4.10. RMSE of estimated Fourier coefficients for case 1 with 2 % noise.

In case 2, (expansion contraction case), the void grows and shrinks at a given location. Two image frames are considered in which void expands during first frame and then it contracts in the next image frame (figure 4.11). The reconstructed phase boundary for case 2 is shown in figure 4.12. EKF is seen to lag and takes a long time to reach the true position. It also fails in estimating the expansion changes. However, EM performs well during void expansion. In the case of second frame, where it contracts, EKF is found to lags behind EM in tracking the boundary. Figures (4.13) and (4.14) show the estimation of location and size of the void. EM has been able to estimate the location and size of the void with good accuracy. RMSE for boundary coefficients is shown in figure 4.15. EM demonstrates better estimation of the Fourier coefficients compared to EKF, therefore, lower RMSE values are registered for EM as compared to EKF. The reconstructed results for case 2 with noise are shown in Figures (4.16~4.19). EM shows better estimation performance in case 2 with noise. As shown in no-noise case, the EKF has been found to lag in tracking the void boundary in expansion process (figure 4.16). The estimation of location (figure

4.17) and size (figure 4.18) of the void reveals better performance of EM. Moreover, as expected, the RMSE values of EM are lower than that of EKF (figure 4.19). The initial parameters used in the numerical simulation for case 2 are shown in Table 4.2.

In case 3, (moving and expanding case), the void changes its position and shape with time (figure 4.20(a)). In this case, we have chosen an ellipse located at center as initial guess figure 4.20(b). The reconstructed phase boundary for case 3 is shown in figure 4.21. EM is able to track the fast changes in the size and location of void better than EKF. The estimation of void location and size for case 3 is shown in figure 4.22 and 4.23. EM tracks the true location trajectory with good accuracy as compared to EKF. The void expands at a faster rate, therefore, the size is estimated less than the actual size by EM and EKF. RMSE for Fourier coefficients is shown in figure 4.24. EM shows better estimation of location as well as the size, therefore, EM has lower RMSE values compared to EKF. The estimation of phase boundary (its location and size) for case 3 with noise is given in figures (4.25~4.27). EM has better estimation of phase boundary in the presence of noise and it can easily be noticed that the location as well as size of the void has been tracked well. The RMSE is shown in figure 4.28 and it is noticed that EM has good approximation of Fourier coefficients. The initial parameters used in the numerical simulation for case 3 are shown in Table 4.3.

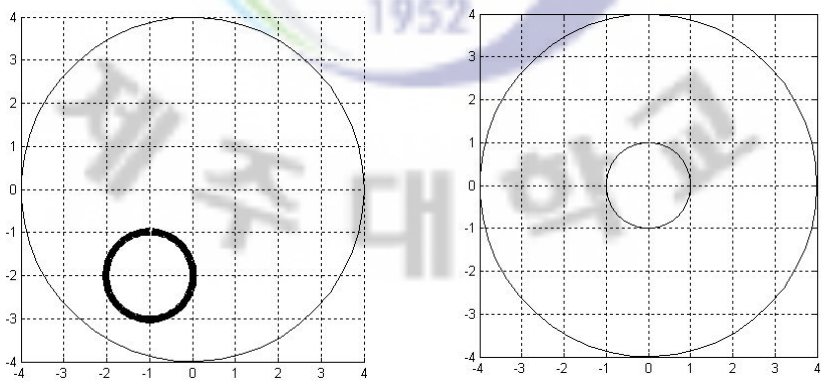

Figure 4.11. Numerical results for case 2 (expanding-contracting scenario) (a) generated (b) initial guess.

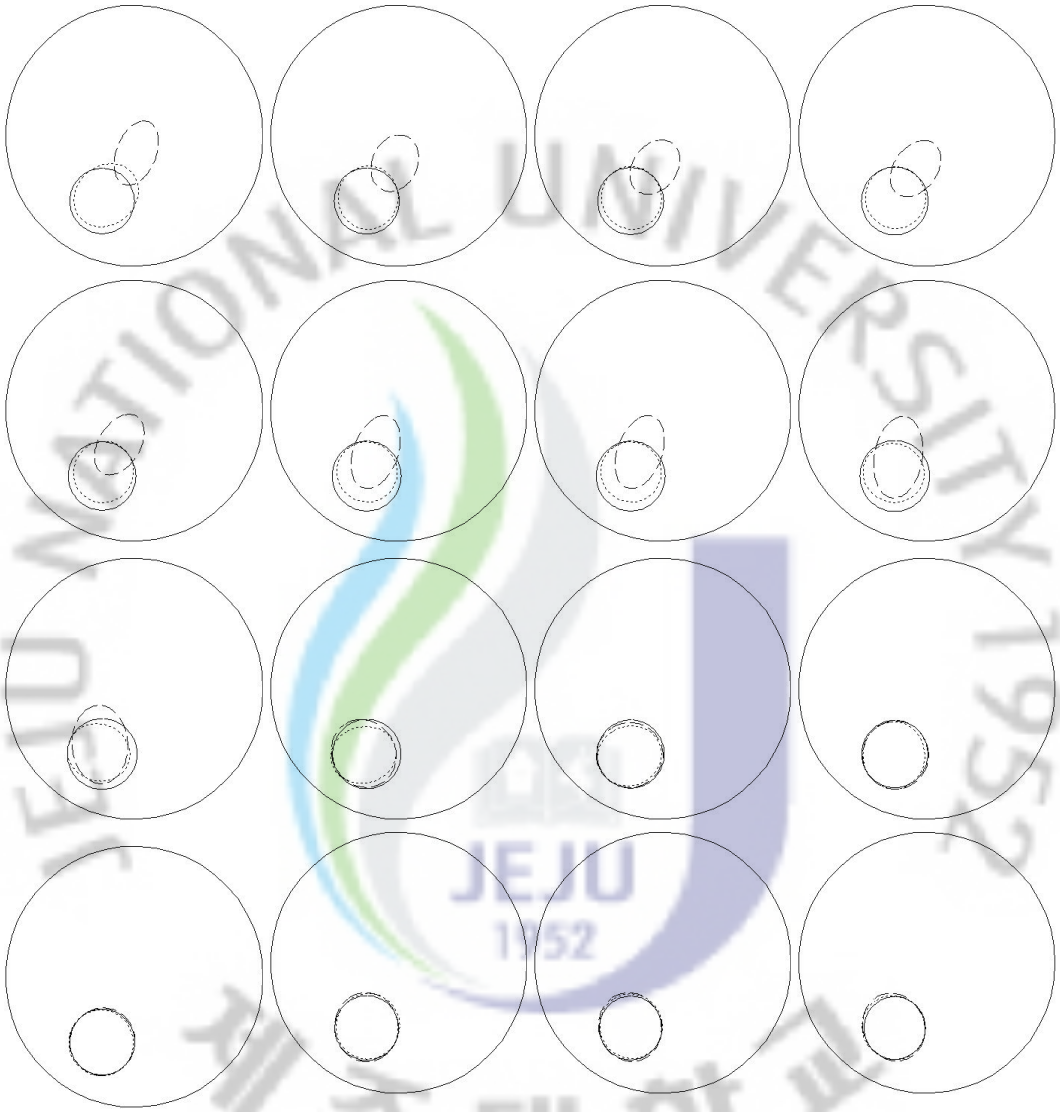

Figure 4.12. Reconstructed phase boundary estimation for case 2 without noise. Alternate images have been displayed. Solid line represents the true boundary, dotted line is with EM algorithm and dashed line is using EKF.

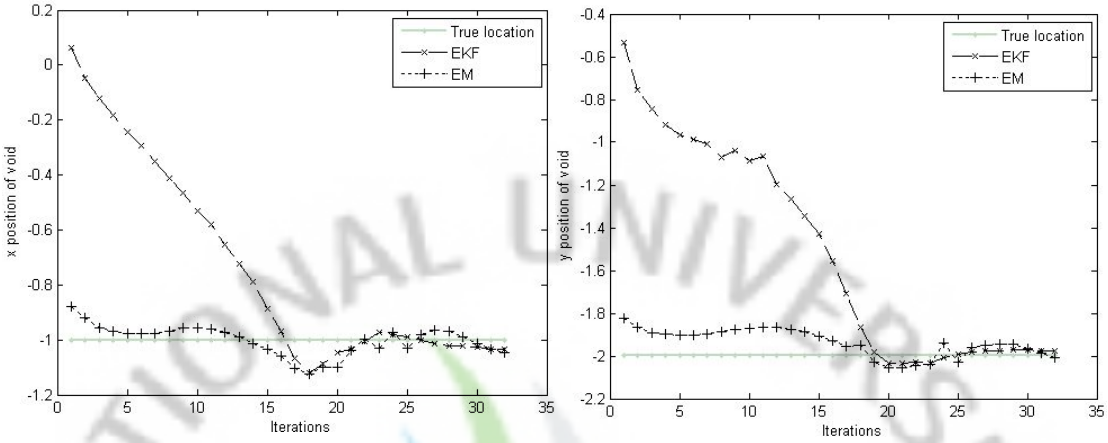

(a) (b)

Figure 4.13. Estimation of boundary location for case 2 without noise (a) x position (b) y position.

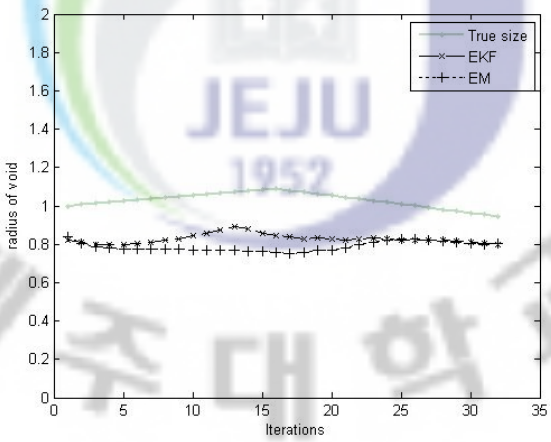

Figure 4.14. Void size estimation for case 2 without noise.

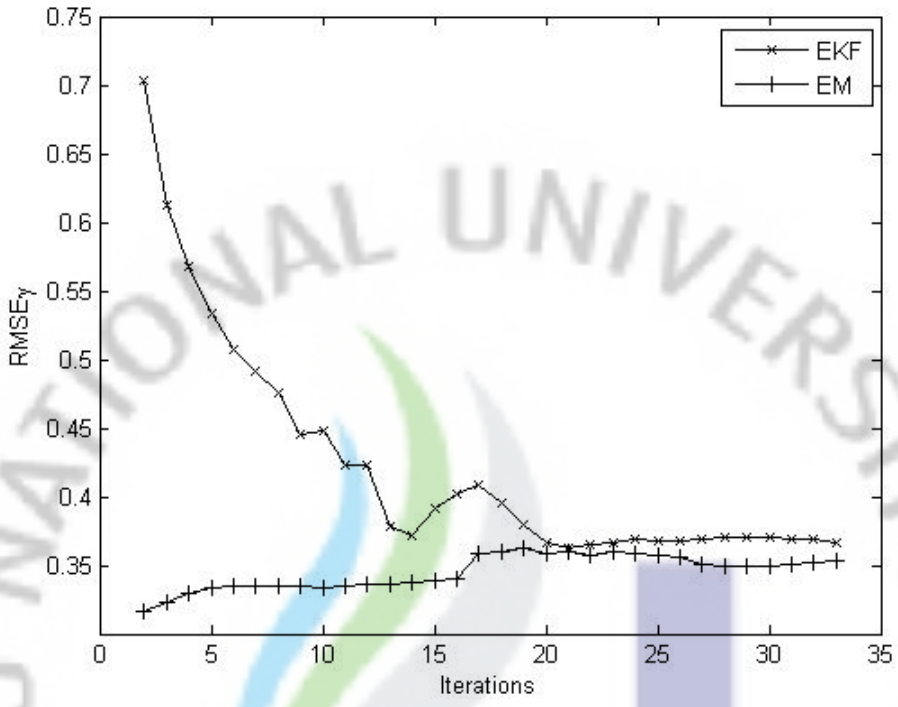

Figure 4.15. RMSE of estimated Fourier coefficients for case 2 without noise.

Table 4.2. Initial settings of model parameters used in EM and EKF for case 2.

Parameters	Noise	
	0 %	2 % white Gaussian Noise
F	$I_M \in \Re^{M\times M}$	$I_M \in \Re^{M\times M}$
Q	$0.01I_M$	$0.01I_M$
R	$5I_L$	$100I_L$
$C_{0\|0}$	I_M	I_M

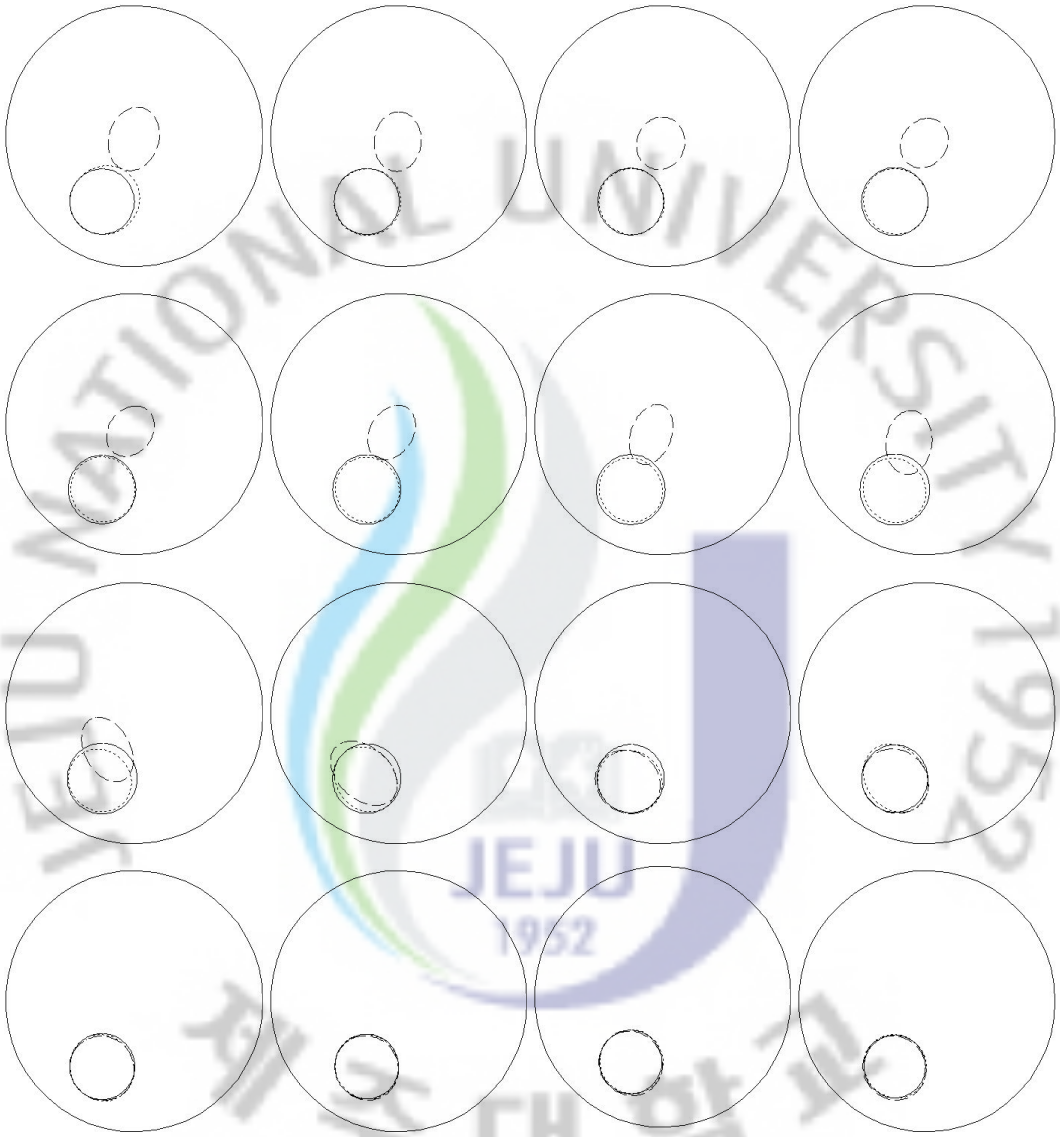

Figure 4.16. Reconstructed phase boundary estimation for case 2 with 2% noise. Alternate images have been displayed. Solid line represents the true boundary, dotted line is with EM algorithm and dashed line is using EKF.

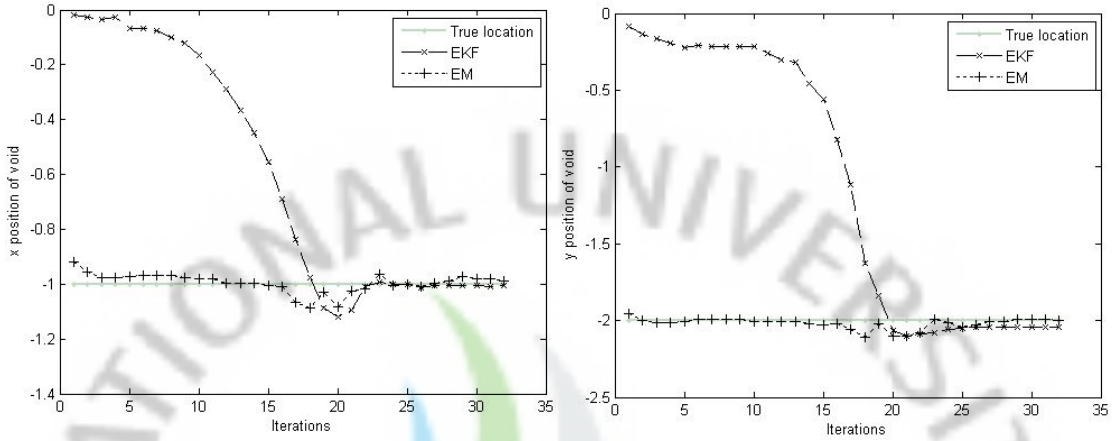

(a) (b)

Figure 4.17. Estimation of boundary location for case 2 with 2% noise (a) x position (b) y position.

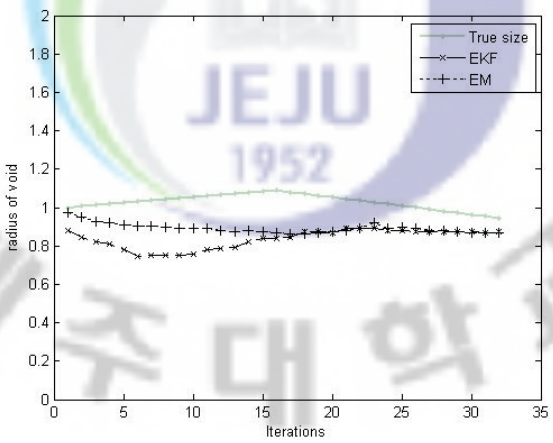

Figure 4.18. Void size estimation for case 2 with 2% noise.

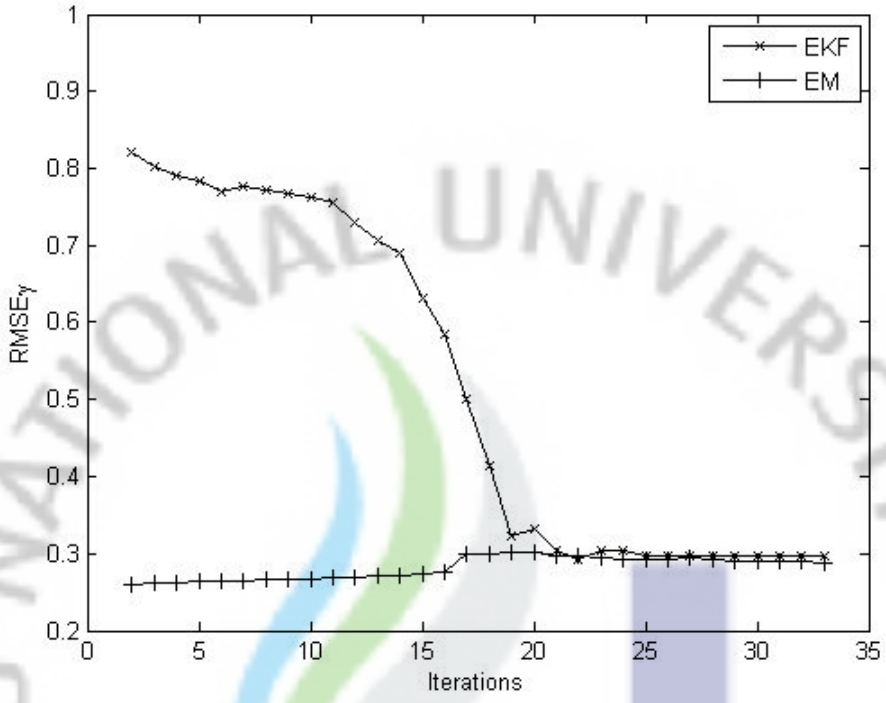

Figure 4.19. RMSE of estimated Fourier coefficients for case 2 with 2 % noise.

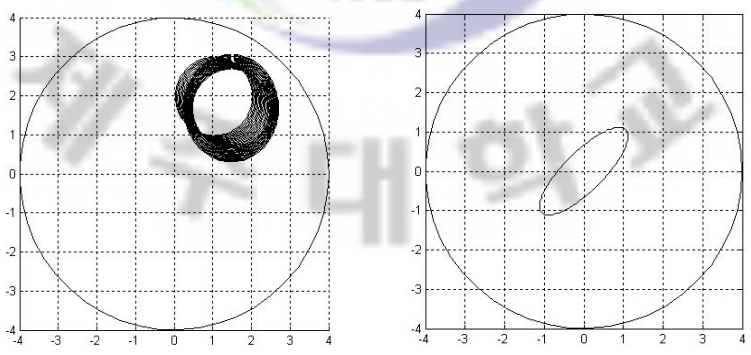

(a) (b)

Figure 4.20. Numerical results for case 3 (moving-expanding scenario) (a) generated scenario (b) initial guess.

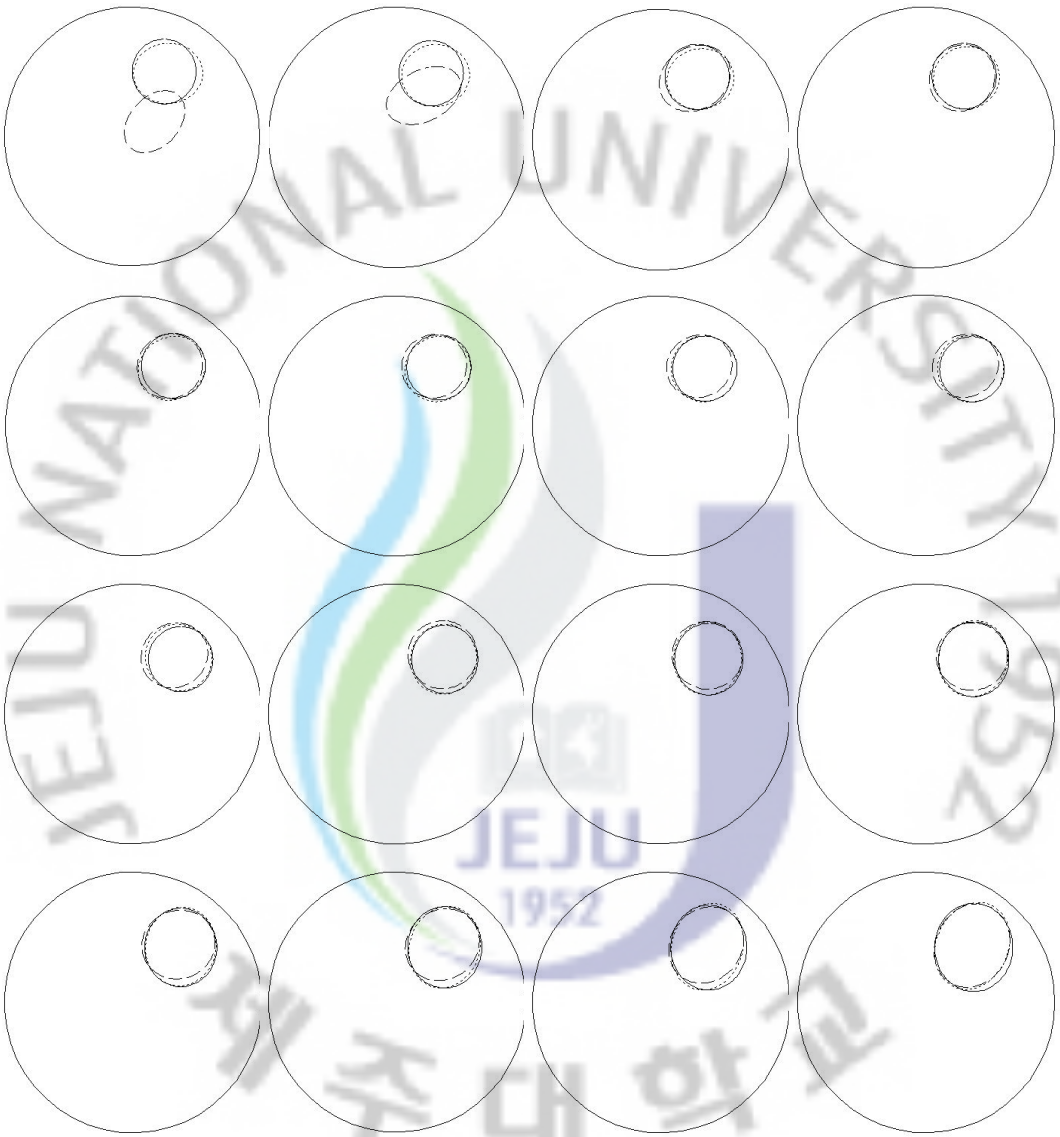

Figure 4.21. Reconstructed phase boundary estimation for case 3 without noise. Alternate images have been displayed. Solid line represents the true boundary, dotted line is with EM algorithm and dashed line is using EKF.

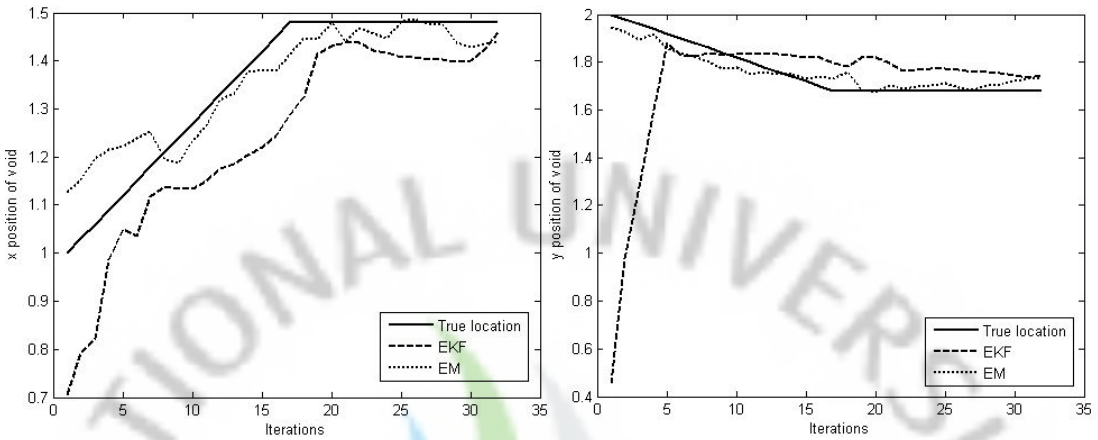

(a) (b)

Figure 4.22. Estimation of boundary location for case 3 without noise (a) x position (b) y position.

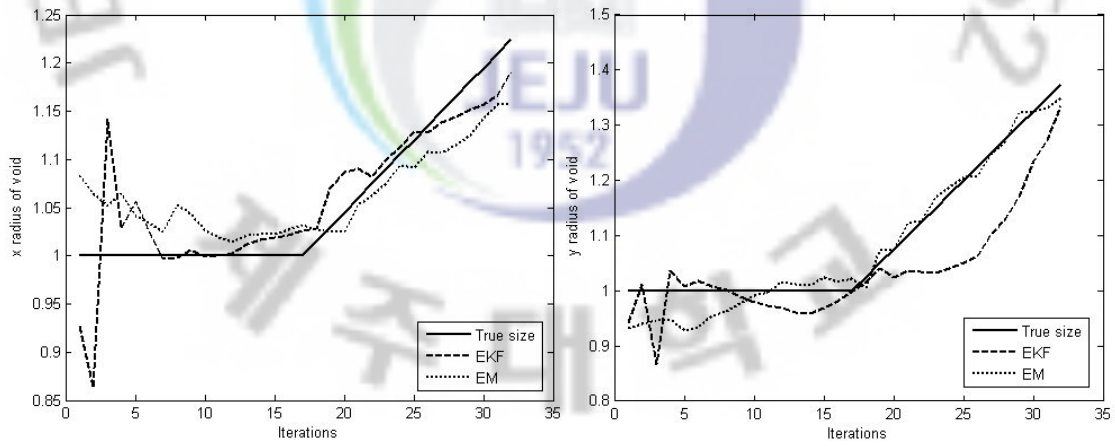

(a) (b)

Figure 4.23. Void size estimation for case 3 without noise (a) radius along x direction (b) radius along y direction.

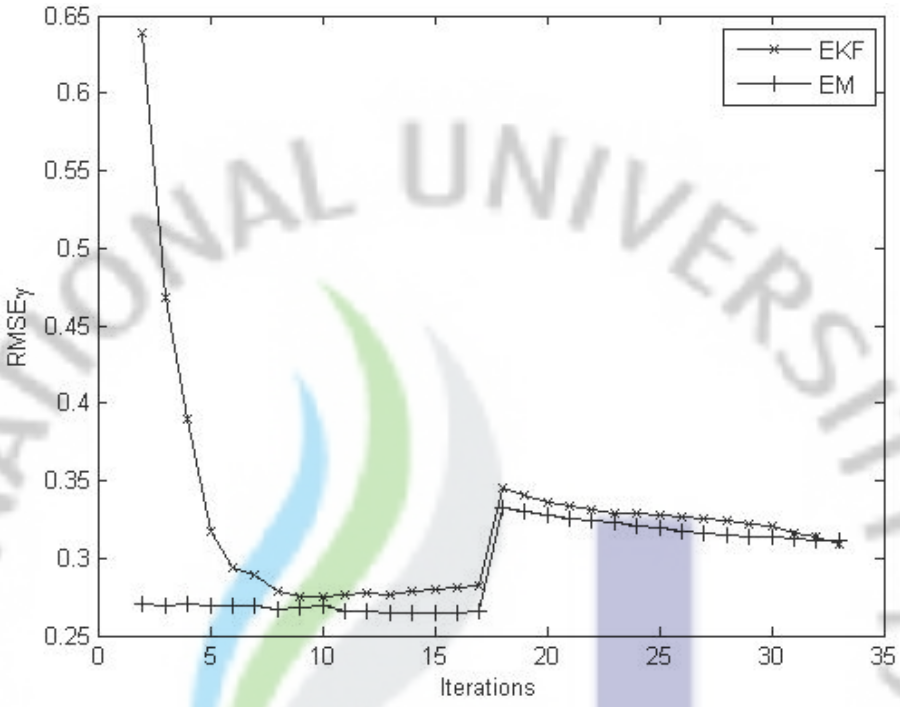

Figure 4.24. RMSE of estimated Fourier coefficients for case 3 without noise.

Table 4.3. Initial settings of model parameters used in EM and EKF for case 3.

Parameters	Noise	
	0 %	2 % white Gaussian Noise
F	$I_M \in \Re^{M\times M}$	$I_M \in \Re^{M\times M}$
Q	$0.005I_M$	$0.01I_M$
R	$500I_L$	$500I_L$
$C_{0\|0}$	I_M	I_M

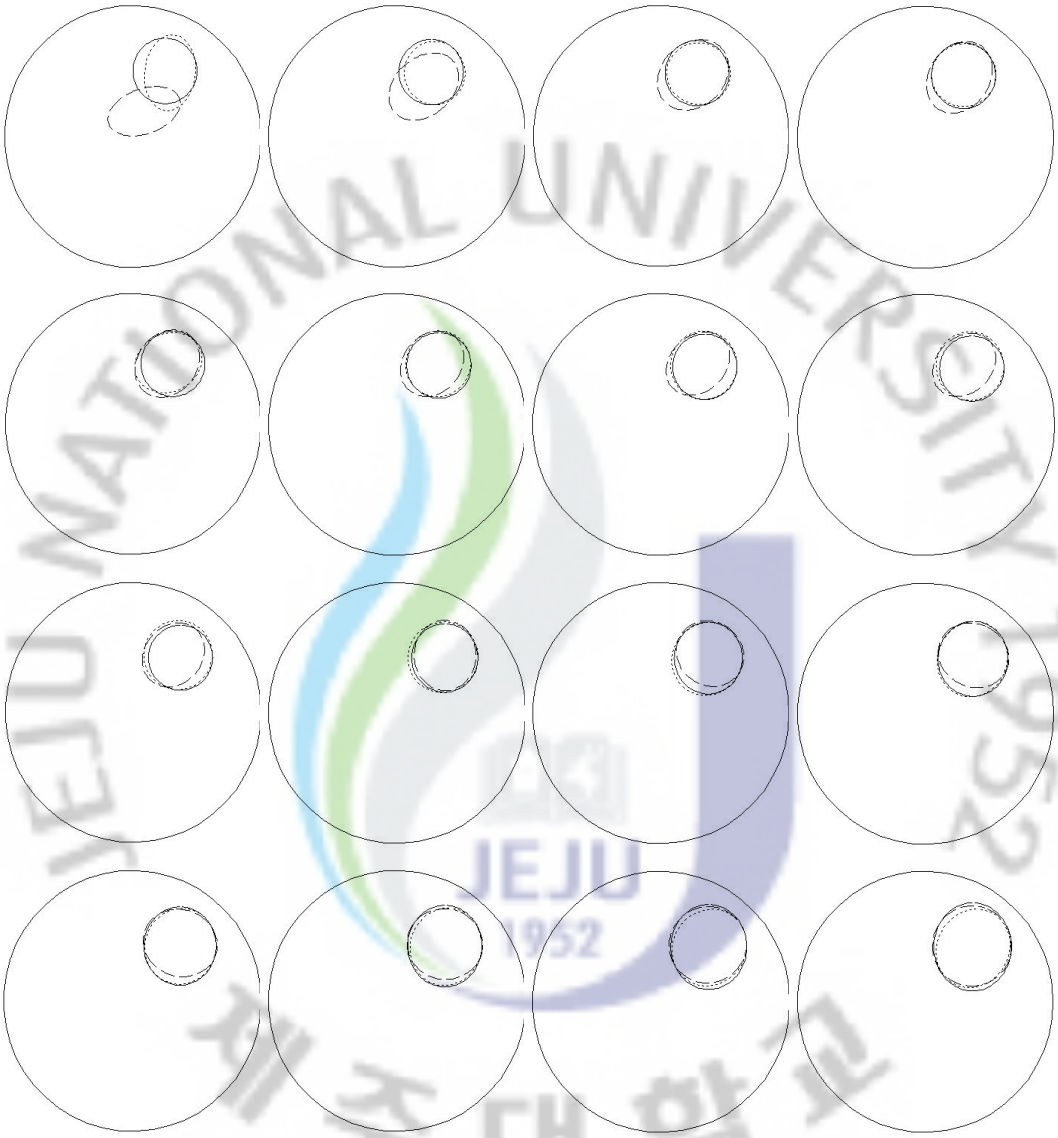

Figure 4.25. Reconstructed phase boundary estimation for case 3 with 2% noise. Alternate images have been displayed. Solid line represents the true boundary, dotted line is with EM algorithm and dashed line is using EKF.

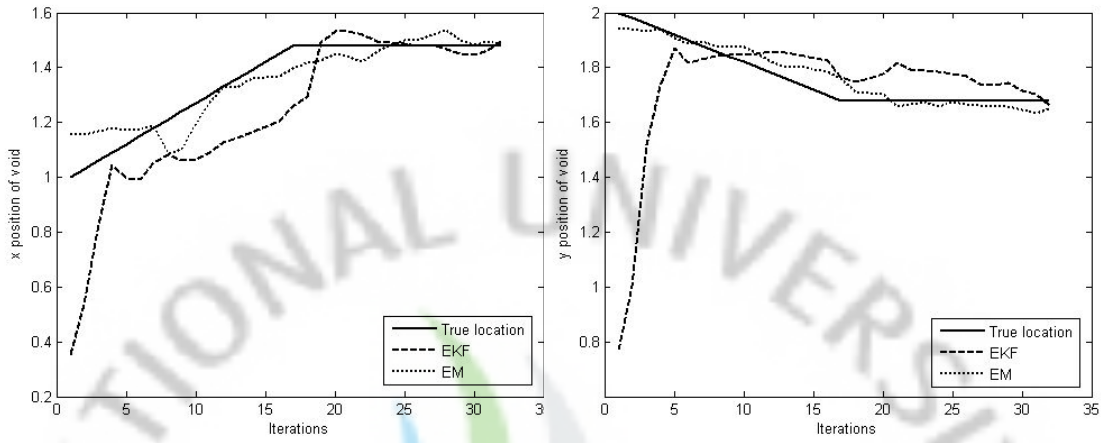

(a) (b)

Figure 4.26. Estimation of boundary location for case 3 with 2% noise (a) x position (b) y position.

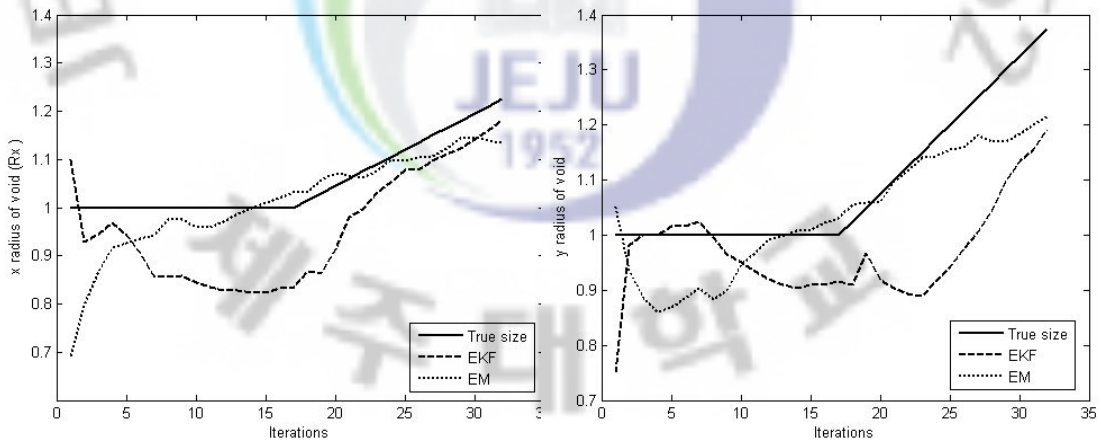

(a) (b)

Figure 4.27. Void size estimation for case 3 with 2% noise (a) radius along x direction (b) radius along y direction.

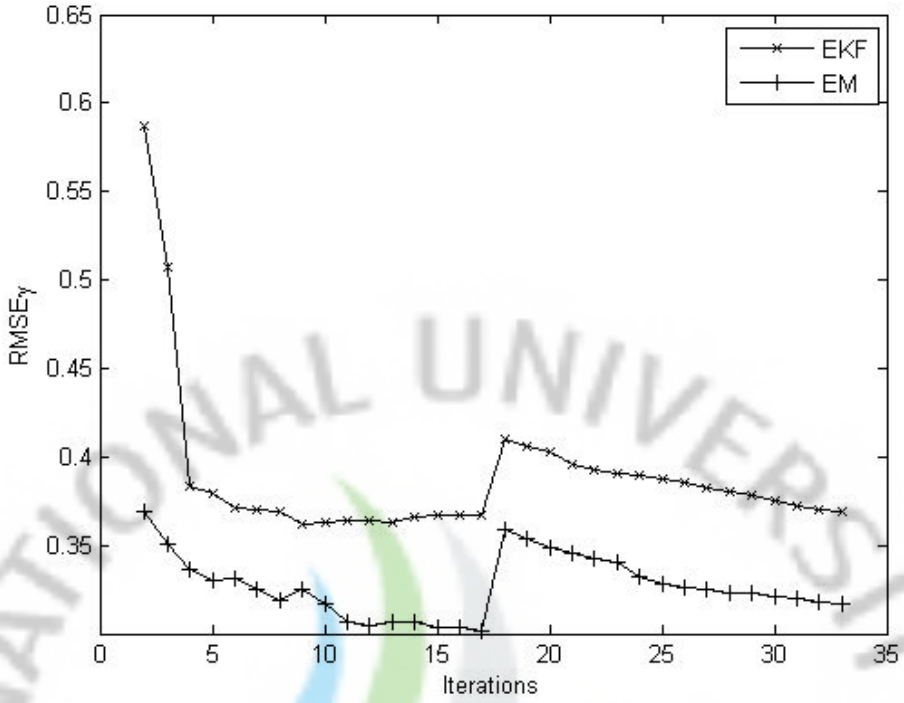

Figure 4.28. RMSE of estimated Fourier coefficients for case 3 with 2 % noise.

4.3.2 Results with experiment data

The visualization of two-phase flows is carried out using the experimental setup as shown in figure 4.29. The experiments are carried out using an experimental phantom in our laboratory. The measurement setup consists of Agilent 4284A precision LCR meter used as a current source and for data acquisition Agilent 43970A with 60-channel high speed data acquisition multimeter is used. The phantom used is of circular type with a radius of 40 mm and for injecting current and measuring voltages 32 stainless steel electrodes each of width 6 mm and 200 mm height are placed around its periphery.

Brine solution of resistivity 300 Ωcm is filled inside the phantom. Plastic rods made of acryl which have infinite conductivity can be used in place of voids to visualize two-phase flow conditions. Acryl rods are placed at various locations inside the phantom during the experiment. Opposite method is used as a current injection mode. In such case, for 32 electrode configuration, we have 32 × 16 measurements available in each frame. Current of magnitude 10 mA is applied across the electrodes and the corresponding voltages are measured. Experiment is performed by moving

the plastic rods at four different locations inside the phantom. The position at which the plastic rod is placed is shown in figure 4.29(c). The position is changed at every eight current patterns. The data obtained is then tested with EM algorithm and is compared against EKF. In solving inverse problem, there is no prior information about the location and size of the void. Therefore as an initial guess a circular boundary with radius 1.1 cm located at the center is chosen. Mesh with 2121 nodes and 3984 triangular elements is used for testing the data.

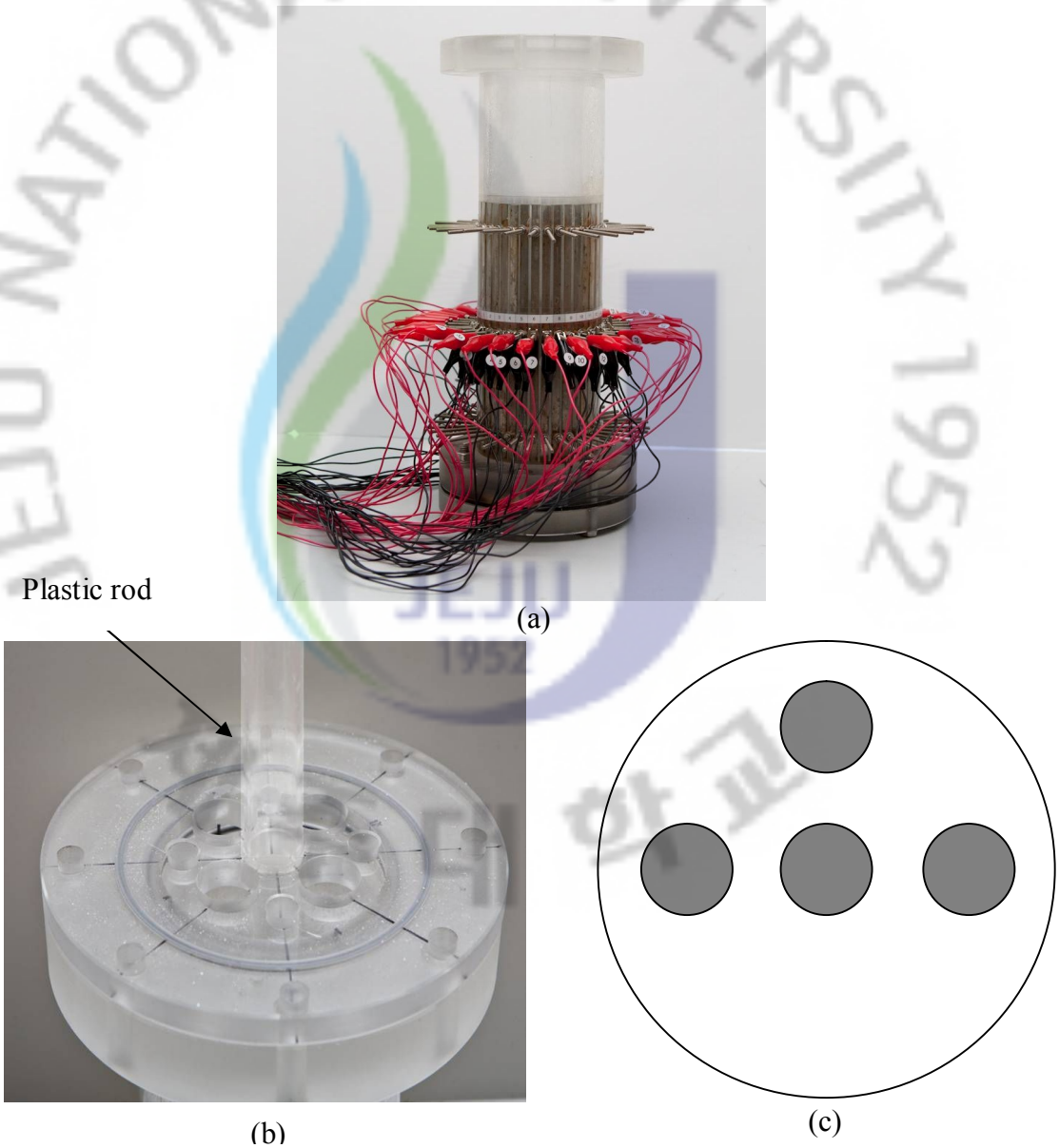

Figure 4.29. EIT measurement system used for two-phase flow visualization (a) phantom used for experiment; (b) plastic rod used as target; and (c) positions where the plastic targets are placed.

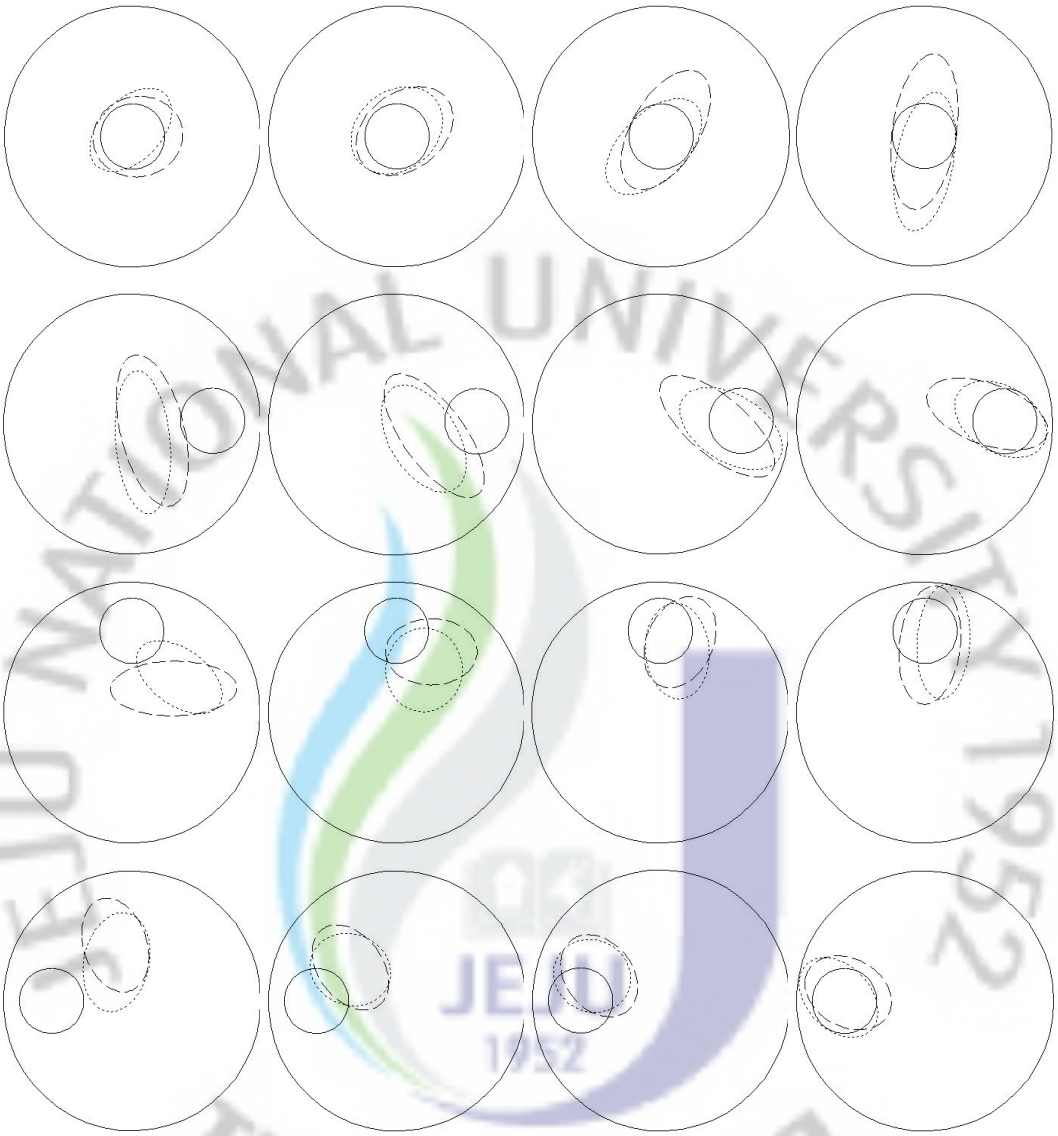

Figure 4.30. Reconstructed phase boundary with experimental data using circular plastic rod. Each row corresponds to different location of plastic rod. Alternate images have been displayed. Solid line represents the true boundary, dotted line is with EM algorithm and dashed line is using EKF.

The reconstructed phase boundary of the plastic rods with experiment data is shown in figure 4.29. In center location the sensitivity is very low, therefore, the size is found to estimate a bigger by both EM and EKF. In other locations, boundary is tracked reasonably well using EM. The estimated location and size of plastic rod is shown in figures (4.30, 4.31). EM has tracked the changes of the plastic rod better as compared to EKF. RMSE is plotted for the estimated Fourier coefficients and it is

found that EM has lower RMSE values than EKF (figure 4.32). The results show that performance of EKF is improved by estimating the model parameters using EM to reduce the uncertainty.

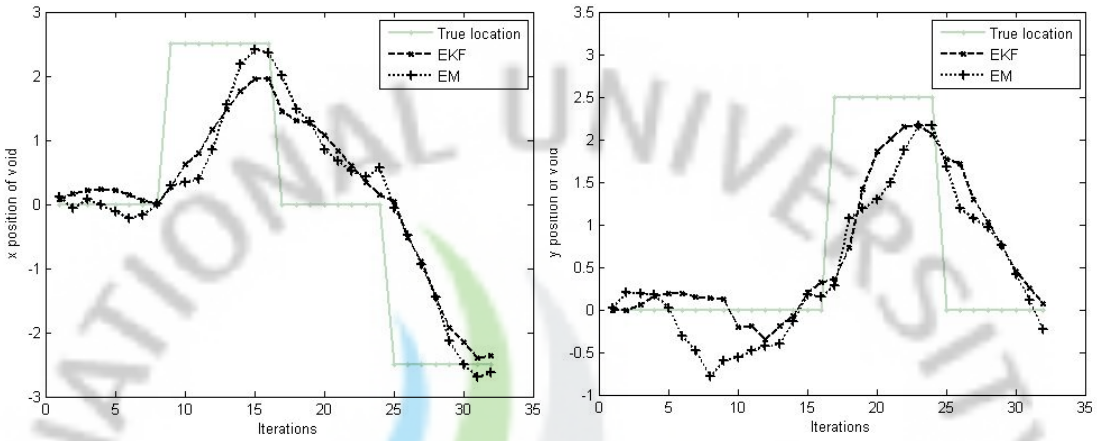

Figure 4.31. Estimation of plastic rod position placed inside the phantom (a) x position (b) y position.

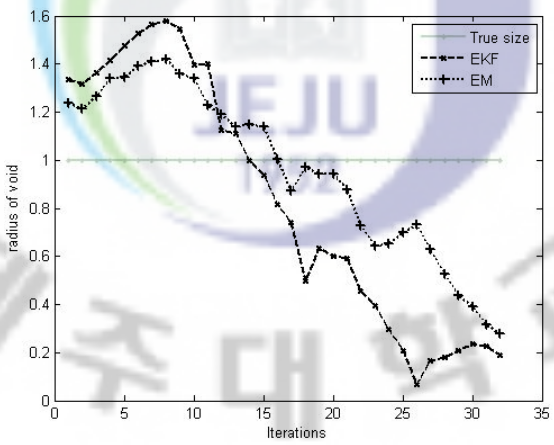

Figure 4.32. Size estimation of plastic rod placed inside the phantom.

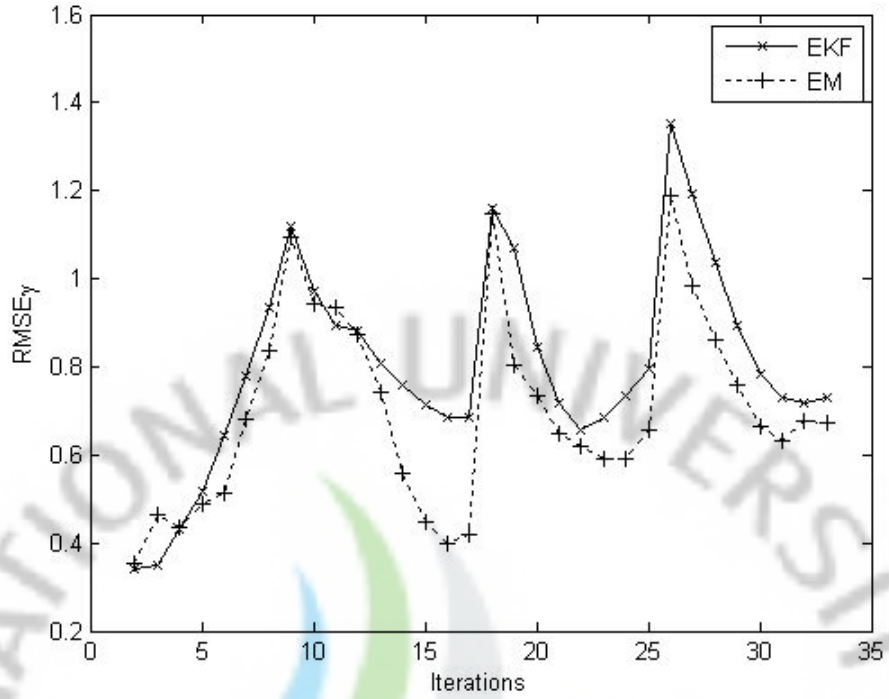

Figure 4.33. RMSE of estimated Fourier coefficients for experimental case.

Table 4.4. Initial settings of model parameters used in EM and EKF for experiment data.

F	Q	R	$P_{0\|0}$	$\gamma_{0\|0}$
$I_\Lambda \in \Re^{\Lambda\times\Lambda}$	$0.5I_\Lambda$	$500I_\Lambda$	$0.5I_\Lambda$	(0,0) r = 1.1

In conventional maximum likelihood estimation procedure, the log-likelihood condition (4.30) is used along with the nonlinear methods to solve for system parameters. These methods are difficult to implement and need to compute the inverse matrix of second order partial equations. Also, these methods do not increase the log-likelihood function value. However, with (4.39~4.43) the model parameters are estimated using EM. These are simple to implement as they are just multivariate regression calculations. The better estimation performance of EM is achieved at the expense of additional computational effort needed to calculate the smoothed estimates $\gamma_{k|n}$, $P_{k|n}$, $P_{k,k-1|n}$ needed to compute model parameters. For this one requires to apply backward recursions where as conventional method need forward

computations to compute (4.30). In the conventional methods, for solving maximum likelihood function, it requires a set of derivates for $\gamma_{k|n}$, $P_{k|n}$ to solve for model parameters which also takes comparable amount of computation.

4.4 Discussion

This paper presents application of expectation maximization algorithm to EIT in estimating the region boundaries in the flow field. The voids formed in the flow field are not stable and move randomly inside the process vessel. In the situations like two-phase flows, the model parameters are difficult to model in a prior form and therefore the algorithms which assume the predefined model parameters (EKF) would not perform satisfactorily. Expectation algorithm, which is a maximum likelihood based estimator, can estimate the model parameters with uncertainty. These estimated model parameters, when used with EKF, improve the estimation performance significantly. The EM algorithm is formulated for the boundary estimation of two-phase flows. Numerical and experimental tests are performed to test the performance of the proposed method. It is found that the performance of EM is better when compared with EKF.

5. Estimation of moving interfacial boundary using expectation maximization algorithm

Flow of two immiscible fluids through pipelines is of importance in several process tomography applications. For example, in petroleum industry it is important to know the amount of water present in the crude oil which is transported. The two fluids are separated by an interfacial boundary and the boundary changes with respect to time. Estimation of the time varying interfacial boundary is very important for the design and monitoring of the process (Fairuzov 2000). EIT is found promising in many tomography applications due to its non intrusive and high data acquisition rate. If the conductivity distribution of the flow field is known *a priori*, then the inverse problem can be transformed to a boundary estimation problem in which the interfacial boundary is estimated based on the voltage measurements. For the application of EIT to estimate the open boundary or free surface, see (Tossavainen *et al.* 2004). In two-phase flows, the interfacial boundary changes before the time to acquire complete set of independent data, therefore, dynamic estimation algorithms are necessary to track the fast changes (Ijaz *et al*. 2008). In (Kim *et al*. 2007b), EKF has been used to track the fast moving interfacial boundary. The interfacial boundary is represented using front points and the front points are treated as the state variables to be estimated. Sensitivity analysis is done by varying the number of front points and the contrast ratio between the two fluids. In EKF, the state distribution is approximated by Gaussian random variable (GRV) and is propagated through a linear approximation of system around the operating point at each time instant. Linearization can only be applied if the Jacobian matrices can be formulated. However, some systems contain discontinuities and the representation of phase interface can be complex. In such cases, derivation of Jacobian matrices is often difficult (Julier *et al.* 2004). Furthermore, this linear approximation causes error in posterior mean and covariance of the transformed GRV. This result in sub-optimal performance and may lead the state to diverge over time. To overcome the limitations with EKF, the unscented transform (UT) was developed as a method to propagate mean and covariance information through a nonlinear transformation (Julier *et al.* 2004). The Kalman filter

based on UT is called as UKF. Ijaz *et al*. (2008) applied UKF to estimate the moving interfacial boundary and compared the performance against EKF. The results show a promising performance of UKF over EKF.

In these Kalman type filters such as EKF or UKF, the model parameters such as the initial states, the state transition matrix, and the noise covariance matrices have to be known in advance. Measurement noise covariance can be computed through experiments. However, the evolution of the interface is complex in real situations therefore it is difficult to represent the state evolution matrix as a prior form as in case of kinematic models. Also, the process noise heavily depends up on the environment surrounding the target. In practical situations, where there is a lot of uncertainty involved, the standard algorithms based on Kalman-type do not give desirable performance. This uncertainty can be overcome with the help of expectation maximization algorithm. In this study, we employ expectation maximization algorithm to estimate the model parameters. The estimated model parameters are then used in EKF to estimate the time varying interfacial boundary. Numerical and experimental studies are performed to evaluate the performance of the proposed method and then it is compared against conventional EKF. Results show promising performance of EM compared to EKF.

5.1 Boundary representation

Consider a stratified two-phase flow through a horizontal circular pipe as shown in figure 5. 1. The two fluids flowing through the pipe are separated by an interfacial boundary. Several methods have been proposed to represent the open boundary between two fluids (Butler and Bonnecase 2000, Tossavainen *et al.* 2004, Tossavainen *et al*. 2006a, Kim *et al*. 2007b, Khambampati *et al*. 2009). Butler and Bonnecaze (2000) considered an open channel filled with conducting liquid and the open boundary was characterized by Chebyshev polynomials, whose coefficients were to be estimated. Another method involves representing the boundary using the mesh nodes and a Bézier curve for the application where a pipe is partially filled with water and has air slug filled in the other portion. A more attractive method has been presented in (Kim *et al.* (2007b)) where the interface is represented with discrete

front points. In this study we also use the same representation as in Kim *et al.* (2007b). Below we describe the front point description of the interface.

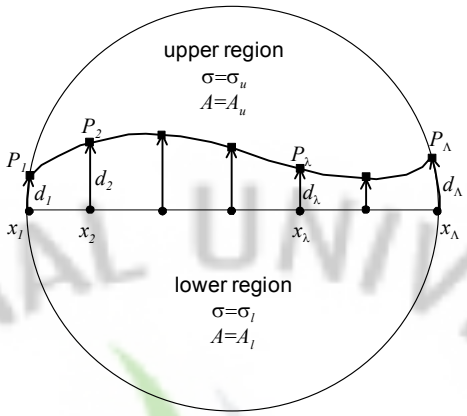

Figure 5.1. Representation of open boundary between two immiscible fluids.

The open boundary between two immiscible liquids is approximated as an interpolation with discrete front points P_λ , $\lambda = 1,2,\cdots,\Lambda$ located on the boundary (Kim *et al*. 2007b). The total number of the front points is Λ . P_1 and P_Λ are the leftmost and the rightmost front points, respectively. The front points are expressed in terms of d_λ . Excluding the end front points, the intermediate front points ($\lambda = 2,...,\Lambda - 1$) are denoted by the vertical distance from the reference point X_λ . The end points are characterized by the arc length in order to restrict the interface to the outer surface of the pipe. The front points on the interface are represented as follows

$$(X_1, Y_1) = \left(-R\cos\frac{d_1}{R}, R\sin\frac{d_1}{R} \right) \tag{5.1}$$

$$(X_\lambda, Y_\lambda) = (x_\lambda, d_\lambda), \ \lambda = 2,\cdots,\Lambda - 1 \tag{5.2}$$

$$(X_\Lambda, Y_\Lambda) = \left(R\cos\frac{d_\Lambda}{R}, R\sin\frac{d_\Lambda}{R} \right). \tag{5.3}$$

The parameter to be estimated is written in the form

$$d = (d_1, d_2, \cdots, d_\Lambda)^{\mathrm{T}} \in \Re^\Lambda. \tag{5.4}$$

Let us assume that the region Ω is divided into disjoint regions S_k given by,

$$\Omega = \bigcup_{k=1}^{2} S_k , \tag{5.5}$$

where two regions exist in domain ($k = 1,2$) as shown in figure 5.1. If $\chi_k(r)$ denotes the characteristic function of sub region S_k, the conductivities of each layer can be expressed as

$$\sigma = \sum_{k=1}^{2} \sigma_k \chi_k(r). \tag{5.6}$$

By substituting (5.5) into FEM formulation we get

$$\mathbf{B}(i,j) = \sum_{k=1}^{2} \int_{\mathrm{supp}(\varphi_i \varphi_j) \cap S_k} \sigma_k \nabla \varphi_i \cdot \nabla \varphi_j d\Omega + \sum_{l=1}^{L} \frac{1}{z_l} \int_{e_l} \varphi_i \varphi_j dS, \quad i,j = 1,2,\cdots,N, \tag{5.7}$$

where $\mathrm{supp}(\varphi_i \varphi_j)$ is a part of domain Ω where both the basis functions are non-zero. The implementation of the integrals of the form (5.7) has been described previously in (Kolehmainen *et al.* 2001, Tossavainen *et al.* 2006, 2007). In the first step, mesh elements Ω_m are classified into the set of elements inside the region $S_k (k = 1,2)$ and the set of elements intercepted by the boundary C (figure 5.2). For the elements that lie in the region S_k, they are assigned their corresponding conductivity values σ_k, however, for the elements that lie on the boundary C, the area weighted conductivity values σ_e are assigned as

$$\sigma_e = \frac{\sigma_1 A_1 + \sigma_2 A_2}{A_1 + A_2}, \tag{5.8}$$

where A_1 and A_2 denote the area of the region above and below the interface, respectively (Figures 5.3(a)-(d)).

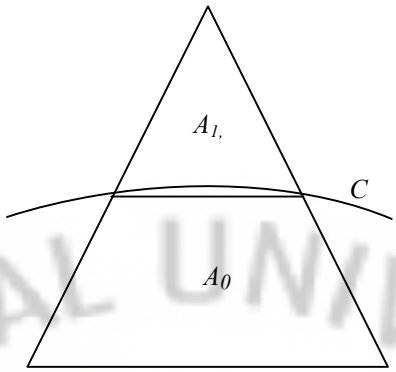

Figure 5.2. Mesh element crossing the interfacial boundary.

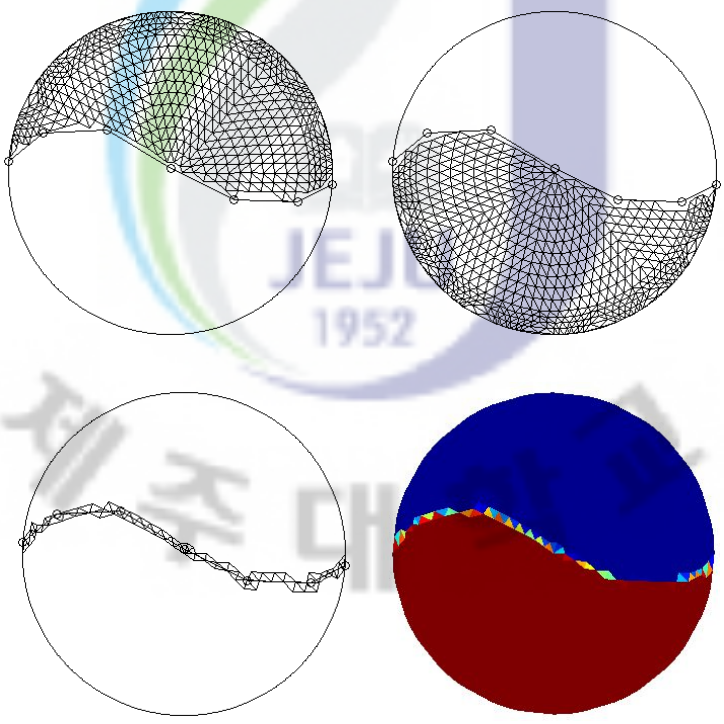

Figure 5.3. Element classification for boundary estimation (a) elements lying above the boundary interface (b) elements lying below the interface (c) elements crossing the boundary interface (d) final conductivity profile of the flow domain.

5.2 Inverse problem

5.2.1 State estimation approach to estimate the moving interfacial boundary

In order to estimate the fast moving changes in the flow process we have to adopt a dynamic estimation approach. The estimation of the parameter d of a discrete-time controlled process is governed by the linear stochastic difference equation given by

$$d_k = F_{k-1} d_{k-1} + w_{k-1}, \tag{5.9}$$

with a measured voltage $V \in \Re^{E\times k}$ that is

$$V_k = U_k(d_k) + v_k, \tag{5.10}$$

where the subscript k is the time index, $F_k \in \Re^{\Lambda\times\Lambda}$ is the state transition model and U_k is the observation model and E is the number of measurement electrodes. The random variables $w_k \in \Re^{\Lambda}$ and $v_k \in \Re^{E}$ denote the process and the measurement noise, respectively. They are assumed to be independent of each other and are modeled as unbiased normal probability distribution

$$p(w_k) \sim N(0, Q_k) \tag{5.11}$$
$$p(v_k) \sim N(0, R_k), \tag{5.12}$$

where $Q_k \in \Re^{\Lambda\times\Lambda}$ and $R_k \in \Re^{E\times E}$ are the process and the measurement noise covariance, respectively. These equations (5.9) and (5.10) are called state-space model. For description about state space models, see chapter 3.

5.3 Interface boundary estimation with EM algorithm

5.3.1 Maximum likelihood function

For the state space representation given in (5.9-5.12), upon applying Markovian property, the likelihood function for the observations can be written as

$$
\begin{aligned}
L &= p(d_k, V_k \mid \theta) \\
&= p(d_0 \mid \theta)\prod_{k=1}^{n} p(d_k \mid d_{k-1}, \theta)\prod_{k=1}^{n} p(V_k \mid d_k, \theta).
\end{aligned} \tag{5.13}
$$

where we call $\theta = \{\mu, \Pi, F, Q, R\}$ the model parameters. Usually, these model parameters are set empirically through experiments. In this study, we use EM algorithm to estimate the model parameters as well as the front point variables representing the interfacial boundary.

5.3.2 Extended Kalman smoother

In Kalman smoother, it has two steps; one is the forward filtering process which is normal EKF computation, and then the backward smoothing considering the measurements *n* samples.

The forward computations for EKS are as follows

$$d_{k|k-1} = F_{k-1} d_{k-1|k-1} \tag{5.14}$$

$$P_{k|k-1} = F_{k-1} P_{k-1|k-1} F_{k-1}^{\mathrm{T}} + Q_{k-1} \tag{5.15}$$

$$K_k = P_{k|k-1} J_k^{\mathrm{T}} (J_k P_{k|k-1} J_k^{\mathrm{T}} + R_k)^{-1} \tag{5.16}$$

$$d_{k|k} = d_{k|k-1} + K_k (V_k - J_k d_{k|k-1}) \tag{5.17}$$

$$P_{k|k} = (I - K_k J_k) P_{k|k-1}. \tag{5.18}$$

The backward smoothing is done with the measurements available by

$$G_{k-1} = P_{k-1|k-1} F_k^{\mathrm{T}} (P_{k|k-1})^{-1} \tag{5.19}$$

$$d_{k-1|n} = d_{k-1|k-1} + G_{k-1}(d_{k|n} - F_k d_{k-1|k-1}) \tag{5.20}$$

$$P_{k-1|n} = P_{k-1|k-1} + G_{k-1}(P_{k|n} - P_{k|k-1}) G_{k-1}^{\mathrm{T}} \tag{5.21}$$

$$P_{k-1,k-2|n} = P_{k-1|k-1} G_{k-2}^{\mathrm{T}} + G_{k-1}(P_{k,k-1|n} - F_k P_{k-1|k-1}) G_{k-2}^{\mathrm{T}}, \tag{5.22}$$

using the initial values

$$d_{n|n} = d_n \tag{5.23}$$

$$P_{n|n} = P_{n|} \tag{5.24}$$

$$P_{n,n-1|n} = (I - K_n J_n^{\mathrm{T}}) F P_{n-1}. \tag{5.25}$$

Given the model parameters $\theta = \{\mu, \Pi, F, Q, R\}$, the expected values of the parameter d_k and their corresponding covariance P_k and cross covariance $P_{k,k-1|n}$ are computed using EKS.

5.3.3 EM algorithm for front point estimation

The EM minimizes the likelihood function (5.13) by iterating the E and M step.

E step: Estimate the hidden variables (d_k) with the assumed model parameters θ .

M step: Estimate the new model parameters that increases the likelihood function (5.13) with the new parameters d_k

The log-likelihood function of the complete data can be written as

$$\log L = \log(p(d_k, V_k \mid \theta)). \tag{5.26}$$

EM is formulated in such a way that the log-likelihood function increases in each step. In the E step the expectation of log-likelihood function is computed and the expected values of the parameter d_k and their corresponding covariance P_k and cross covariance $P_{k,k-1|n}$ are computed through Kalman smoother described in earlier section. These smoothed values are then used to compute the new model parameters as follows

$$F = B A^{-1} \tag{5.27}$$

$$Q = \frac{1}{n}(C - B A^{-1} B^{\mathrm{T}}) \tag{5.28}$$

$$R = \frac{1}{n}\sum_{k=1}^{n} J_k^{\mathrm{T}} p_{k|n} J_k + \{(V_k - J_k d_{k|n})(V_k - J_k d_{k|n})^{\mathrm{T}}\} \tag{5.29}$$

$$\mu(r+1) = d_{1|n} \tag{5.30}$$

$$\prod(r+1) = p_{1|n}, \tag{5.31}$$

where

$$A = \sum_{k=1}^{n} (P_{k-1|n} + d_{k-1|n} d_{k-1|n}^{\mathrm{T}}) \tag{5.32}$$

$$B = \sum_{k=1}^{n} \left(P_{k,k-1|n} + d_{k|n} d_{k-1|n}^{\mathrm{T}} \right) \tag{5.33}$$

$$C = \sum_{k=1}^{n} \left(P_{k|n} + d_{k|n} d_{k|n}^{\mathrm{T}} \right). \tag{5.34}$$

5.3.4 Computation of Jacobian for front points

In the inverse solver for the implementation of EM algorithm to estimate the unknown state variables d_λ ($\lambda = 1,2,\cdots,\Lambda$), the Jacobian should be formulated. Using the FEM formulation for CEM (2.24-2.32), the Jacobian for front points $\partial \hat{\mathbf{U}} / \partial d_\lambda$ ($\lambda = 1,2,\cdots,\Lambda$) can be expressed as follows

$$\frac{\partial \hat{\mathbf{U}}}{\partial d_\lambda} = \tilde{\mathbf{M}} \mathbf{A}^{-1} \frac{\partial \mathbf{A}}{\partial d_\lambda} \mathbf{A}^{-1} \tilde{\mathbf{I}} = \tilde{\mathbf{R}}^{\mathrm{T}} \frac{\partial \mathbf{A}}{\partial d_\lambda} \mathbf{b}, \tag{5.35}$$

where $\tilde{\mathbf{R}} = \mathbf{A}^{-1} \tilde{\mathbf{M}}^T \in \Re^{(N+L-1)\times E}$ is the pseudo resistance matrix, $\mathbf{A}$ is the stiffness matrix in FEM formulation, $\mathbf{b}$ is the solution vector in the FEM formulation. In $\mathbf{A}$, the matrix $\mathbf{B}$ is the only term dependent on d_λ and the Jacobian will be

$$\frac{\partial \hat{\mathbf{U}}}{\partial d_\lambda} = -\begin{pmatrix} \tilde{\mathbf{R}}_1 \\ \tilde{\mathbf{R}}_2 \end{pmatrix}^{\mathrm{T}} \begin{pmatrix} \frac{\partial \mathbf{B}}{\partial d_\lambda} & \mathbf{0} \\ \mathbf{0} & \mathbf{0} \end{pmatrix} \begin{pmatrix} \boldsymbol{\alpha} \\ \boldsymbol{\beta} \end{pmatrix} = -\begin{pmatrix} \tilde{\mathbf{R}}_1^{\mathrm{T}} & \tilde{\mathbf{R}}_2^{\mathrm{T}} \end{pmatrix} \begin{pmatrix} \frac{\partial \mathbf{B}}{\partial d_\lambda} \boldsymbol{\alpha} \\ \mathbf{0} \end{pmatrix} = -\tilde{\mathbf{R}}_1^{\mathrm{T}} \frac{\partial \mathbf{B}}{\partial d_\lambda} \boldsymbol{\alpha}. \tag{5.36}$$

From the definition (5.1-5.3), the derivative $\partial \mathbf{B} / \partial d_\lambda$ is written as

$$\frac{\partial \mathbf{B}}{\partial d_1} = \frac{\partial \mathbf{B}}{\partial X_1} \frac{\partial X_1}{\partial d_1} + \frac{\partial \mathbf{B}}{\partial Y_1} \frac{\partial Y_1}{\partial d_1} = \frac{Y_1}{R} \frac{\partial \mathbf{B}}{\partial X_1} - \frac{X_1}{R} \frac{\partial \mathbf{B}}{\partial Y_1},$$

$$\frac{\partial \mathbf{B}}{\partial d_\lambda} = \frac{\partial \mathbf{B}}{\partial Y_\lambda}, \qquad \lambda = 2,\cdots,\Lambda - 1 \tag{5.37}$$

$$\frac{\partial \mathbf{B}}{\partial d_\Lambda} = -\frac{Y_\Lambda}{R} \frac{\partial \mathbf{B}}{\partial X_\Lambda} + \frac{X_\Lambda}{R} \frac{\partial \mathbf{B}}{\partial Y_\Lambda}.$$

Since we are considering a stratified flow of two immiscible liquids with distinct electrical properties, so the matrix $\mathbf{B}$ will be

$$\mathbf{B}(i,j) = \sum_{r=l,u} \sigma_r \int_{A_r} \nabla\varphi_i \cdot \nabla\varphi_j d\Omega + \sum_{\ell=1}^{L} \frac{1}{z_\ell} \int_{e_\ell} \varphi_i \varphi_j dS, \;, \; i,j = 1,2,\cdots,N, \qquad (5.38)$$

where the subscript 'l' and 'u' denote the lower and the upper region, respectively (see figure 5.1). The derivative $\partial\mathbf{B} / \partial d_\lambda$ can then be obtained as

$$\begin{aligned} \frac{\partial \mathbf{B}}{\partial d_\lambda} &= \lim_{\delta d_\lambda \to 0} \frac{\mathbf{B}(X_\lambda + \delta X_\lambda, Y_\lambda + \delta Y_\lambda) - \mathbf{B}(X_\lambda, Y_\lambda)}{\delta d_\lambda} \\ &= \lim_{\delta d_\lambda \to 0} \frac{(\sigma_l - \sigma_u)}{\delta d_\lambda} \sum_{m|\Omega_m \subset \mathbf{supp}(\varphi_i\varphi_j)} \int_{\delta A_u \cap \Omega_m} \nabla\varphi_i \cdot \nabla\varphi_j d\Omega. \end{aligned} \qquad (5.39)$$

The detailed derivation for the above expression (5.39) to calculate Jacobian can be found in Kim *et al*. (2007b), Ijaz *et al*. (2008).

5.4 Results

5.4.1 Numerical results

In this section, the numerical results obtained using EM are reported. Stratified flow of two conducting immiscible liquids through a cylindrical pipe of diameter 28 cm with 16 electrodes of width 2.5 cm each around its periphery is considered. For generation of measurement data, the flow area is discretized into 2088 triangular meshes with 1109 nodes and the cubic spline interpolation with the prescribed front points is used to describe the interface. In the image reconstruction, a slightly coarser mesh structure with 1968 triangular elements and 1049 nodes are used and the interface is approximated with a piecewise linear interpolation function based on the front points. The use of different interpolations to describe the interface and the different mesh structures for the simulated data generation and for the inverse solution will support the freedom from the inverse crime. The conductivity of each region is assumed to be known and initially set to 1/1500 S/cm for the upper region

and 1/300 S/cm for the lower region. Therefore a contrast ratio of 1:5 is considered for the two regions. Opposite method is used as a current injection mechanism. Two dynamic cases are considered in which the interface is assumed to change within time to acquire a single measurement. First-order kinematic models are used to describe the evolution of the true interface. To simulate the actual conditions, random noise of zero-mean Gaussian process noise having *STD* 1% of the value of the corresponding computed voltage is added to the computed voltage. The performance of EM is compared with EKF and as a performance index root mean square error of estimated front points and voltage is calculated

The RMSE for the parameter d, RMSE_d, is defined as

$$\mathrm{RMSE}_d = \frac{\| d_{estimated} - d_{true} \|}{\| d_{true} \|}. \tag{5.40}$$

The RMSE for the boundary voltages, RMSE_U, is defined as

$$\mathrm{RMSE}_U = \frac{\| U_{estimated} - U_{meas} \|}{\| U_{meas} \|}. \tag{5.41}$$

In case 1, where the interface is assumed to be flat and the front points have the same value (d = 5) and with time the interface at the left side moves towards up and the right side front points moves downwards with respect to time. The evolution of the true interface with respect to time is shown in figure 5.4(a). As an initial condition (figure 5.4b), we choose the initial interface to be a straight surface at (y = 3). The reconstructed interfacial boundary for case 1 without noise is shown in figure 5.5 and the RMSE for boundary and voltages are shown in figures 5.6-5.7, respectively. As can be observed in figures 5.5-5.7, the proposed EM algorithm has been successful in tracking the moving boundary with good accuracy as compared to EKF. The parameters used in the simulation for the initial setting of the inverse algorithms are given in Table 5.1. Figure 5.8 shows the reconstructed interfacial boundary for case 1, in which 1 % white Gaussian noise has been added to the simulated voltage data. The RMSE values for the estimated parameter d and voltage U are given in figures 5.9-5.10. In the presence of noise, EKF has been found to have wobbles in the interface and failed to track the interface. However, EM estimates the

interface with good accuracy. The better performance of the EM compared to EKF can also be visualized through RMSE plots, where EM has lower values for both parameter *d* and voltage *U*. The parameters used for initial settings of the inverse solver for case 1 with 1 % noise are given in Table 5.1.

In case 2, the opposite of the above scenario is considered where the front points on the left side of the interface moves down wards while the right most front points move upwards. The generated true scenario and the initial condition used for case 2 are given in figure 5.11. Figure 5.12 shows the reconstructed interfacial boundary for case 2 without noise. The RMSE for the parameter *d* and voltage *U* are given in figures 5.13-5.14. The results for the phase boundary reveal that except for the last image frame, EM has better estimation of the boundary, especially, near the center region where the interface is wavy. The better performance of EM can be observed in the RMSE plots where EM is found to have lower values than EKF. Figure 5.15 shows the reconstructed interfacial boundary for case 2 with 1 % noise. The performance deteriorates in EKF especially near the center region in the presence of noise. On the other hand EM is fairly successful in estimating the boundary. The RMSE plots for the estimated front points and voltage for case 2 with 1 % noise is shown in figures 5.16-5.17. The figures reveal the performance gain of EM when compared to EKF. The parameters used in the initial setting for case 2 are shown in Table 5.2.

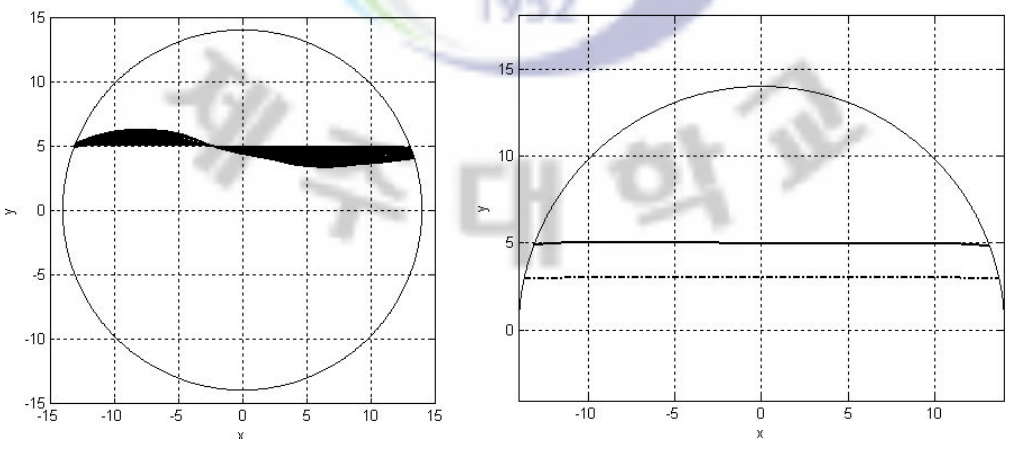

(a) (b)

Figure 5.4. Evolution of interface for numerical simulations with case 1 without noise (a) generated true scenario where interface changes with respect to time (b) initial condition used in inverse calculation.

Figure 5.5. Reconstructed phase boundary estimation for case 1 without noise. Alternate images have been displayed. Solid line represents the true boundary and dotted, dashed line represents estimated boundary using EM algorithm, EKF, respectively.

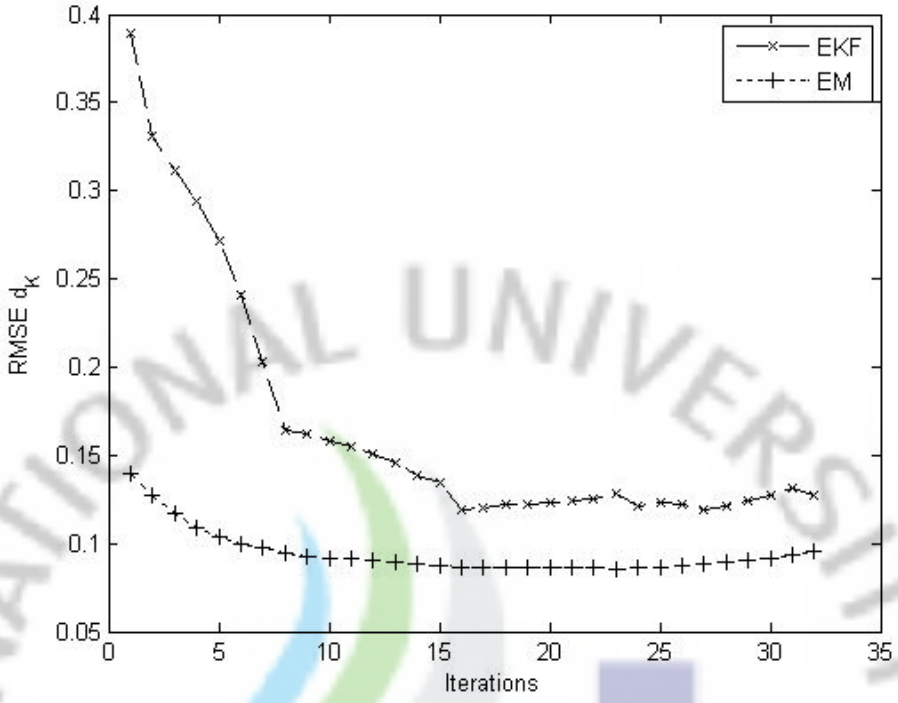

Figure 5.6. RMSE of estimated front points for case 1 without noise.

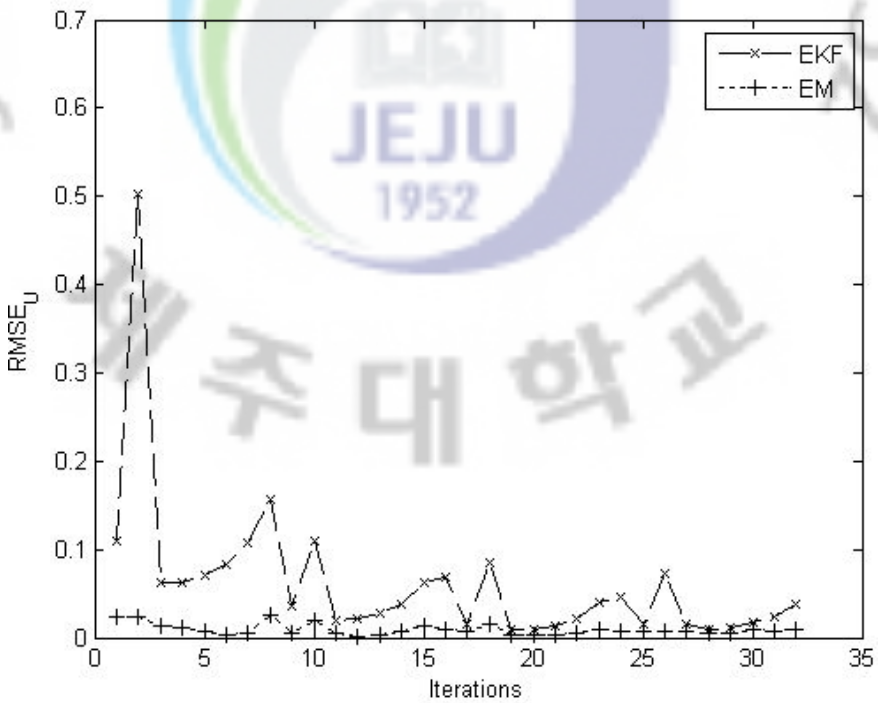

Figure 5.7. RMSE voltage for case 1 without noise.

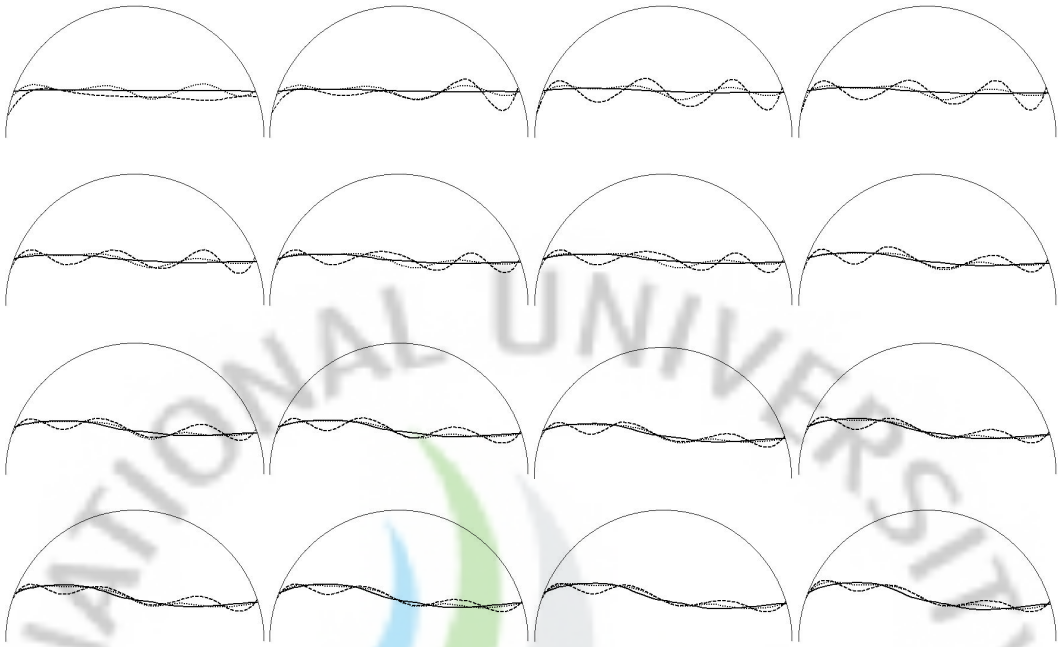

Figure 5.8. Reconstructed phase boundary estimation for case 1 with 1% noise. Alternate images have been displayed. Solid line represents the true boundary, dotted line is with EM algorithm and dashed line is using EKF.

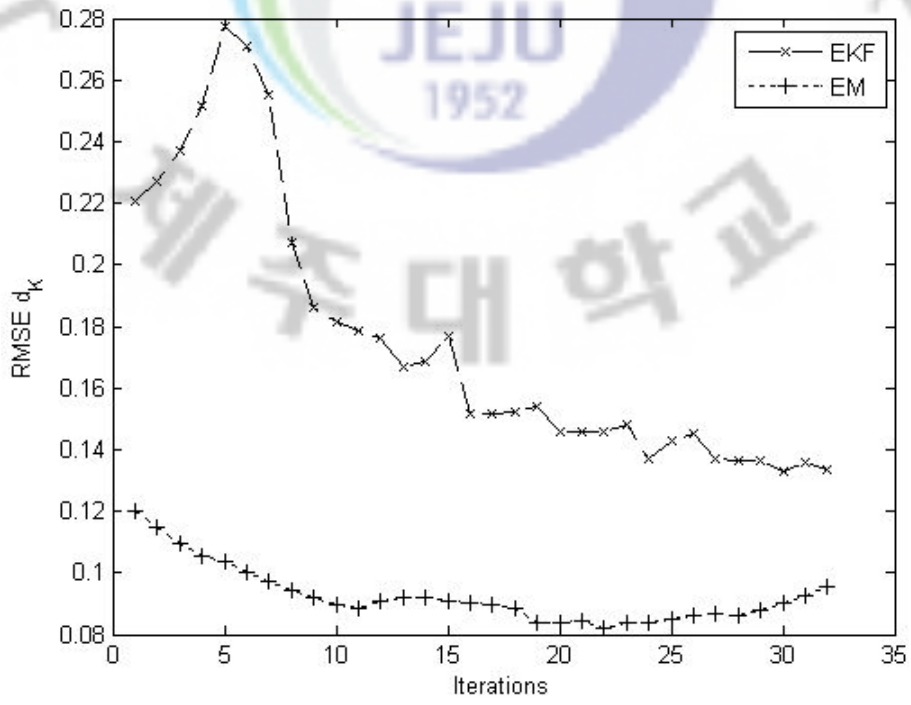

Figure 5.9. RMSE of estimated front points for case 1 with 1% noise.

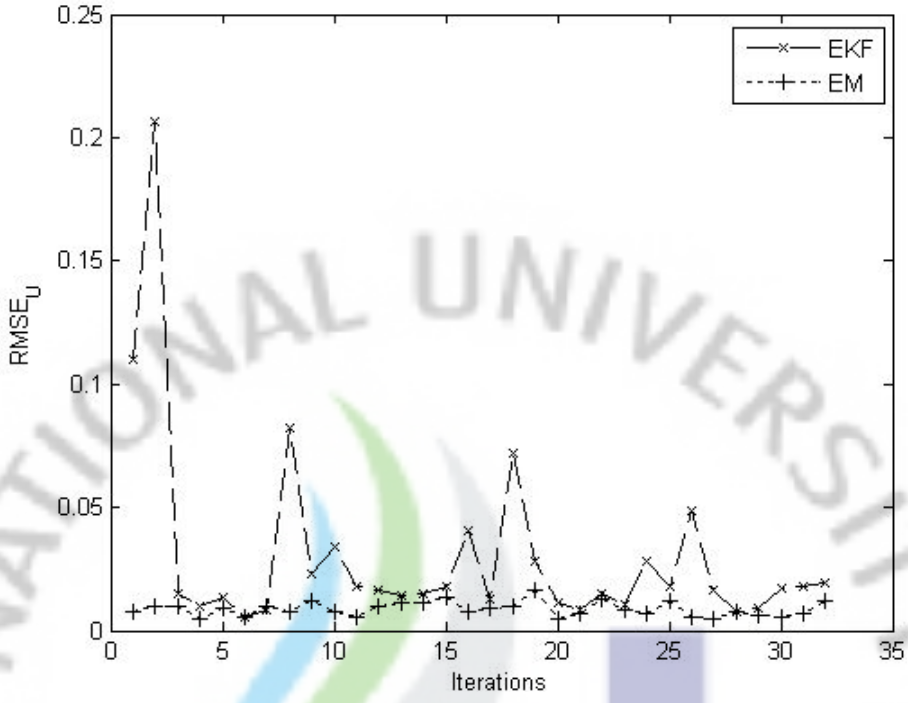

Figure 5.10. RMSE voltage for case 1 with 1% noise.

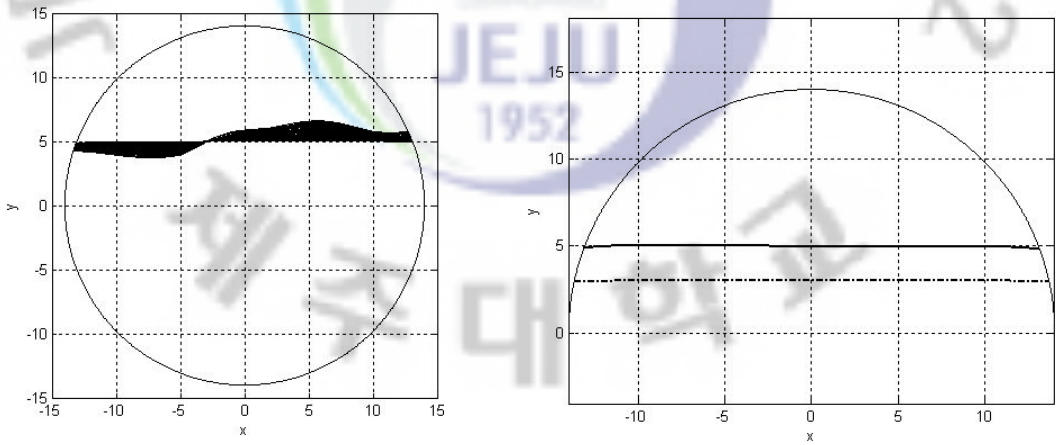

(a) (b)

Figure 5.11. Evolution of interfacial boundary for numerical simulations with case 2 (a) evolution of true interface with current pattern (b) initial condition (dashed dot line) used in inverse calculation.

Figure 5.12. Reconstructed phase boundary estimation for case 2 without noise. Alternate images have been displayed. Solid line represents the true boundary, dotted line is with EM algorithm and dashed line is using EKF.

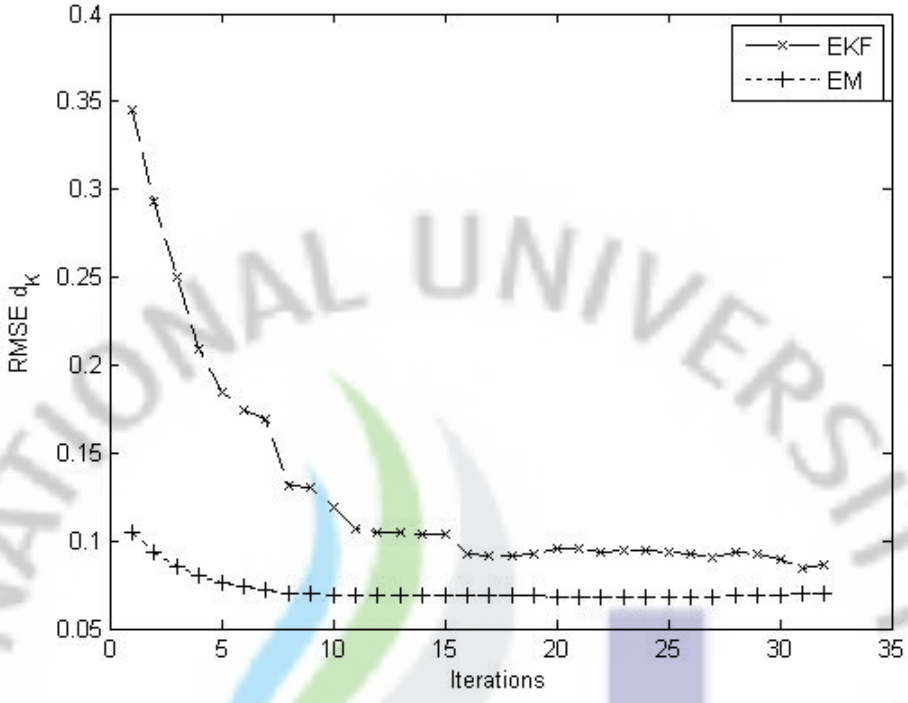

Figure 5.13. RMSE of estimated front points for case 2 without noise.

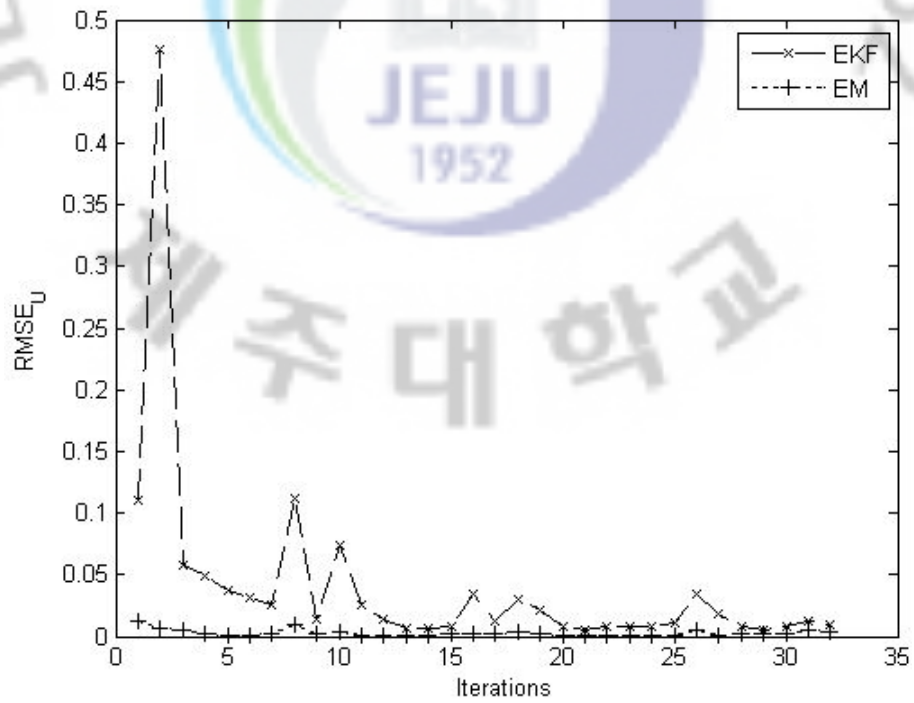

Figure 5.14. RMSE voltage for case 2 without noise.

Figure 5.15. Reconstructed phase boundary estimation for case 2 with 1% noise. Alternate images have been displayed. Solid line represents the true boundary, dotted line is with EM algorithm and dashed line is using EKF.

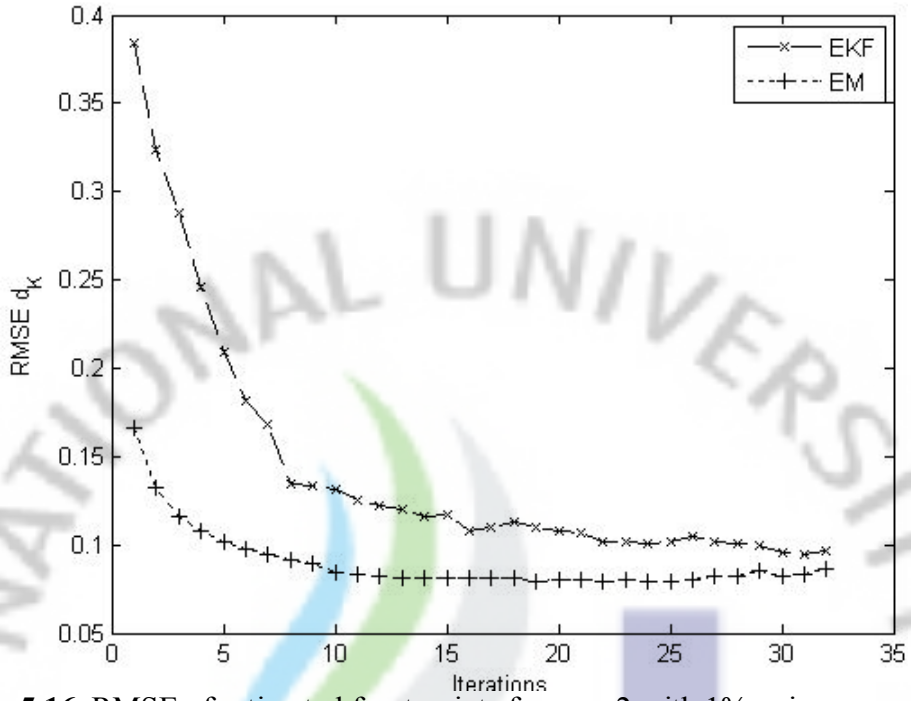

Figure 5.16. RMSE of estimated front points for case 2 with 1% noise.

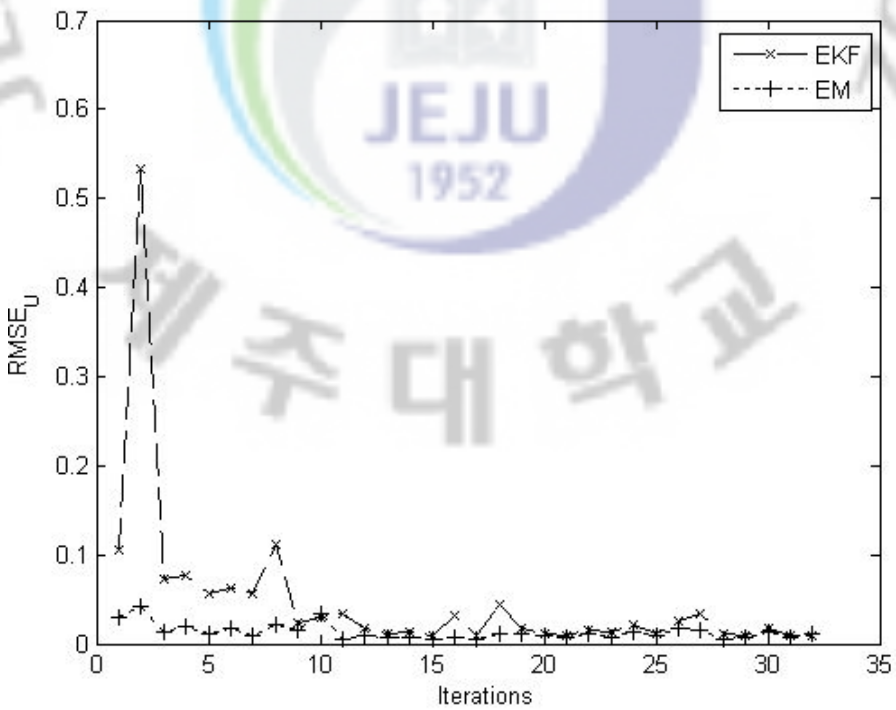

Figure 5.17. RMSE voltage for case 2 with 1% noise.

Table 5.1. Iinitial settings of model parameters used in EM and EKF for case 1.

Parameters	Noise	
	0 %	1% white Gaussian Noise
F	$I_\Lambda \in \Re^{\Lambda\times\Lambda}$	$I_\Lambda \in \Re^{\Lambda\times\Lambda}$
Q	$0.01I_\Lambda$	$0.01I_\Lambda$
R	$10I_L$	$10I_L$
$C_{0\|0}$	$0.1I_\Lambda$	$0.1I_\Lambda$

Table 5.2. Initial settings of model parameters used in EM and EKF for case 2.

Parameters	Noise	
	0 %	1% white Gaussian Noise
F	$I_\Lambda \in \Re^{\Lambda\times\Lambda}$	$I_\Lambda \in \Re^{\Lambda\times\Lambda}$
Q	$0.01I_\Lambda$	$0.05I_\Lambda$
R	$10I_L$	$10I_L$
$C_{0\|0}$	$0.1I_\Lambda$	$0.1I_\Lambda$

5.4.2 Experimental studies

The experimental setup consists of a circular phantom with a radius of 150 mm and a height of 100 mm. 16 electrodes were considered mounted around the phantom (each of width 10 mm). Mesh with 2032 elements and 1097 nodes is used for solving the inverse solution. As for the current injection protocol, opposite current patterns are used. Traditionally, for 16 electrodes configuration, there are 8 opposite current patterns. However, since the goal of the current research is to use dynamic scenarios, a subset of opposite current patterns is considered in each image frame. Experiment for two immiscible fluids is performed using gelatin (4 mS/cm) and brine solution (6mS/cm) as shown in figure 5.18. The two fluids form the boundary and the position of the interface between gelatin and brine solution is varied by removing the gelatin layer based on guide placed below the phantom. Initially the gelatin brine interface is located at y = -10 and the interface is static for the eight current patterns

time injection and later the interface is changed by cutting the gelatin layer after every four current patterns.

Figure 5.19 shows the reconstructed interfacial boundary for the experimental case study. In figure 5.19, images are illustrated after every two frames and the parameters used to set the initialize the inverse solver is given in Table 5.3. In reconstructing the interfacial boundary the interface is represented using seven front points. If the interface is wavier then higher number of front points are necessary, however, it should be noted that as the number of front points increases the estimation performance is effected. It is observed that EM estimates the interface fairly reasonable as compared to EKF. EM tracks the interface all the way whereas EKF is found to lag with true interface. Moreover, near the center of the phantom the interface is not tracked effectively because the sensitivity is low at the center of the phantom. This can be solved if current injection pattern is designed considering the distinguishability analysis. Figures 5.20-5.21 show the comparison of RMSE values for parameter d and voltage U, respectively. It is noticed that EM has RMSE values when compared to EKF which explains the superior estimation performance of interfacial boundary.

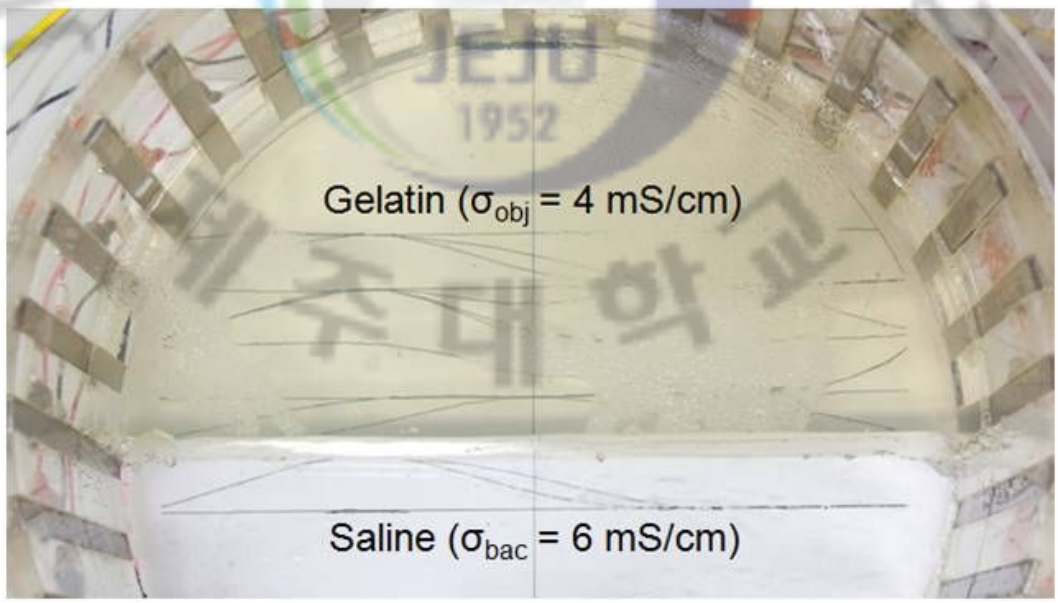

Figure 5.18. Experiment setup for interfacial boundary estimation. Gelatin of conductivity 4 mS/cm and saline of conductivity 6 mS/cm are used as immiscible fluids inside the phantom. The interfacial boundary in between these two is estimated.

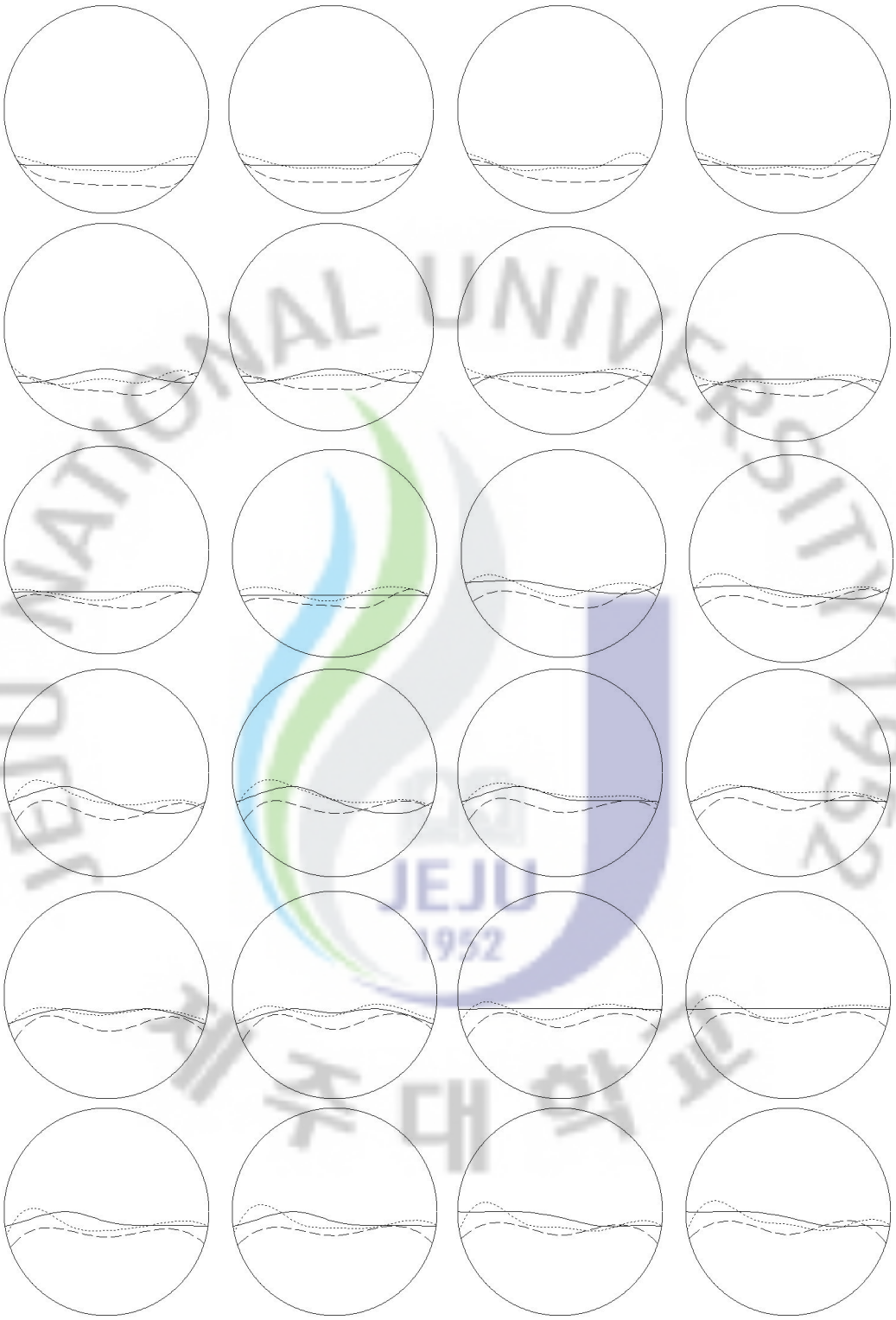

Figure 5.19. Reconstructed phase boundary estimation for experiment data. Alternate images have been displayed. Solid line represents the true boundary, dotted line is with EM algorithm and dashed line is using EKF.

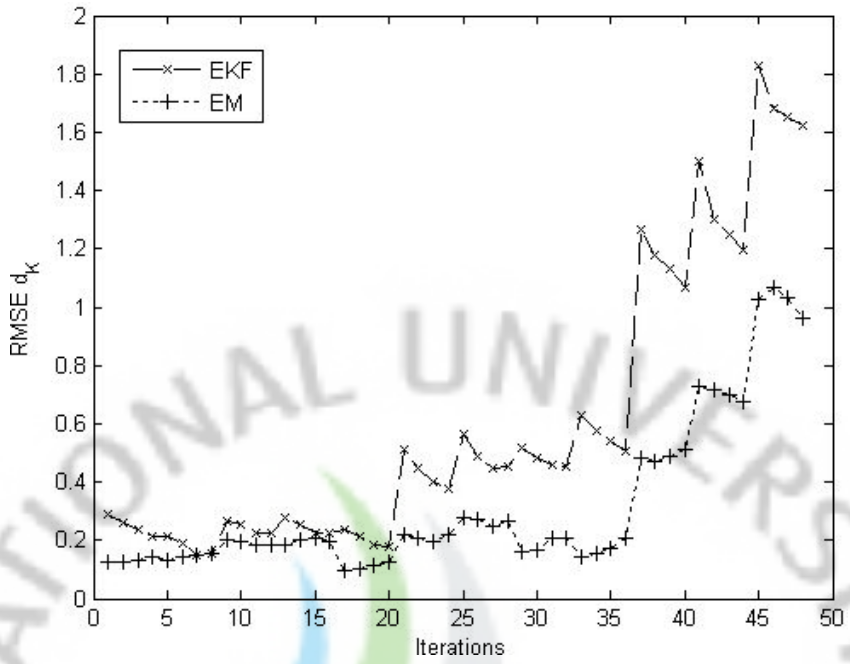

Figure 5.20. RMSE of estimated front points for experiment data.

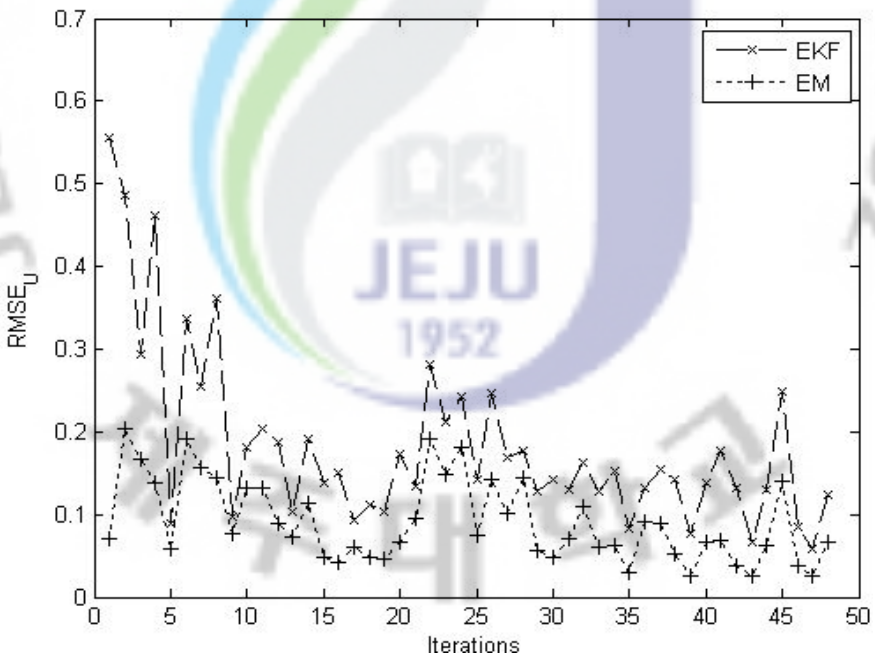

Figure 5. 21. RMSE voltage for experiment data.

Table 5.3. Initial setting of model parameters used in EM and EKF for experiments.

F	Q	R	$P_{0\|0}$	$P_{0\|0}$
$I_\Lambda \in \Re^{\Lambda\times\Lambda}$	$0.05I_\Lambda$	$5000I_L$	$0.1I_\Lambda$	y =-10

6. Conclusions

In this study, electrical impedance tomography is used to estimate the boundary in the flow field as an application of process tomography. If the flow distribution is known *a priori* then the conductivity distribution is used as additional information for the solution and the unknowns are the boundary, location and the shape of the anomaly. The anomaly can be voids in case of closed boundary and interfacial boundary between two fluids for an open boundary problem.

If the boundary is assumed to be smooth, the closed boundary is represented using truncated Fourier series where the Fourier coefficients characterize the boundary. In open boundary, the boundary is represented as an interpolation of discrete front points. It is assumed that the flow undergoes a fast transient such that the boundary properties changes before the time to obtain a full set of independent measurement data. The conventional static imaging reconstruction techniques usually do not give desirable results, therefore, dynamic methods are required to achieve better estimation performance.

Extended Kalman filter is the standard algorithm used in dynamic estimation. However, in the implementation of extended Kalman filter, the model parameters such as the initial states, the state evolution matrix and the noise covariance matrices have to be predefined. Usually these parameters are determined empirically or through trial and error method. In real situations, the flow process is very complex and has a lot of uncertainties involved therefore it is difficult to represent the model parameters in a prior form. In such cases, the performance of conventional EKF would not give satisfactory performance. In the present approach, expectation maximization algorithm is formulated for boundary estimation and the problem is transformed into a state estimation problem and the time varying state parameters are estimated along with the model parameters. Numerical and experimental studies are performed to evaluate the performance of the proposed method.

With respect to closed boundary problem, the voids formed are not stable and therefore move randomly inside the flow domain. The motion of the void is represented using first-order kinematic model and three cases such as moving, expanding and moving-expanding are considered. In the inverse computations it was

assumed that we do not have the knowledge of the model parameters and using EM algorithm these model parameters are estimated. Through numerical simulations, with and without noise, it was found that the EM has better estimation of fast moving closed boundaries compared to that of EKF. Through experiment studies it was observed that it was possible to estimate boundary of plastic targets which can be visualized as that of voids with good accuracy using EM algorithm.

Interfacial boundary estimation is represented using 10 front points and the fast moving boundary is represented using first-order kinematic model. Numerical simulations have been successful up to contrast ratio 1:5. Also, we tested the proposed method with 1 % measurement noise. Experiments have been performed using gelatin and brine as two fluids inside the phantom. The results with experiments show that EM algorithm has been able to better track the interfacial boundary with good efficiency as compared to EKF.

The present work is focused on two-dimensional boundary estimation and it can easily be extended to three dimensions. The currently employed technology for boundary estimation is using EIT and it is applicable to other tomography techniques. Generalized EM algorithm is formulated in this study and hence can easily adapt to other applications. Future work can include boundary estimation in three dimension and methods to improve the convergence of EM by improving the E and M steps.

Summary

Visualization of two-phase flows provides an insight into the characteristics of flow parameters and thus helps in monitoring the flow process. Electrical impedance tomography (EIT), which offers high temporal characteristics, has potential to monitor fast transient processes. In EIT, current is applied through the current source across the electrodes attached to the boundary of the process vessel and the excited voltages are measured on the surface of the electrode. Based on the current-voltage relationship the internal conductivity distribution is reconstructed. In two-phase flows, the conductivities distribution can be known *a priori*. Using this prior information, the boundary between the two phases can be estimated. The phase boundaries can be classified as open and closed boundary type depending on the topology of the boundary. Closed boundary problem involves estimation of voids in the flow process. A typical open boundary problem is to estimate the interfacial boundary between the two immiscible fluids. Closed boundary is represented using truncated Fourier series where as the open boundary is represented as an interpolation of discrete front points. The boundary between the two phases is time variant and the flow process is quite complicated. To track the fast moving boundary changes, dynamic estimation algorithms are necessary.

In dynamic estimation, the inverse problem is treated as a state estimation problem and the time varying boundary coefficients are the state variables to be estimated. For the application of Kalman-type estimators like extended Kalman filter (EKF), unscented Kalman filter (UKF), the exact dynamics of the evolution, the initial states, and the noise covariance of process and measurement models have to be predefined. In practice, prior information about the evolution of the object is not known therefore random-walk model is often used. In some cases, kinematic models such as constant velocity and constant acceleration are employed. The values of noise covariance are set through experience or manually tuned which is a major drawback of EKF for parameter estimation. In real situations, the dynamics of the evolution are complex and it is difficult to model the evolution of the boundary in a prior form. Also, process noise depends on the dynamics of the target and the

environment surrounding it. In situations, when there is uncertainty in determining the model parameters, the estimation performance of the Kalman-type filters is affected. Therefore, in this study, we apply the expectation-maximization algorithm (EM) as an inverse algorithm to reduce model uncertainties in estimating the closed and open boundaries. EM is formulated for boundary estimation using Kalman smoother approach. The model parameters (state evolution matrix, noise covariance matrices and initial states) are estimated using expectation (E) and maximization (M) steps. The advantage with EM is that it always tries to increase the log-likelihood function, thereby guaranteeing the convergence. In this study, EM is applied for boundary estimation in two applications. One involves estimation of voids in flow process (closed boundary) while the other is estimation of moving interfacial boundary between two immiscible fluids (open boundary). Numerical and experimental studies have been performed for the above mentioned applications and the estimation performance is compared against EKF. The results show that EM has better estimation performance of the dynamic changes in the boundary (location, shape and size) as compared to conventional EKF.

References

Antoniadis N and Hero A 1994 Time delay estimation for filtered Poisson processes using an EM type algorithm *IEEE Trans. Sig. Proc.* 42 2112-2123

Baker L E 1989 Principles of the impedance technique *IEEE Eng. Med. Biol. Mag.* 8 11-15

Barber D C and Brown B H 1984 Applied Potential tomography *J phys. E: Sci Instrum* 17 723-733

Bar-Shalom Y and Li X R 1993 Estimation and Tracking: Principles, Techniques and Softwares, Artech House.

Barker R D and Moore J 1998 The application of time-lapse electrical tomography in groundwater studies *The Leading Edge* 17 1454-1458

Boyles R A 1980 Convergence results for EM algorithm. *Technical Report No 13 Division of Statistics*, University of California, Davis

Brown B H 2001 Medical impedance tomography and process impedance tomography: a brief review *Meas. Sci.Technol.* 12 991–6

Butler J E and Bonnecaze R T 2000 Inverse method for imaging a free surface using electrical impedance tomography *Chem. Eng. Sci.* 55 1193-204

Byrne W 1992 Alternating minimization and Boltzman machine learning *IEEE Trans. Neural Net.* 3 612-620

Cheney M and Isaacson D 1992 Distinguishability in impedance imaging *IEEE Trans. Biomed. Eng.* 39 852-860

Cheng K S, Isaacson D, Newell J C and Gisser D G 1988 Error comparison for different current patterns in electrical impedance tomography *In proc 10 th Intl Conf IEEE Eng Med Biol Society* 37 60-65

Cheng K S, Isaacson D, Newell J C and Gisser D G 1989 Electrode models for electric current computed tomography *IEEE Trans. Biomed. Eng.* **36** 918-924

Cherepenin V A, Karpov A Y, Korjenevsky A V, Kornienko V N, Kultiasov Y S, Ochapkin M B, Trochanova O V, and Meister J D 2002 Three-dimensional EIT imaging of breast tissues: System design and clinical testing *IEEE Trans. Med. Imag.* 21 662–667

Cherepenin V, Karpov A, Korjenevsky A, Kornienko V, Mazaletskaya A and Mazourov D 2001 A 3D electrical impedance tomography (EIT) system for breast cancer detection. *Physiol. Meas.* 22 9–18

Casas A, Himi M, Diaz Y, Pinto V, Font X and Tapias J C 2008 Assessing aquifer vulnerability to pollutants by electrical resistivity tomography (ERT) at a nitrate vulnerable zone in NE Spain *Environ. Geol.* 54 515-520

Choi M H, Kao T J, Isaacson D, Saulnier G J and Newell J C 2004 A simplified model of mammography geometry for breast cancer imaging with electrical impedance tomography, in *Proc. 26th Annu. Int. Conf. IEEE EMBS*, San Francisco 1310-1313

Cartwright D J 2001 Underlying Principles of the Boundary Element Method, Billerica, MA: *Computational Mechanics*

Chung E T, Chan T F and Tai X C 2005 Electrical impedance tomography using level set representation and total variational regularization *J. Comput. Phys.* 205 357–372.

Daily W, Ramirez A 1992 Electrical resistivity tomography of vadose water movement *water resource research* 28 1429-1442

Dempster A P, Laird N M and Rubin D B 1977 Maximum Likelihood from incomplete data via the EM algorithm *J. R. Statist.Soc.* B 39, 1-38

Dickin F and Wang M 1996 Electrical resistance tomography for process tomography *Meas.Sci.Technol* 7 247-260

Doerstling B H 1995 *A 3-D reconstruction algorithm for the linearized inverse boundary value problem for Maxwell's equations*. PhD thesis, Rensselaer Polytechnic Institute, Troy, New York.

Fairuzov Y V 2000 Numerical simulation of transient flow of two immiscible liquids in pipeline *AIChe J.* 46 1332-9

Friedman A and Vogelius M 1989 Determining cracks by boundary measurements *Indiana University Mathematics Journal* 38 527-556

Gelb A 1981 *Applied Optimal Estimation* MIT press

Gisser D C, Isaacson D and Newell J C 1988 Theory and performance of adaptive current tomography system *Clinical Physics and Physiological Meas.* 9 35-42

Gladden L F and Alexander P 1996 Application of nuclear magnetic resonance imaging in process engineering *Meas. Sci. Technol.* 7 423-435

Ghaharamani Z and Hinton G E 1996 Parameter estimation for linear dynamic systems Technical report CRG-TR-96-2

Ghaharamani Z and Beal M J 1999 Learning nonlinear dynamical systems using an em algorithm Advances in Neural Information Processing Systems 11 MIT press

Goodrich R L and Caines P E 1979 Linear system identification from nonstationary cross-sectional data *IEEE Trans. Aut. Cont. AC* 24 403-411

Gupta N K and Mehra R K 1974 Computational aspects of maximum likelihood estimation and reduction in sensitivity function calculations *IEEE Trans. Aut. Cont. AC* 19 774-783

Holder D S 1992 Electrical impedance tomography (EIT) of brain function *Brain Topogr.* 5 87–93

Holand F A and Bragg R 1995 *Fluid Flow for Chemical Engineers* (London: Edward Arnold Publisher)

Han D K and Prosperetti A 1999 A shape decomposition technique in electrical impedance tomography *J. Comput. Phys.* 155 75-95

Isaacson D 1986 Distinguishability of conductivities by electric current computed tomography *IEEE Trans. Med. Imag.* M1-5 91-95

Isaacson D and Cheney M 1990 Current problems in impedance imaging In Colton D, Ewing R and Rundell W, editors *Inverse problems in partial differential equations* chapter 9 pages 141-149 SIAM Philadelphia

Ijaz U Z, Khambampati A K, Lee J S, Kim S, and Kim K Y 2008 Nonstationary phase boundary estimation in electrical impedance tomography using unscented Kalman filter *J. Comput. Phys.* 227 7089-7112

Ijaz U Z, Chung S I, Khambampati A K, Kim K Y and Kim S 2008 Electrical resistance imaging of a time-varying interface in stratified flows using an unscented Kalman filter 19(6) 065501-0605512

Jain H, Isaacson D, Edic P M and Newell J C 1997 Electrical impedance tomography of complex conductivity distributions with noncircular boundary *IEEE Trans. Biomed. Eng.* 44 1051-1060

Jeon H J, Kim J H, Choi B Y, Kim K Y, Kim M C, and Kim S 2005 Electrical Impedance Imaging of Binary Mixtures with Boundary Estimation Approach Based on Multilayer Neural Network *IEEE Sensors Journal* 5(2) 313-319

Jiang C 1994 The use of mixture models to detect effects of major genes on quantitative charecteristics in a plant-breeding experiment *Genetics* 136 383-394

Jones O C, Lin J T, Ovacik L and Shu H 1993 Impedance imaging relative to gas-liquid systems *Nuclear Engineering and Design* 141 159-176

Julier S J and Jeffery K U 1997 A New Extension of the Kalman Filter to nonlinear Systems. In The Proceedings of AeroSense: The 11th International Symposium on Aerospace/Defense Sensing, Simulation and Controls, Multi Sensor Fusion, Tracking and Resource Management II, SPIE.

Julier S J and Uhlmann J K 2004 Unscented filtering and nonlinear estimation *Proceedings of the IEEE* 92(3) 401-422.

Kerner T E, Hartov A, Soho S K, Poplack S P and Paulsen K D 2002 b Imaging the breast with EIS: an initial study of exam consistency *Physiol. Meas.* 23 221–36

Kerner T E, Paulsen K D, Hartov A, Soho S K and Poplack S P 2002a Electrical impedance spectroscopy of the breast: clinical results in 26 subjects *IEEE Trans. Med. Imag.* 21 638–45.

Khambampati A K, Rashid A, Kim S, Soleimani M and Kim K Y 2009 Unscented Kalman filter approach to track moving interfacial boundary in sedimentation process using three-dimensional electrical impedance tomography *Proc. R. Soc. A.* 367 3095-3120

Kim B S, Boverman G, Newell J C, Saulnier G J and Isaacson D 2007a The complete electrode model for EIT in mammography geometry *Physiol. Meas.*28 S57-S69

Kim, K Y, Kim B S, Kim M C, Lee K J, Ko Y J and Kim S 2005 Electrical impedance imaging of two-phase flows undergoing rapid transient: Part II. Effect of input current pattern *Int. Commun. Heat Mass Transfer* 32 649-657

Kim K Y, Kim B S, Kim M C, Lee Y J and Vauhkonen M 2001 Image reconstruction in time varying electrical impedance tomography based on the extended Kalman filter *Meas. Sci. Technol.* 12 1032-1039

Kim S, Ijaz U Z, Khambampati A K, Kim K Y, Kim M C and Chung S I 2007b Moving interfacial boundary estimation in stratified flows of two immiscible liquids using electrical resistance tomography *Meas. Sci. Technol.* 18(5) 1257-1269

Koksal and Eyuboglu 1995 Determination of optimum injected current patterns in electrical impedance tomography *Physiol. Meas.* 16 A99-109.

Kortschak B and Brandstätter B 2005 A FEM-BEM approach using level-sets in electrical capacitance tomography, *Compel* 24 591–605

Kolehmainen V, Arridge S R, Lionheart W R B, Vauhkonen M and Kaipio J P 1999 Recovery of region boundaries of piecewise constant coefficients of elliptic PDE from boundary data *Inverse Probems.* 15 1375-1391

Ledolter J 1979 A recursive approach to parameter estimation in regression and time series problems Comm. *Statist Theor. Meth. A* 8 1227-1245

Lionheart W R B 2004 EIT reconstruction algorithms: pitfalls, challenges and recent developments *Physiol. Meas.* 23 125-42

Little R and Rubin D 1983 On jointly estimating parameters and missing data by maximizing the complete data likelihood *Am. Statistn.* 37 218-200

Li X R and Zhang Y 1996 Multiple model estimation with variable structure *IEEE trans. Automatic. Control* 41 478-493

Li X R 1997 Canonical transform for tracking with kinematic models *IEEE Trans. Aerospace and Electronic systems* 33 1212-1224

Malmivuo J and Plonsey R 1995 *Bioelectromagnetism.* Oxford university press New York

Mann R, Dickin F J, Wang M, Dyakowski T, Williams R A, Edwards R B, Forrest A E and Holden P J 1997 Application of electrical resistance tomography to interrogate mixing processes at plant scale *Chem. Eng. Sci.* 52 2087-2097

Mazor E, Averbuch A, Bar-Shalom Y and Dayan J 1996 Interacting multiple model methods in target tracking: A survey *IEEE trans. Aerospace and electronic systems* 34 103-123

Mueller J L, Isaacson D and Newell J C 2001 Reconstruction of conductivity changes due to ventilation and perfusion from EIT data collected on a rectangular electrode array *Physiol. Meas.* 22 97–106

Maillol J M, Seguin M K, Gupta O P, Akhauri H M and Sen N 1999 Electrical resistivity tomography survey for delineating uncharted mine galleries in West Bengal, India. *Geophys. Prospect., Eur. Assoc. Geosci. Eng.* 47 103–116.

Meads L N, Bently L R, Mendoza C A 2003 Application of electrical resistivity imaging to the development of a geological model for a proposed Edmonton landfill site *Canadian Geotechnical Journal.* 40 499-523

Ming L, ChongZhao H and Panzhi L 2007 Expectation maximization algorithm based nonlinear target tracking with adaptive state transition matrix and noise covariance *10th International Conference on Information Fusion.* Qubec Canada 1-7

Newell J C, Gisser D C and Isaacson D 1988 An electric current tomograph *IEEE Trans. Biomed. Eng.* 35 823-833

Osterman K S, Kerner T E, Williams D B, Hartov A, Poplack S P and Paulsen K D 2000 Multifrequency electrical impedance imaging: preliminary in vivo experience in breast *Physiol. Meas.* 21 99–109

Ola P, Paivarinta L and Sommersalo E 1993 An inverse boundary value problem in electrodynamics *Duke Math J* 70 617-653

Oscher S and Sethian J A 1988 Fronts propagating with curvature-dependant speed Algorithms based on Hamilton-Jacobi formulations *J. of Comp. phys.* 79 12-49

Paulson K, Breckon W and Pidcock M 1992 Optimal measurements in electrical impedance tomography *In Proc 14th Intl Conf IEEE Eng. Med. Biol. Society* 1730-1731

Pinheiro P A T, Loh W W and Dickin F J 1997 Smoothness-constrained inversion for two-dimensional electrical resistance tomography *Meas. Sci.Technol.* 8 293-302

Polydorides N and Lionheart WRB 2002 A MATLAB toolkit for three-dimensional electrical impedance tomography: A contribution to the electrical impedance and diffuse optical reconstruction software project, *Meas. Sci. Technol.* 13 1871-1883

Perry R H, Green D W and Maloney J O 1997 *Perry's Chemical Engineers Handbook* (New York: McGraw-Hill)

Reynolds J M, Taylor D I 1996 Use of geophysical surveys during the planning, construction and remediation of landfills in S.P. Bentley *Engineering Geology of waste disposal: The Geological society of London* 11 93-98

Rondi L and Santosa F 2001 Enhanced electrical impedance tomography via the Mumford-Shah functional *Control, Optimisation, and Calculus of Variations*, 6 517-538

Radhakrishnan K, Unnikrishnan A, Balakrishnan KG 2006 EM based extended Kalman filter for estimation of rotor time-constant of induction motor *IEEE ISIE 2006 Montreal*, Quebec, Canada 2434-2438

Sam R and Ghahramani Z 2001 An EM algorithm for identification of nonlinear dynamical systems in Kalman Filtering and Neural Networks S. Haykin, Ed. New York: Wiley, 175–220

Shumway R H and Stoffer D S 1981 Time series smoothing and forecasting using the EM algorithm. *Technical report No. 27*, Division of statistics, University of California, Davis.

Somersalo E, Cheney M and Isaacson D 1992 Exsistence and uniqueness for electrode models for electirc current computed tomography *SIAM J. Appl. Math.* 52 4 1023-1040

Somersalo E, Isaacson D and Cheney M 1992 A linearized inverse boundary value problem for Maxwell equations *J comput. Appl. Math.* 42 123-136

Spies B and Ellis R 1995 Cross-borehole resistivity tomography of a pilot scale, insitu verification test *Geophysics* 60 886-898

Shollenberger K A, Torczynski J R, Adkin D R, O'hern T J and Jackson N B 1997 Gamma-densitometry tomography of gas holdup spatial distribution and industrial-scale bubble colum *Chem. Eng. Sci.* 52 2037-2048

Shollenberger K A, Torczybski J R, Adkin D R, O'hern T J and Jackson N B 1997 Gamma-densitometry tomograph of gas holdup spatial distribution and industrial-scale bubble column *Chem Eng, Sci.* 52 2037-2048

Shumway R H and Stoffer D S 1982 An approach to time series smoothing and forecasting using the EM algorithm *J. Time Ser. Anal.* 3 253-264

Tossavainen O-P, Vauhkonen M, Heikkinen L M and Savolainen T 2004 Estimating shape and free surfaces with electrical impedance tomography *Meas. Sci. Technol.* 15 1402-1411

Tossavainen O-P, Kolehmainen V and Vauhkonen M 2006 Free-surface and admittivity estimation in electrical impedance tomography *Int. J. Numer. Math. Eng.* **66** 1991-2013

Tossavainen O-P, Vauhkonen M, Heikkinen L M and Savolainen T 2004 Estimating shape and free surfaces with electrical impedance tomography *Meas. Sci. Technol.* 15 1402-1411

Vauhkonen M 1997 Electrical impedance tomography and prior information PhD Thesis, University of Kuopio, Finland

Vauhkonen M, Karjalainen P A and Kaipio J P 1998 A Kalman filter approach to track fast impedance changes in electrical impedance tomography *IEEE Trans. Biomed. Eng.* 45 486-493

Webster J G. 1990 Electrical Impedance Tomography (Bristol: Adam Hilger)

Wu C F 1981 On the convergence of the EM algorithm. Technical Report No. 642, Department of statistics, University of Wisconsin, Madison

Xu L, Han L, Xu A and Yang J 1997 Application of ultrasonic tomography to monitoring gas/liquid flow *Chem. Eng. Sci.* 52 2171-2183

Yorkey T J. Webster J G 1987 A comparison of impedance tomographic reconstruction algorithms *Clin. Phys. Physiol. Suppl A* 8 55-62